Universiteit
Leiden
The Netherlands

Pre-implantation and placental development in humans and mice

He, N.

Citation
He, N. (2017, October 24). *Pre-implantation and placental development in humans and mice*. Retrieved from https://hdl.handle.net/1887/58876

Version:	Not Applicable (or Unknown)
License:	Licence agreement concerning inclusion of doctoral thesis in the Institutional Repository of the University of Leiden
Downloaded from:	https://hdl.handle.net/1887/58876

Note: To cite this publication please use the final published version (if applicable).

Cover Page

Universiteit Leiden

The following handle holds various files of this Leiden University dissertation:
http://hdl.handle.net/1887/58876

Author: He, N.
Title: Pre-implantation and placental development in humans and mice
Issue Date: 2017-10-24

Pre-implantation and placental development in humans and mice

Proefschrift

ter verkrijging van
de graad van Doctor aan de Universiteit Leiden,
op gezag van Rector Magnificus prof.mr. C.J.J.M. Stolker,
volgens besluit van het College voor Promoties
te verdedigen op

dinsdag 24 oktober 2017
klokke 11:15 uur

door

Nannan He

geboren te Jiaozuo, China in 1989

Promotores
Prof. dr. C.L. Mummery
Prof. dr. F.M. Helmerhorst

Co-promotor
Dr. S.M. Chuva de Sousa Lopes

Promotiecommissie
Prof. dr. J.J. Goeman
Prof. dr. C.B.M. Oudejans (VU University Medical Center, Amsterdam)
Prof. dr. J. Gribnau (Erasmus University Medical Center, Rotterdam)
Dr. L.A.J. van der Westerlaken

CONTENTS

Chapter 1 8
General introduction
Chapter 2 28
On the development of extragonadal and gonadal human germ cells
Chapter 3 48
Transcriptomic data analysis indicates X chromosome inactivation in human pre-implantation embryos
Chapter 4 72
Human extravillous trophoblasts penetrate decidual veins and lymphatics before remodeling spiral arteries during early pregnancy
Chapter 5 90
Spatial pattern of methylation in *IGF2/H19* ICR1 in human first-trimester placenta
Chapter 6 100
At term, XmO and XpO mouse placentas show differences in glucose metabolism in the trophectoderm-derived outer zone
Chapter 7 118
General discussion and future perspectives
Appendix
Summary 130
Samenvatting 132
论文概述 134
List of Publications 136
Curriculum Vitae 137
Acknowledgements 138

CHAPTER 1

General introduction

Primordial germ cells and gametogenesis in humans and mice

The immortal life cycle of mammalian germ cells

In mammals, germ cells are immortal and highly specialized for transmitting genetic information through generations [1, 2]. Following the segregation of the germline from the somatic lineage early in embryogenesis [3], primordial germ cells (PGCs), the progenitors of haploid gametes, originate outside the early post-implantation embryo at the border with the extraembryonic part of the embryo. The PGCs then migrate across the embryo to reach the developing gonad [4, 5]. Through spermatogenesis or oogenesis in the gonads, PGCs differentiate into sperms or oocytes via meiosis (Figure 1) [3]. Following the fusion of sperm with an mature oocyte, the haploid genomes of each parent are unified, resulting in a totipotent one-cell zygote [6]. The zygote, which represents the earliest developmental stage of embryogenesis, will develop into an embryo and eventually a complete organism together with all of its extraembryonic structures [7]. These extraembryonic structures mediate implantation in the uterine wall and the following gas exchange and nutrient supply. From the post-implantation epiblast, PGCs are specified [8-10].

Origin and migration of human and mouse PGCs

Due to the limited access to very early human embryos and more importantly restrictions to the allowed time in culture (14 days), little is known about PGCs formation in humans [10]. During weeks 5-6 of gestation (W5-W6, or weeks 3-4 post conception), PGCs are observed in human embryos in the yolk sac wall close to the allantois [11]. Subsequently, they migrate through the dorsal hind gut mesentery to the gonadal primordia [12] and arrive at the prospective ovary or testis around W7 [13]. By contrast, mouse PGC precursors are known to be induced in epiblast-derived embryonic ectoderm at embryonic day (E)6.25, located between extraembryonic and embryonic ectoderm [14]. At E7.25, PGCs are present at the base of the mesodermal allantois [10, 15]. From there they migrate through the developing hindgut, along the midline of the embryo, and reach the genital ridges at around E10.5 [4, 16]. However, some PGCs may stop migrating on their way to the gonads or become lodged in extragonadal organs such as adrenal glands [17, 18]. Ectopic PGCs are often associated with extragonadal germ cell tumors in humans [19]. Therefore, the development of human extragonadal PGCs and their fate deserve further investigation.

Gametogenesis in humans and mice

Following gonadal colonization, both human and mouse PGCs differentiate into oogonia in females and spermatogonia in males upon sex determination [10, 20]. In the female ovaries, after mitotic arrest, oogonia enter meiotic prophase as primary oocytes and after birth arrest at the diplotene stage of meiosis [21]. After puberty, hormonal stimulation during ovulation of each menstrual cycle causes maturation and release of the dominant oocyte. After the first meiotic division is completed, the mature oocyte arrests at metaphase II stage, ready to be

fertilized [22, 23]. In the male testes, spermatogonia proliferate and then arrest in the G0/G1 phase of the mitotic division [24]. In contrast to females, male germ cells do not enter meiosis before birth [25]. After birth, the germ cells resume mitotic proliferation. Until puberty, some of spermatogonia in the seminiferous tubules enter meiosis I and differentiate into primary spermatocytes. Secondary spermatocytes are produced after meiosis I and then after the second meiotic division, haploid spermatids are formed. These spermatids subsequently differentiate morphologically into sperms through changes in cellular organization and shape [26].

Pre-implantation development and implantation in humans and mice

The pre-implantation development period, which includes fertilization, cell cleavage, morula and blastocyst formation, comprises the initial stages of mammalian development. It takes place before the embryo implants into the mother's uterus (Figure 2) [27]. Fertilization represents one of the most important and fascinating processes in biology, because the union of sperm and mature oocyte at fertilization triggers the recombination of paternal and maternal genetic information to form the diploid genome of a new and unique individual [7]. Understanding the stages of pre-implantation development and the underlying regulatory cellular and molecular mechanisms offers essential implications for assisted reproductive technology (ART).

In preparation for implantation and pregnancy, uterine endometrium transforms into a differentiated maternal tissue "decidua" through a remarkable event known as decidualization [28, 29] in response to estrogen and progesterone. The decidua is characterized by vascular remodelling, differentiation of stromal cells into large rounded decidual cells, angiogenesis and secretory transformation of uterine glands [28, 30].

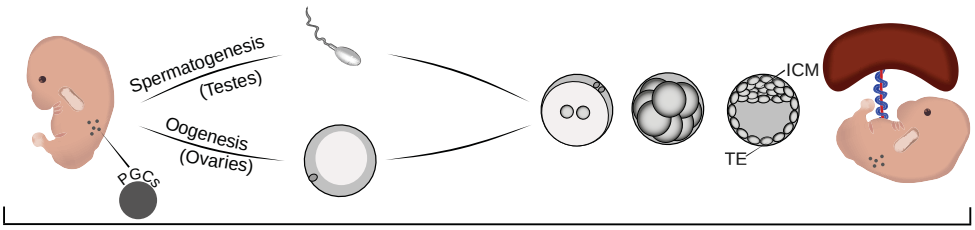

Figure 1. The immortal life cycle of mammalian germ cells.

Once the unipotent primordial germ cells (PGCs) are specified just outside the embryo proper during early embryogenesis, they migrate to the developing fetal gonads. There, they develop into female oogonia or male spermatogonia upon sex determination. Subsequently, germ cells undergo meiosis and produce mature sperms or oocytes depending on the sex. When the oocyte is fertilized by sperm, a totipotent zygote is formed. Through cell cleavage divisions and differentiation, the zygote develops into a blastocyst with pluripotent inner cell mass (ICM) and trophectoderm (TE). PGCs are specified from the ICM-derived epiblast cells, thus completing the cycle.

Human pre-implantation development

Pre-implantation embryos are morphologically similar in humans and mice, although the timing is quite different from each other (Figure 2) [31].

In humans, simultaneously with sperm-oocyte fusion, the second meiotic division of the oocyte is complete and the second polar body is extruded [26]. In the one-cell zygote, paternal and maternal haploid pronuclei move towards each other and they both undergo DNA replication before entering the first mitotic division [32] to produce a 2-cell embryo within one day after fertilization. Afterwards, the embryo undergoes a series of mitotic cell divisions (known as cleavage divisions) and produces sequentially smaller embryonic cells (called blastomeres).

As cleavage divisions continue, the embryo "compacts" to form a solid ball of cells (morula) by day 4 of development (Figure 2). Products of several genes are involved in this compaction and the following cavitation process, including the sodium-potassium ATPase transport system and tight junction proteins [33]. The sodium/potassium ATPases on the cell membrane transport sodium from outside environment into the morula, followed by water flow into the embryo and formation of blastocoelic fluid. When a large cavity (blastocoel) is formed, the embryonic cells form a compact mass (called the inner cell mass or ICM) at one side of this cavity and a thin outer shell of epithelium (called trophectoderm or TE) [34]. Now the embryo is referred to as a blastocyst. In the blastocyst, TE cells adjacent to the ICM are polar TE, whereas the cells surrounding the blastocoel are mural TE [35].

By day 6 in humans, the developing blastocyst "hatches" from the protective *zona pellucida* [36], an acellular membrane that has protected the embryo as it has moved from the

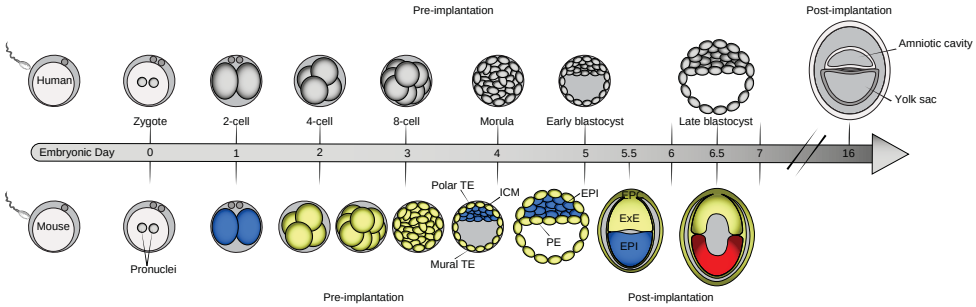

Figure 2. Stages and X chromosome status of pre-implantation and post-implantation development in humans and mice.

Simultaneously with sperm-oocyte fusion, the one-cell zygote is formed. By day 1, a 2-cell embryo is produced after the first mitotic division. As cleavage divisions continue, the embryo undergoes compaction and cell differentiation and develops into morula and then blastocyst. The blastocyst is composed of trophectoderm (TE) and the inner cell mass (ICM) which further differentiate into pluripotent epiblast (EPI) and primitive endoderm (PE). The implantation of the human hatched blastocyst occurs at around E6.5. During gastrulation at around E16, EPI gives rise to three primary germ layers while PE gives rise to the yolk sac. The extraembryonic cytotrophoblasts and syncytiotrophoblast cells are derived from TE. Being different from human post-implantation embryos, mouse post-implantation embryos become an egg cylinder within 1 day. The TE differentiates into giant cells, the extraembryonic ectoderm (ExE) and the ectoplacental cone (EPC). In the E6.5 embryo, epiblast cells give rise to the three germ layers. Colors indicate X chromosome inactivation status in cells. Yellow: imprinted X inactivation (Xp inactive, XaXi); blue: Xp reactivation (XaXa); red: random X inactivation (either Xm or Xp inactive).

oviduct where cleavage takes place, into the uterus. The blastocyst is then ready to attach to the endometrial lining of the uterus. At around 6.5 days, the polar TE cells undergo syncytial fusion of mononucleated cells and produce the first syncytiotrophoblast, which is able to invade the uterine lining [37]. Implantation is only facilitated during a limited reception-ready phase (the "implantation window"), on days 7-10 of development in humans [38]. This restricted period is regulated by appropriate levels of ovarian estrogen and progesterone, which synchronize the timing of embryo development with uterine receptivity [39]. The complex but highly organized implantation process can be classified into three phases [40]: (1) apposition - close apposition of the blastocyst to the uterine lining; (2) adhesion - attachment of the blastocyst to endometrial surface epithelium; and (3) penetration - invasion of the embryo through the epithelial surface and into the endometrial stroma. Successful implantation, a crucial step in the establishment and development of normal pregnancy, depends on the interaction between receptive decidua and a good-quality blastocyst at the right time [41].

Mouse pre-implantation development

While this pre-implantation period lasts approximately one week in humans, mouse embryos undergo the same events in 4.5 days (Figure 2) [31]. Embryonic cells start to compact and differentiate at the morula stage around E2.5. By E3.5, with lineage segregation and the formation of cavitation, a blastocyst is formed. Between E3.5 and E4.5, the ICM further differentiates and segregates into primitive endoderm (PE) and the pluripotent epiblast (EPI). These pre-implantation cell fate decisions are concisely regulated by cell signaling and subsequent lineage-specific transcription factors [42, 43]. At E4.5, the blastocyst with three segregated cell lineages (TE, EPI and PE) hatches out of the *zona pellucida* and initiates implantation [42].

Post-implantation development in humans and mice

Human post-implantation development

Following human implantation at day 7, the invasive syncytiotrophoblast, derived from polar TE, penetrates the uterine surface epithelium and thus draws the blastocyst deeper into the uterine wall [44]. The bilaminar embryonic disc comprises the EPI and the PE layers, both derived from ICM (Figure 2). By day 8, the amniotic cavity has appeared separating EPI from amnion while the syncytiotrophoblast grows and expands continuously. By day 9, the embryo becomes fully embedded within the uterine lining. The amniotic cavity expands, and trophoblastic *lacunae* appear in the syncytiotrophoblast which covers the embryo completely. On days 10-11, PE-derived primary yolk sac appears [45]. On days 11-13, the PE cells proliferate to produce the definitive (secondary) yolk sac whereas the primary yolk sac breaks up. An extraembryonic space, the chorionic cavity, is established. Its outer boundary, referred to as the chorion, is composed of trophoblasts and the underlying extraembryonic mesoderm [46]. During gastrulation on days 14-16, ingressing EPI cells converge at the midline and ingress at the primitive streak, replacing primitive endoderm to produce definitive endoderm [47]. Some EPI cells differentiate into embryonic mesoderm lying between the EPI layer and the definitive

endoderm layer. Cell movements in gastrulation transform the human embryo into a multi-layered organism with three primary germ layers (ectoderm, definitive endoderm and embryonic mesoderm) (Figure 2) [48].

Mouse post-implantation development

Being quite distinct from human post-implantation embryo structures (Figure 2) [48], cells of the mouse blastocyst proliferate rapidly and transform the embryo into an egg cylinder within 24 hours after implantation [42]. Mural TE differentiates into primary trophoblastic giant cells [49], whereas polar TE subsequently differentiates into the ectoplacental cone (EPC) and the extraembryonic ectoderm (ExE) [50]. As the egg cylinder elongates, a luminal space is established within the EPI through polarization and hollowing, thereby transforming the EPI into a cup-shaped polarized epithelium [51]. The same process of polarization and hollowing also occurs in the ExE, the lumen eventually fusing to form the pro-amniotic cavity during E5.5–E5.75. The PE differentiates into parietal endoderm covering inner surface of mural trophectoderm and visceral endoderm cells covering the elongating egg cylinder (Figure 2) [42]. In the E6.5 mouse embryo, the primitive streak is formed in the posterior region of the EPI, which indicates the initiation of gastrulation [52]. Epiblast cells proliferate to cells that pass through the primitive streak, thereby giving rise to the mesoderm and the definitive endoderm which replaces the visceral endoderm [53]. Those EPI cells not moving through the primitive streak become the ectoderm. Together, these are the three primary germ layers (embryonic ectoderm, embryonic mesoderm and definitive endoderm) of the mouse embryo (Figure 2) [54]. A set of signaling pathways, including the WNT, BMP, Nodal and FGF pathways have been shown to be involved in this gastrulation process largely through gene deletion studies [55, 56]. At E7.25, PGCs arise from the epiblast, at the base of the mesodermal allantois [10].

Early placentation in humans and mice

During human and mouse implantation, decidua has three portions renamed by their relationship to the implantation site [28, 57]: (1) Decidua basalis, which underlies the implantation site; (2) Decidua capsularis, which lies between the uterine lumen and the implantation site; (3) Decidua parietalis, which is the rest decidua. The decidua basalis forms the basal plate which is the maternal part of the placenta.

Human early placentation

In the first week of development, the human embryo obtains nutrients by simple diffusion [58]. As the blastocyst attaches to the uterine epithelium, the formation of the placenta begins [59]. From day 8, TE-derived invasive trophoblasts penetrate the decidual stroma and the trophoblastic *lacunae* within the syncytiotrophoblast start to contact with maternal capillaries [31, 37]. During days 11-13, the cytotrophoblasts, acting as stem cells, proliferate and bud into the overlying syncytiotrophoblasts. The cytotrophoblast cells, together with an outer layer of syncytiotrophoblasts, grow out into the *lacunae*, thus forming primary villi [60]. Thereafter, the extraembryonic mesoderm cells proliferate and penetrate into the primary villi, forming

secondary villi. By week 3, within the villous mesoderm core, hematopoietic progenitor cells develop and give rise to placental blood cells [61]. The villi containing the first placental blood vessels are referred to as tertiary villi [62].

Due to the rapid placental growth during early pregnancy as well as apoptosis in the syncytiotrophoblast layer [63], the villous cytotrophoblast cells continuously proliferate, differentiate and fuse into the outer syncytiotrophoblasts [64]. This differentiation and fusion process involves syncytin genes encoding proteins which can induce cell-cell fusion [65, 66]. In the distal part of the anchoring villi, cytotrophoblasts proliferate and differentiate into cell columns, where trophoblast cells acquire an invasive phenotype during differentiation. These invading trophoblasts, known as extravillous trophoblasts (EVTs), detach from the cell columns and start to migrate into the decidua and even the myometrium [67, 68]. This trophoblast differentiation process is tightly regulated by oxygen tension and proper interplay of transcription factors, hormones, growth factors and other signaling molecules [69]. Four subsets of EVTs have been identified: (1) Interstitial EVTs, which invade the decidual stroma and even into the inner third of the myometrium; (2) Endovascular EVTs, which can migrate into maternal remodelled spiral arteries in a retrograde fashion [70] and into maternal uterine veins [71]; (3) Intramural EVTs, which are present in vascular wall of the remodeled spiral arteries [72]; (4) "Epithelial" EVTs, which line the basal plate together with maternal endothelial cells [73].

EVTs are observed to "block" or "plug" the opening of spiral arteries into the intervillous space at W8-W12 [74]. Because of these "blocks" or "plugs", the maternal circulation to the placenta is restricted, thereby creating an hypoxic placental environment which is vital for regulating trophoblast cells differentiation during early pregnancy [75]. In addition, EVTs have been shown to be involved in the process of arterial remodelling together with macrophages and uterine natural killer (uNK) cells [76]. Initially, unremodelled decidual arteries consist of an intact endothelium and several well-organized smooth muscle cell (SMC) layers. Before EVT invasion of the spiral arteries, leukocytes infiltrate the vascular wall, synchronized with disorganization of the SMC layers and loss of endothelial cells. Under subsequent remodelling by interstitial and endovascular EVTs, decidual arteries lose endothelium and SMC layers entirely [77]. Remodelled decidual arteries lack maternal vasomotor control [78] and therefore become low-resistance, heavily dilated vessels that provide increased blood flow towards the placenta to meet the requirements of the growing fetus. At about W12, the open connection between maternal circulation and intervillous space is completely established [78, 79]. In this process, proper EVT invasion in decidual vasculature regulates oxygen tension for placental development [75] which is vital for successful pregnancy [80, 81]. On the contrary, insufficient EVTs invasion in maternal decidua is reported to result in inadequate blood perfusion of the placenta and subsequent pregnancy complications including preeclampsia and intrauterine growth restriction [82, 83]. Thus, characterizing the invasion of fetal EVTs in maternal decidua basalis in early pregnancy will help to identify the underlying mechanism and reveal potential therapeutic strategies for some pregnancy complications.

Mouse early placentation

In mice, the mesoderm-derived allantois contacts with chorion at E8.5 [84]. This event, called "chorioallantoic fusion", starts the formation of early placenta. Thereafter, fetal components of the placental vascular network undergo extensive branching and grow into the folds of the chorion [84]. At the same time, chorionic trophoblast cells, in direct apposition with endothelium of the fetal vessels, differentiate into multiple layers of trophoblast cells: two layers of syncytiotrophoblast cells and another layer of mononuclear trophoblast cells [85]. Maternal blood flows through the small spaces among trophoblast cells at around E10.5, resulting in a functional placenta exchanging maternal and fetal blood [86]. By E14.5, the placenta finally develops into the definitive placenta [87].

Mouse placentation shows many differences from humans [88]. Crucially, in contrast to human extensive trophoblast invasion into decidua and decidual vessels, mouse trophoblast invasion is very shallow [89]. Therefore, transformation of mouse uterine arteries is dependent on maternal (uNK) cells rather than fetal trophoblasts [90].

Late placentation in humans and mice

The placenta is the first fully-formed organ in mammals. It supports the directional and selective transport of nutrients, gases and waste between maternal and fetal circulations during intrauterine development [91]. It maintains pregnancy and supports fetal development and growth. Therefore, placental dysfunction may lead to pregnancy complications causing risk to mother and fetus [92]. Mouse and human placentae are haemochorial, meaning that the maternal blood directly contacts fetal trophoblast cells [93, 94]. The other two types of placenta, epitheliochorial placenta (as observed in horse, cow and pig) and endotheliochorial placenta (as described in cat and dog) have a barrier between fetal villi and maternal blood [94, 95].

Human late placentation

In humans, the chorionic surface is entirely covered by chorionic villi during the first 8 weeks. As the gestational sac enlarges, chorionic villi on the decidua capsularis undergoes progressive regression into a smooth surface called "chorion laeve" [96, 97]. The chorion laeve fuses with decidua parietalis by the end of the third month. Chorionic villi on the decidua basalis become larger and more extensively branched.

By the end of the fourth month of pregnancy, the human placenta has attained its definitive structure and function (referred to as "definitive placenta"), consisting of fetal terminal chorionic villi and maternal decidua (Figure 3A) [98, 99]. The villi are composed of an inner EPI-derived mesenchymal core and two layers of TE-derived trophoblast epithelium (a layer of mononuclear cytotrophoblast cells and a layer of multinucleated syncytiotrophoblast cells) [37]. The chorionic villi either attach to the decidua basalis as anchoring villi or float within the intervillous space as floating villi [69].

The high-flow low-resistance maternal remodelled arteries accommodate massively

increased maternal blood perfusion into the intervillous space [78]. The relatively high arterial pressure allows exchange between maternal and fetal blood to take place. This must cross four layers of tissue (the placental barrier): two villous trophoblast layers (one layer of syncytiotrophoblasts and one layer of cytotrophoblasts), the connective tissue (extraembryonic mesoderm) in the core of villi and the fetal capillary endothelium [100]. After exchange of fetal and maternal blood at the external microvillous surface of chorionic villi, the single umbilical vein carries oxygenated blood and nutrient to the fetus. Then the two umbilical arteries transport deoxygenated fetal blood and waste product back to the placenta [101]. In-flowing maternal arterial blood pushes venous blood back to decidual veins through venous orifices in the basal plate. Thus, the maternal blood traverses the intervillous space of the placenta freely without preformed channels.

Mouse late placentation

Since E11.5, mouse definitive chorioallantoic placenta is established, composed of distinct structural layers [102]: maternal decidua with spiral arteries perfusion, an outer layer of trophoblast giant cells (TGCs) interfacing with the maternal decidua, followed by the junctional zone [glycogen cells (GCs) and spongiotrophoblasts], the labyrinth (trophoblast cells and extraembryonic mesoderm endothelial cells) and finally the chorionic plate facing the embryo [84, 103, 104] (Figure 3B). The GCs, which have high glycogen content and are sensitive to glucagon signaling, may be serving as a potential source of energy [105].

Maternal spiral arteries traverse the decidua basalis and converge to form centrally located arterial "canals" which carry maternal blood to the base of labyrinth [89] (Figure 3B). In the labyrinth, fetal and maternal blood exchanges, with the well-organized cell layers (a layer of mononuclear trophoblasts, a bilayer of syncytiotrophoblasts and an endothelial cell layer of the fetal vasculature) serving as the barrier between maternal-fetal exchange [101]. Afterwards, venous deoxygenated blood drains from the labyrinth through venous channels in the junctional zone into venous sinuses in the decidua basalis [89].

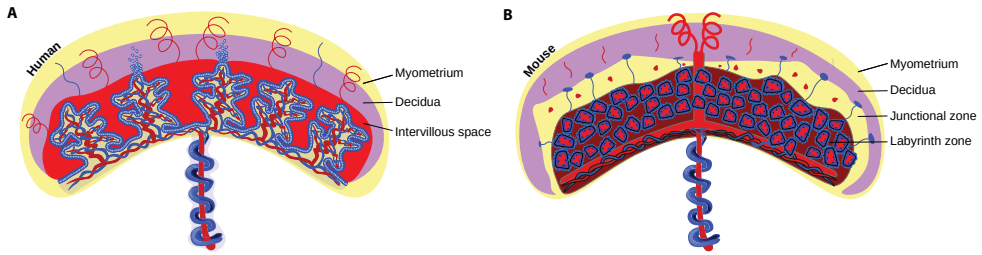

Figure 3. Anatomical comparison of definitive placenta in humans and mice.

(**A**) Structure of the human definitive placenta. The placenta is composed of maternal decidua and fetal chorionic villi. Chorionic villi consist of mesenchyme core, an inner cytotrophoblasts layer and an outer syncytiotrophoblasts layer. In the distal part of anchoring villi, extravillous trophoblast (EVT) cells detach from the distal part of cytotrophoblasts columns and invade the maternal decidua. (**B**) Structure of the mouse definitive placenta. The placenta is composed of maternal decidua, junctional zone and labyrinth zone. In the labyrinth, maternal blood is separated from fetal capillaries by three trophoblast layers: a mononuclear trophoblast cell layer and a bilayer of syncytiotrophoblasts.

Epigenetic regulation in germ cells, peri-implantation and placental development

Epigenetic regulation is crucial for various biological processes. Two epigenetic regulation processes established in early development [106], X chromosome inactivation (XCI) and genomic imprinting, are essential for dosage control of X-linked genes and parent-of-origin-specific genes in certain cells at certain stages.

X chromosome inactivation

In mammals, XCI is the mechanism to achieve dosage compensation of X-genes between females and males, in which one of the two X chromosomes becomes inactivated (Xi) in female somatic cells [106, 107]. XCI is regulated by X inactivation centre (Xic) [108, 109], which includes the non-coding locus *XIST* and its antisense transcript *TSIX* as a repressor [110]. *XIST* RNA coats the future inactive X chromosome, thus trigging the silencing of the whole X chromosome. This is followed by DNA methylation at CpG-rich promoters, histone H3 lysine 27 trimethylation (H3K27me3) and H4 hypoacetylation [106, 111]. Individuals, even with abnormal numbers of X chromosomes, silence all but one of the X chromosomes [112]. For example, Turner syndrome patients (45,XO) harboring a single X chromosome [113] show no inactivation of this unique X chromosome. Klinefelter syndrome patients (47, XXY) display one active and one inactive X chromosomes [114]. Additionally, a fraction of X-genes are revealed to escape X inactivation on the Xi and are known as “escapees”. A higher percentage of escapees along chromosome X are reported in humans (around 15%) than in mice (about 3%) [115, 116]. Many of the escapees are located in the pseudoautosomal regions [117], where genes are present on both X and Y chromosomes.

XCI has been investigated by several approaches including *XIST* RNA-FISH [118], H3K27 trimethylation [119], human androgen receptor gene assay (HUMARA) [120], retinitis pigmentosa 2 (*RP2*)-based assay [121] and allele-specific expression analysis of the informative single-nucleotide polymorphisms (SNPs) enabling parental origin to be assigned [122-124].

The dynamic XCI status during early development has been more extensively studied in mice than in humans, because of the availability of genetic substrains of mice [125-127]. After fertilization, X inactivation is initiated during pre-implantation development of mouse female embryos, closely related to the early lineage segregation [125]. The first XCI wave occurs at the two- to four-cell stage and results in the imprinted inactivation of Xp in all cells of the embryo (Figure 2). At the blastocyst stage, the Xp remains silent in the TE and PE [103, 126, 127] while the Xp becomes reactivated in the EPI at E3.5. Shortly thereafter, during the second XCI wave, either the Xm or the Xp is silenced in a random fashion, resulting in random XCI in epiblast cells (Figure 2) [128]. This is followed by reactivation of the silent X, in preparation for the equal segregation during meiosis, in female PGCs between E8.5 and E12.5, but not in the female somatic cells [119]. During placentation, mouse TE-derived cells maintain imprinted XCI. Therefore, TE-derived cells in the placenta contain an obligatorily silenced

Xp in females, including the TGCs, the spongiotrophoblasts and GCs in the outer zone and the syncytiotrophoblasts, mononuclear trophoblasts in the labyrinth zone [102]. By contrast, EPI-derived cells in the placenta, including the chorionic plate of the placenta and the fetal endothelial cells in the labyrinth zone, show random XCI.

The process of XCI in humans is less well-known than in mice. The inactivated X chromosomes in human PGCs are already reactivated at W4 [122]. During pre-implantation development at E3-E7, X-linked genes are thought to maintain biallelic expression in all lineages [118, 129]. Previous research regarding XCI in human placenta has resulted in conflicting views, supporting random [124, 130-133], non-random [134] and preferential paternal XCI [135-139]. These conflicting results may be due to high heterogeneity, clonal growth and a mixture of TE-derived and EPI-derived cells in placenta.

Genomic imprinting

In mammals, normally both maternal and paternal alleles of genes are expressed. However, genomic imprinting affects a subset of genes (known as imprinted genes) in both male and female offsprings, resulting in monoallelic expression of either maternal or paternal allele [106]. Most imprinted genes are located in clusters [140] that are regulated by transcription of a non-coding RNA. Imprinted genes play an essential role in embryonic and extraembryonic growth and development in mammals [141, 142].

IGF2/H19 locus, which is located on human chromosome 11 and on mouse chromosome 7, is one well-studied imprinted gene cluster [143, 144]. The location of its imprinting control region (ICR) is between protein-coding *IGF2* gene and noncoding *H19* gene [145]. The ICR on the maternal chromosome is bound by the insulator protein CTCF, and therefore is unmethylated. This allows activation of the *H19* promoter and inactivates of the *IGF2* promoter. As a result, the maternal chromosome has transcription of *H19* but not *IGF2*. In contrast, the ICR is methylated on the paternal chromosome and *IGF2* is transcribed [144].

A couple of techniques have been used to detect imprinting patterns [146], including DNA methylation at ICRs and allele-specific expression analysis of informative SNPs. Sperms and mature oocytes carry imprinted chromosomes. After fertilization, the imprint is maintained in each cell division during peri-implantation and placental development [147]. Genome-wide epigenetic reprogramming in human and mouse PGCs results in erasure of parental imprints before sex determination [147]. Upon sex determination, male and female germ cells acquire paternal and maternal imprints respectively on the chromosomes.

Aims and outline of this thesis

Pre-implantation and placental development in humans and mice has been investigated over several centuries. Although much is known about early development in mice, how differentiation and implantation are regulated at the molecular level in humans is limited. Since incorrect development and implantation is thought to be a cause of pregnancy failure and risk, the work in this thesis aimed to fill some of these gaps and specifically address the following aspects related to pre-implantation and placental development in humans and mice.

The main question of **Chapter 2** is what is the development of human (extra)gonadal germ cells between first and second trimesters regarding expression of germ cell markers and meiosis markers. Are there ectopic germ cells and do they enter meiosis in synchrony with the gonadal germ cells?

The main aim of **Chapter 3** is to investigate the status of XCI in human pre-implantation embryos. Do TE-derived cells show different XCI pattern from ICM-derived cells at E5-E7? If there is X inactivation, whether the XCI pattern is imprinted or random?

The focus of **Chapter 4** is on the invasion of decidual vasculature by human extravillous trophoblast cells from W5.5 till the end of first trimester. Do the EVTs invade arteries, veins and lymphatics? When does the invasion occur?

In **Chapter 5**, the investigation is extended towards the spatial pattern of methylation of the *IGF2/H19* imprinting control region in multiple sites of collection in human first-trimester placental villi. Do the multiple sites of placental villi show the same imprinting pattern? Is the imprinting pattern of *IGF2/H19* in human first-trimester placental villi the same as in the embryo?

The aim of **Chapter 6** is to compare the consequences of Turner syndrome harboring either a single paternally inherited (Xp) or maternally inherited (Xm) chromosome in mouse E18.5 placenta, in order to study whether the transcriptional level of Xp is equal to Xm.

Finally in **Chapter 7**, we combine and further discuss the findings obtained in chapters 2-6. Future perspectives are also proposed.

References

1. Surani MA, Hayashi K, Hajkova P: Genetic and epigenetic regulators of pluripotency. Cell 2007, 128:747-762.
2. Wylie C: Germ cells. Cell 1999, 96:165-174.
3. Lesch BJ, Page DC: Genetics of germ cell development. Nat Rev Genet 2012, 13:781-794.
4. Richardson BE, Lehmann R: Mechanisms guiding primordial germ cell migration: strategies from different organisms. Nat Rev Mol Cell Biol 2010, 11:37-49.
5. Starz-Gaiano M, Lehmann R: Moving towards the next generation. Mech Dev 2001, 105:5-18.
6. Flesch FM, Gadella BM: Dynamics of the mammalian sperm plasma membrane in the process of fertilization. Biochim Biophys Acta 2000, 1469:197-235.
7. Clift D, Schuh M: Restarting life: fertilization and the transition from meiosis to mitosis. Nat Rev Mol Cell Biol 2013, 14:549-562.
8. Hayashi Y, Saitou M, Yamanaka S: Germline development from human pluripotent stem cells toward disease modeling of infertility. Fertility and sterility 2012, 97:1250-1259.
9. Hayashi K, de Sousa Lopes SMC, Surani MA: Germ cell specification in mice. Science 2007, 316:394-396.
10. de Sousa Lopes SMC, Roelen BA: On the formation of germ cells: the good, the bad and the ugly. Differentiation 2010, 79:131-140.
11. Witschi E: Migration of the germ cells of human embryos from the yolk sac to the primitive gonadal folds. Contrib Embryol 1948, 32:67-80.
12. Mollgard K, Jespersen A, Lutterodt MC, Yding Andersen C, Hoyer PE, Byskov AG: Human primordial germ cells migrate along nerve fibers and Schwann cells from the dorsal hind gut mesentery to the gonadal ridge. Mol Hum Reprod 2010, 16:621-631.
13. Heeren A, van Iperen L, Klootwijk DB, de Melo Bernardo A, Roost MS, Gomes Fernandes MM, Louwe LA, Hilders CG, Helmerhorst FM, van der Westerlaken LA, Chuva de Sousa Lopes SM: Development of the follicular basement membrane during human gametogenesis and early folliculogenesis. BMC Dev Biol 2015, 15:4.
14. Johnson AD, Alberio R: Primordial germ cells: the first cell lineage or the last cells standing? Development 2015, 142:2730-2739.
15. Ginsburg M, Snow MH, McLaren A: Primordial germ cells in the mouse embryo during gastrulation. Development 1990, 110:521-528.
16. Saitou M, Yamaji M: Primordial germ cells in mice. Cold Spring Harb Perspect Biol 2012, 4.
17. Upadhyay S, Zamboni L: Ectopic germ cells: natural model for the study of germ cell sexual differentiation. Proc Natl Acad Sci U S A 1982, 79:6584-6588.
18. Mamsen LS, Brochner CB, Byskov AG, Mollgard K: The migration and loss of human primordial germ stem cells from the hind gut epithelium towards the gonadal ridge. Int J Dev Biol 2012, 56:771-778.
19. Gobel U, Schneider DT, Calaminus G, Haas RJ, Schmidt P, Harms D: Germ-cell tumors in childhood and adolescence. GPOH MAKEI and the MAHO study groups. Ann Oncol 2000, 11:263-271.
20. McMurray CT: Mechanisms of trinucleotide repeat instability during human development. Nature Reviews Genetics 2010, 11:786-799.
21. Tam P, Snow M: Proliferation and migration of primordial germ cells during compensatory growth in mouse embryos. Development 1981, 64:133-147.
22. Nikolic A, Volarevic V, Armstrong L, Lako M, Stojkovic M: Primordial germ cells: current knowledge and perspectives. Stem cells international 2015, 2016.
23. Virant-Klun I: Postnatal oogenesis in humans: a review of recent findings. Stem cells and cloning: advances and applications 2015, 8:49.
24. McLaren A: Mammalian germ cells: birth, sex, and immortality. Cell structure and function 2001, 26:119-122.
25. Hassold T, Hunt P: To err (meiotically) is human: the genesis of human aneuploidy. Nature Reviews Genetics 2001, 2:280-291.

26. Sathananthan AH: Ultrastructure of human gametes, fertilization and embryos in assisted reproduction: a personal survey. Micron 2013, 44:1-20.
27. Garcia-Herrero S, Cervero A, Mateu E, Mir P, Póo M, Rodrigo L, Vera M, Rubio C: Genetic Analysis of Human Preimplantation Embryos. Current Topics in Developmental Biology 2016.
28. Plaisier M: Decidualisation and angiogenesis. Best Pract Res Clin Obstet Gynaecol 2011, 25:259-271.
29. Ramathal CY, Bagchi IC, Taylor RN, Bagchi MK: Endometrial decidualization: of mice and men. In Seminars in reproductive medicine. © Thieme Medical Publishers; 2010: 017-026.
30. Gellersen B, Brosens IA, Brosens JJ: Decidualization of the human endometrium: mechanisms, functions, and clinical perspectives. In Seminars in reproductive medicine. © Thieme Medical Publishers; 2007: 445-453.
31. Niakan KK, Han J, Pedersen RA, Simon C, Pera RAR: Human pre-implantation embryo development. Development 2012, 139:829-841.
32. Hamatani T, Carter MG, Sharov AA, Ko MS: Dynamics of global gene expression changes during mouse preimplantation development. Developmental cell 2004, 6:117-131.
33. Watson AJ, Barcroft LC: Regulation of blastocyst formation. Frontiers in bioscience: a journal and virtual library 2001, 6:708.
34. Hardy K, Handyside AH, Winston R: The human blastocyst: cell number, death and allocation during late preimplantation development in vitro. Development 1989, 107:597-604.
35. Chia CM, Winston R, Handyside AH: EGF, TGF-alpha and EGFR expression in human preimplantation embryos. Development 1995, 121:299-307.
36. Krupinski P, Chickarmane V, Peterson C: Simulating the mammalian blastocyst--molecular and mechanical interactions pattern the embryo. PLoS Comput Biol 2011, 7:e1001128.
37. Huppertz B: The anatomy of the normal placenta. Journal of clinical pathology 2008, 61:1296-1302.
38. Xiao Y, Sun X, Yang X, Zhang J, Xue Q, Cai B, Zhou Y: Leukemia inhibitory factor is dysregulated in the endometrium and uterine flushing fluid of patients with adenomyosis during implantation window. Fertil Steril 2010, 94:85-89.
39. Smith SK: Regulation of angiogenesis in the endometrium. Trends in Endocrinology & Metabolism 2001, 12:147-151.
40. Wang H, Dey SK: Roadmap to embryo implantation: clues from mouse models. Nature Reviews Genetics 2006, 7:185-199.
41. Kapiteijn K, Koolwijk P, van der Weiden RM, van Nieuw Amerongen G, Plaisier M, van Hinsbergh VW, Helmerhorst FM: Human embryo-conditioned medium stimulates in vitro endometrial angiogenesis. Fertil Steril 2006, 85 Suppl 1:1232-1239.
42. Bedzhov I, Graham SJ, Leung CY, Zernicka-Goetz M: Developmental plasticity, cell fate specification and morphogenesis in the early mouse embryo. Phil Trans R Soc B 2014, 369:20130538.
43. Frum T, Ralston A: Cell signaling and transcription factors regulating cell fate during formation of the mouse blastocyst. Trends in Genetics 2015, 31:402-410.
44. Benirschke K, Burton GJ, Baergen RN: Early development of the human placenta. In Pathology of the human placenta. Springer; 2012: 41-53
45. Enders A, King B: Development of the human yolk sac. In The human yolk sac and yolk sac tumors. Springer; 1993: 33-47
46. Bourne G: The foetal membranes: a review of the anatomy of normal amnion and chorion and some aspects of their function. Postgraduate medical journal 1962, 38:193.
47. Chu L-F, Leng N, Zhang J, Hou Z, Mamott D, Vereide DT, Choi J, Kendziorski C, Stewart R, Thomson JA: Single-cell RNA-seq reveals novel regulators of human embryonic stem cell differentiation to definitive endoderm. Genome biology 2016, 17:173.
48. Tang WW, Kobayashi T, Irie N, Dietmann S, Surani MA: Specification and epigenetic programming of the human germ line. Nature Reviews Genetics 2016, 17:585-600.
49. Cross J: How to make a placenta: mechanisms of trophoblast cell differentiation in mice–a review. Placenta 2005, 26:S3-S9.

50. Carney E, Prideaux V, Lye S, Rossant J: Progressive expression of trophoblast-specific genes during formation of mouse trophoblast giant cells in vitro. Molecular reproduction and development 1993, 34:357-368.
51. Bedzhov I, Zernicka-Goetz M: Self-organizing properties of mouse pluripotent cells initiate morphogenesis upon implantation. Cell 2014, 156:1032-1044.
52. Kojima Y, Tam OH, Tam PP: Timing of developmental events in the early mouse embryo. In Seminars in cell & developmental biology. Elsevier; 2014: 65-75.
53. Robb L, Tam PP: Gastrula organiser and embryonic patterning in the mouse. In Seminars in cell & developmental biology. Elsevier; 2004: 543-554.
54. Tam PP, Loebel DA: Gene function in mouse embryogenesis: get set for gastrulation. Nature Reviews Genetics 2007, 8:368-381.
55. Olivera-Martinez I, Storey KG: Wnt signals provide a timing mechanism for the FGF-retinoid differentiation switch during vertebrate body axis extension. Development 2007, 134:2125-2135.
56. Kojima Y, Kaufman-Francis K, Studdert JB, Steiner KA, Power MD, Loebel DA, Jones V, Hor A, de Alencastro G, Logan GJ: The transcriptional and functional properties of mouse epiblast stem cells resemble the anterior primitive streak. Cell Stem Cell 2014, 14:107-120.
57. Lim HJ, Wang H: Uterine disorders and pregnancy complications: insights from mouse models. The Journal of clinical investigation 2010, 120:1004-1015.
58. Harris SE, Gopichandran N, Picton HM, Leese HJ, Orsi NM: Nutrient concentrations in murine follicular fluid and the female reproductive tract. Theriogenology 2005, 64:992-1006.
59. Aplin JD: The cell biological basis of human implantation. Best Practice & Research Clinical Obstetrics & Gynaecology 2000, 14:757-764.
60. Handwerger S: New insights into the regulation of human cytotrophoblast cell differentiation. Molecular and cellular endocrinology 2010, 323:94.
61. Dempsey EW: The development of capillaries in the villi of early human placentas. Developmental Dynamics 1972, 134:221-237.
62. Demir R, Kaufmann P, Castellucci M, Erbengi T, Kotowski A: Fetal vasculogenesis and angiogenesis in human placental villi. Cells Tissues Organs 1989, 136:190-203.
63. Huppertz B, Kadyrov M, Kingdom JCP: Apoptosis and its role in the trophoblast. American Journal of Obstetrics and Gynecology 2006, 195:29-39.
64. Simpson R, Mayhew T, Barnes P: From 13 weeks to term, the trophoblast of human placenta grows by the continuous recruitment of new proliferative units: a study of nuclear number using the disector. Placenta 1992, 13:501-512.
65. Mi S, Lee X, Li X-p, Veldman GM, Finnerty H, Racie L, Lavallie E, Tang X-Y, Edouard P, Howes S: Syncytin is a captive retroviral envelope protein involved in human placental morphogenesis. Nature 2000, 403:785-789.
66. Blaise S, de Parseval N, Bénit L, Heidmann T: Genomewide screening for fusogenic human endogenous retrovirus envelopes identifies syncytin 2, a gene conserved on primate evolution. Proceedings of the National Academy of Sciences 2003, 100:13013-13018.
67. Brosens JJ, Pijnenborg R, Brosens IA: The myometrial junctional zone spiral arteries in normal and abnormal pregnancies: a review of the literature. Am J Obstet Gynecol 2002, 187:1416-1423.
68. Knofler M: Critical growth factors and signalling pathways controlling human trophoblast invasion. Int J Dev Biol 2010, 54:269-280.
69. Ji L, Brkić J, Liu M, Fu G, Peng C, Wang Y-L: Placental trophoblast cell differentiation: physiological regulation and pathological relevance to preeclampsia. Molecular aspects of medicine 2013, 34:981-1023.
70. Harris LK: Review: Trophoblast-vascular cell interactions in early pregnancy: how to remodel a vessel. Placenta 2010, 31 Suppl:S93-98.
71. Moser G, Weiss G, Sundl M, Gauster M, Siwetz M, Lang-Olip I, Huppertz B: Extravillous trophoblasts invade more than uterine arteries: evidence for the invasion of uterine veins. Histochem Cell Biol 2016.
72. Lyall F, Robson SC, Bulmer JN: Spiral Artery Remodeling and Trophoblast Invasion in Preeclampsia and Fetal Growth RestrictionNovelty and Significance. Hypertension 2013, 62:1046-1054.

73. Byrne S, Challis E, Williams JL, Pringle JH, Hennessy JM, Ockleford CD: A mosaic cell layer in human pregnancy. Placenta 2010, 31:373-379.
74. Burton GJ, Jauniaux E, Watson AL: Maternal arterial connections to the placental intervillous space during the first trimester of human pregnancy: the Boyd collection revisited. Am J Obstet Gynecol 1999, 181:718-724.
75. James JL, Stone PR, Chamley LW: The regulation of trophoblast differentiation by oxygen in the first trimester of pregnancy. Hum Reprod Update 2006, 12:137-144.
76. Lyall F: Mechanisms regulating cytotrophoblast invasion in normal pregnancy and pre-eclampsia. Australian and New Zealand journal of obstetrics and gynaecology 2006, 46:266-273.
77. Harris L: Review: trophoblast-vascular cell interactions in early pregnancy: how to remodel a vessel. Placenta 2010, 31:S93-S98.
78. Pijnenborg R, Vercruysse L, Hanssens M: The uterine spiral arteries in human pregnancy: facts and controversies. Placenta 2006, 27:939-958.
79. Jauniaux E, Watson AL, Hempstock J, Bao YP, Skepper JN, Burton GJ: Onset of maternal arterial blood flow and placental oxidative stress. A possible factor in human early pregnancy failure. Am J Pathol 2000, 157:2111-2122.
80. Plaisier M, Dennert I, Rost E, Koolwijk P, van Hinsbergh VW, Helmerhorst FM: Decidual vascularization and the expression of angiogenic growth factors and proteases in first trimester spontaneous abortions. Hum Reprod 2009, 24:185-197.
81. Plaisier M, Rodrigues S, Willems F, Koolwijk P, van Hinsbergh VW, Helmerhorst FM: Different degrees of vascularization and their relationship to the expression of vascular endothelial growth factor, placental growth factor, angiopoietins, and their receptors in first-trimester decidual tissues. Fertil Steril 2007, 88:176-187.
82. Burke SD, Karumanchi SA: Spiral artery remodeling in preeclampsia revisited. Hypertension 2013, 62:1013-1014.
83. Fisher SJ: Why is placentation abnormal in preeclampsia? Am J Obstet Gynecol 2015, 213:S115-122.
84. Rossant J, Cross JC: Placental development: lessons from mouse mutants. Nat Rev Genet 2001, 2:538-548.
85. Cross JC: Genetic insights into trophoblast differentiation and placental morphogenesis. In Seminars in cell & developmental biology. Elsevier; 2000: 105-113.
86. Dzierzak E, Robin C: Placenta as a source of hematopoietic stem cells. Trends in molecular medicine 2010, 16:361-367.
87. Latos PA, Hemberger M: From the stem of the placental tree: trophoblast stem cells and their progeny. Development 2016, 143:3650-3660.
88. Carter AM: Animal models of human placentation–a review. Placenta 2007, 28:S41-S47.
89. Adamson SL, Lu Y, Whiteley KJ, Holmyard D, Hemberger M, Pfarrer C, Cross JC: Interactions between trophoblast cells and the maternal and fetal circulation in the mouse placenta. Dev Biol 2002, 250:358-373.
90. Moffett A, Loke C: Immunology of placentation in eutherian mammals. Nature Reviews Immunology 2006, 6:584-594.
91. Jansson T: Placenta plays a critical role in maternal-fetal resource allocation. Proc Natl Acad Sci U S A 2016, 113:11066-11068.
92. Ray JG, Vermeulen MJ, Schull MJ, McDonald S, Redelmeier DA: Metabolic syndrome and the risk of placental dysfunction. Journal of Obstetrics and Gynaecology Canada 2005, 27:1095-1101.
93. Enders AC, Blankenship TN: Comparative placental structure. Advanced drug delivery reviews 1999, 38:3-15.
94. Carter AM, Enders AC: Comparative aspects of trophoblast development and placentation. Reproductive Biology and Endocrinology 2004, 2:46.
95. PrabhuDas M, Bonney E, Caron K, Dey S, Erlebacher A, Fazleabas A, Fisher S, Golos T, Matzuk M, McCune JM: Immune mechanisms at the maternal-fetal interface: perspectives and challenges. Nature immunology 2015, 16:328-334.
96. Pijnenborg R, Vercruysse L, Brosens I: Deep placentation. Best Pract Res Clin Obstet Gynaecol 2011, 25:273-285.

97. Ilancheran S, Moodley Y, Manuelpillai U: Human fetal membranes: a source of stem cells for tissue regeneration and repair? Placenta 2009, 30:2-10.

98. Gude NM, Roberts CT, Kalionis B, King RG: Growth and function of the normal human placenta. Thrombosis research 2004, 114:397-407.

99. Georgiades P, Ferguson-Smith A, Burton G: Comparative developmental anatomy of the murine and human definitive placentae. Placenta 2002, 23:3-19.

100. Kulvietis V, Zalgeviciene V, Didziapetriene J, Rotomskis R: Transport of nanoparticles through the placental barrier. The Tohoku journal of experimental medicine 2011, 225:225-234.

101. Dilworth M, Sibley C: Review: Transport across the placenta of mice and women. Placenta 2013, 34:S34-S39.

102. Rai A, Cross JC: Development of the hemochorial maternal vascular spaces in the placenta through endothelial and vasculogenic mimicry. Dev Biol 2014, 387:131-141.

103. Cross JC, Baczyk D, Dobric N, Hemberger M, Hughes M, Simmons DG, Yamamoto H, Kingdom JC: Genes, development and evolution of the placenta. Placenta 2003, 24:123-130.

104. Malassine A, Frendo JL, Evain-Brion D: A comparison of placental development and endocrine functions between the human and mouse model. Hum Reprod Update 2003, 9:531-539.

105. Coan PM, Conroy N, Burton GJ, Ferguson-Smith AC: Origin and characteristics of glycogen cells in the developing murine placenta. Dev Dyn 2006, 235:3280-3294.

106. Inbar-Feigenberg M, Choufani S, Butcher DT, Roifman M, Weksberg R: Basic concepts of epigenetics. Fertil Steril 2013, 99:607-615.

107. Lyon MF: Gene action in the X-chromosome of the mouse (Mus musculus L.). Nature 1961, 190:372-373.

108. Brown CJ, Ballabio A, Rupert JL, Lafreniere RG, Grompe M, Tonlorenzi R, Willard HF: A gene from the region of the human X inactivation centre is expressed exclusively from the inactive X chromosome. Nature 1991, 349:38-44.

109. Brown CJ, Lafreniere RG, Powers VE, Sebastio G, Ballabio A, Pettigrew AL, Ledbetter DH, Levy E, Craig IW, Willard HF: Localization of the X inactivation centre on the human X chromosome in Xq13. Nature 1991, 349:82-84.

110. Galupa R, Heard E: X-chromosome inactivation: new insights into cis and trans regulation. Curr Opin Genet Dev 2015, 31:57-66.

111. Okamoto I, Heard E: Lessons from comparative analysis of X-chromosome inactivation in mammals. Chromosome research 2009, 17:659-669.

112. Augui S, Nora EP, Heard E: Regulation of X-chromosome inactivation by the X-inactivation centre. Nature Reviews Genetics 2011, 12:429-442.

113. Cockwell A, MacKenzie M, Youings S, Jacobs P: A cytogenetic and molecular study of a series of 45, X fetuses and their parents. Journal of medical genetics 1991, 28:151-155.

114. Iitsuka Y, Bock A, Nguyen DD, Samango-Sprouse CA, Simpson JL, Bischoff FZ: Evidence of skewed X-chromosome inactivation in 47, XXY and 48, XXYY Klinefelter patients. American journal of medical genetics 2001, 98:25-31.

115. Carrel L, Willard HF: X-inactivation profile reveals extensive variability in X-linked gene expression in females. Nature 2005, 434:400-404.

116. Berletch JB, Yang F, Disteche CM: Escape from X inactivation in mice and humans. Genome biology 2010, 11:213.

117. Gray KA, Yates B, Seal RL, Wright MW, Bruford EA: Genenames.org: the HGNC resources in 2015. Nucleic Acids Res 2015, 43:D1079-1085.

118. Okamoto I, Patrat C, Thepot D, Peynot N, Fauque P, Daniel N, Diabangouaya P, Wolf JP, Renard JP, Duranthon V, Heard E: Eutherian mammals use diverse strategies to initiate X-chromosome inactivation during development. Nature 2011, 472:370-374.

119. de Sousa Lopes SMC, Hayashi K, Shovlin TC, Mifsud W, Surani MA, McLaren A: X chromosome activity in mouse XX primordial germ cells. PLoS Genet 2008, 4:e30.

120. Allen RC, Zoghbi HY, Moseley AB, Rosenblatt HM, Belmont JW: Methylation of HpaII and HhaI sites near

the polymorphic CAG repeat in the human androgen-receptor gene correlates with X chromosome inactivation. Am J Hum Genet 1992, 51:1229-1239.

121. Machado FB, Machado FB, Faria MA, Lovatel VL, da Silva AFA, Radic CP, De Brasi CD, Rios ÁFL, de Sousa Lopes SMC, da Silveira LS: 5 me CpG Epigenetic Marks Neighboring a Primate-Conserved Core Promoter Short Tandem Repeat Indicate X-Chromosome Inactivation. PloS one 2014, 9:e103714.
122. Guo F, Yan L, Guo H, Li L, Hu B, Zhao Y, Yong J, Hu Y, Wang X, Wei Y, et al: The Transcriptome and DNA Methylome Landscapes of Human Primordial Germ Cells. Cell 2015, 161:1437-1452.
123. Petropoulos S, Edsgard D, Reinius B, Deng Q, Panula SP, Codeluppi S, Plaza Reyes A, Linnarsson S, Sandberg R, Lanner F: Single-Cell RNA-Seq Reveals Lineage and X Chromosome Dynamics in Human Preimplantation Embryos. Cell 2016, 165:1012-1026.
124. Moreira de Mello JC, de Araujo ES, Stabellini R, Fraga AM, de Souza JE, Sumita DR, Camargo AA, Pereira LV: Random X inactivation and extensive mosaicism in human placenta revealed by analysis of allele-specific gene expression along the X chromosome. PLoS One 2010, 5:e10947.
125. Okamoto I, Otte AP, Allis CD, Reinberg D, Heard E: Epigenetic dynamics of imprinted X inactivation during early mouse development. Science 2004, 303:644-649.
126. Payer B, Lee JT: X chromosome dosage compensation: how mammals keep the balance. Annu Rev Genet 2008, 42:733-772.
127. Reik W, Lewis A: Co-evolution of X-chromosome inactivation and imprinting in mammals. Nat Rev Genet 2005, 6:403-410.
128. Silva J, Nichols J, Theunissen TW, Guo G, van Oosten AL, Barrandon O, Wray J, Yamanaka S, Chambers I, Smith A: Nanog is the gateway to the pluripotent ground state. Cell 2009, 138:722-737.
129. Sahakyan A, Plath K: Transcriptome Encyclopedia of Early Human Development. Cell 2016, 165:777-779.
130. Looijenga LH, Gillis AJ, Verkerk AJ, van Putten WL, Oosterhuis JW: Heterogeneous X inactivation in trophoblastic cells of human full-term female placentas. Am J Hum Genet 1999, 64:1445-1452.
131. Migeon BR, Do TT: In search of nonrandom X inactivation: studies of the placenta from newborns heterozygous for glucose-6-phosphate dehydrogenase. Basic Life Sci 1978, 12:379-391.
132. Mohandas TK, Passage MB, Williams JW, 3rd, Sparkes RS, Yen PH, Shapiro LJ: X-chromosome inactivation in cultured cells from human chorionic villi. Somat Cell Mol Genet 1989, 15:131-136.
133. Willemsen R, Bontekoe CJ, Severijnen LA, Oostra BA: Timing of the absence of FMR1 expression in full mutation chorionic villi. Hum Genet 2002, 110:601-605.
134. Dhara SK, Benvenisty N: Gene trap as a tool for genome annotation and analysis of X chromosome inactivation in human embryonic stem cells. Nucleic Acids Res 2004, 32:3995-4002.
135. Goto T, Wright E, Monk M: Paternal X-chromosome inactivation in human trophoblastic cells. Mol Hum Reprod 1997, 3:77-80.
136. Harrison KB: X-chromosome inactivation in the human cytotrophoblast. Cytogenet Cell Genet 1989, 52:37-41.
137. Harrison KB, Warburton D: Preferential X-chromosome activity in human female placental tissues. Cytogenet Cell Genet 1986, 41:163-168.
138. Ropers HH, Wolff G, Hitzeroth HW: Preferential X inactivation in human placenta membranes: is the paternal X inactive in early embryonic development of female mammals? Hum Genet 1978, 43:265-273.
139. Uehara S, Tamura M, Nata M, Ji G, Yaegashi N, Okamura K, Yajima A: X-chromosome inactivation in the human trophoblast of early pregnancy. J Hum Genet 2000, 45:119-126.
140. Delaval K, Feil R: Epigenetic regulation of mammalian genomic imprinting. Current opinion in genetics & development 2004, 14:188-195.
141. Tycko B, Morison IM: Physiological functions of imprinted genes. Journal of cellular physiology 2002, 192:245-258.
142. Frost JM, Moore GE: The importance of imprinting in the human placenta. PLoS Genet 2010, 6:e1001015.
143. van den Berg IM, Laven JS, Stevens M, Jonkers I, Galjaard RJ, Gribnau J, van Doorninck JH: X chromosome inactivation is initiated in human preimplantation embryos. Am J Hum Genet 2009, 84:771-779.

144. Autuoro JM, Pirnie SP, Carmichael GG: Long noncoding RNAs in imprinting and X chromosome inactivation. Biomolecules 2014, 4:76-100.

145. Abramowitz LK, Bartolomei MS: Genomic imprinting: recognition and marking of imprinted loci. Current opinion in genetics & development 2012, 22:72-78.

146. Tost J, Jammes H, Dupont J-M, Buffat C, Robert B, Mignot T-M, Mondon F, Carbonne B, Siméoni U, Grangé G: Non-random, individual-specific methylation profiles are present at the sixth CTCF binding site in the human H19/IGF2 imprinting control region. Nucleic acids research 2006, 34:5438-5448.

147. Barlow DP, Bartolomei MS: Genomic imprinting in mammals. Cold Spring Harbor perspectives in biology 2014, 6:a018382.

CHAPTER 2

On the development of extragonadal and gonadal human germ cells

A. Marijne Heeren[1,#a,*], **Nannan He**[1,*], Aline F. de Souza[1,2], Angelique Goercharn-Ramlal[1,#b], Liesbeth van Iperen[1], Matthias S. Roost[1], Maria Gomes Fernandes[1], Lucette A.J. van der Westerlaken[3], Susana M. Chuva de Sousa Lopes[1,4]

[1]Department of Anatomy and Embryology, Leiden University Medical Center, Leiden, The Netherlands

[2]Department of Veterinary Medicine, Faculty Animal Sciences and Food Engineering, University of São Paulo, Pirassununga, São Paulo, Brazil; and Department of Surgery, Faculty Veterinary Medicine and Animal Sciences, University of São Paulo, São Paulo, Brazil

[3]Department of Gynaecology, Leiden University Medical Center, The Netherlands

[4]Department for Reproductive Medicine, Ghent University Hospital, Ghent, Belgium

[#a]Current address: Department of Obstetrics and Gynaecology, VU University Medical Center, Amsterdam, The Netherlands

[#b]Current address: Department of Human Genetics, Radboud University Medical Center, Nijmegen, The Netherlands

[*]Equal first authorship contribution

Biology Open 2016, 5:185-194.

Abstract

Human germ cells originate in an extragonadal location and have to migrate to colonize the gonadal primordia around 7 weeks of gestation, W7 (or 5 weeks post conception). Many germ cells are lost along the way and should enter apoptosis, but some escape and can give rise to extragonadal germ cells tumors. Due to the common somatic origin of gonads and adrenal cortex, we investigated whether ectopic germ cells were present in the human adrenals. Germ cells expressing DDX4 and/or POU5F1 were present in male and female human adrenals in the first and second trimester. However, in contrast to what has been described in mice, where 'adrenal' and 'ovarian' germ cells seem to enter meiosis in synchrony, we were unable to observe meiotic entry in human 'adrenal' germ cells until W22. By contrast, 'ovarian' germ cells at W22 showed a pronounced asynchronous meiotic entry. Interestingly, we observed that immature POU5F1+ germ cells in both first and second trimester ovaries still expressed the neural crest-marker TUBB3, reminiscent of their migratory phase. Our findings highlight species-specific differences in early gametogenesis between mice and humans. We report the presence of a population of ectopic germ cells in the human adrenals during development.

Introduction

In humans, primordial germ cells (PGCs) originate outside the gonadal primordia, in the posterior part of the yolk sac, close to the allantois and hindgut wall and undergo a phase of proliferation and migration towards the gonadal ridge [1, 2]. Normally, these PGCs reach gonadal primordia around week 7 of gestation (W7, or week 5 post conception) to become enclosed in either seminiferous tubules or ovarian cords, respectively in male and female embryos [3].

However, some PGCs in humans may stop migrating along the way to the gonads [4] or become lodged in extragonadal organs. The most obvious ectopic organ to lodge PGCs would be the adrenal glands (or adrenals). This is because the somatic gonad and adrenal cortex, both steroid-producing organs, have a common somatic origin and both organs are colonized by migratory neural crest cells [2, 5, 6]. In mice and bovine, ectopic germ cells have been described in the adrenal glands [7-9]. Ectopic germ cells present along the migratory pathway are most of the times eliminated by apoptosis [10, 11]; however, when lodged in the adrenal glands some of these ectopic germ cells survive and are able to undergo meiosis to become oocytes in both females and males [7, 9]. This suggests that the adrenal glands may provide a microenvironment that induces (or allows) germ cells to undergo a female sex differentiation pathway. Interestingly, these adrenal 'oocytes' seem to develop synchronous with gonadal 'oocytes' regarding growth, meiotic entry and they even develop a *zona pellucida* [9], in agreement with the current view of a default female pathway in the urogenital region, initiated by exposure to retinoic acid (RA) and blocked in the male gonad by local degradation of RA or related metabolites [12-14].

In different animal models, PGCs follow different 'routes' to reach the gonads, including the gut and abdominal mesentery in mice [15] or the vasculature in chicken [16]. Interestingly, it has been suggested that in humans, PGCs may migrate along the peripheral nervous system [2, 4]. Sympathetic nerve fibers were also found in the adrenal glands and indeed human ectopic PGCs could enter the adrenal glands via these fibers [4].

Here, we have investigated the presence of ectopic human germ cells in the adrenals during human development (from W8.4 until W22) and investigated how these ectopic germ cells developed by comparing the dynamics of expression of early, late and meiotic germ cell markers between the adrenal and the gonadal germ cells. 'Adrenal' germ cells seem to upregulate the late marker DDX4, but we were unable to observe 'adrenal' germ cells entering meiosis until W22. However, we show that meiotic entry in human female gonads is an asynchronous process that is still taking place after W22. We discuss possible ways of how the human germ cells reach the adrenals and on the fate of those 'adrenal' germ cells.

Material & Methods

Animals and ethics statement

The mouse E15.5 female embryos (n=7) used in this study were part of a collaboration

with Dr A. McLaren (University of Cambridge, UK, who sadly passed away on 7 July 2007) and were obtained according to the UK Home Office guidelines. The embryos were fixed overnight in 4% paraformaldehyde (PFA, Merck, Darmstadt, Germany) and stored in 100% methanol at –20°C. After rehydration, the embryos were embedded in 4% low-melting agarose (Life Technologies, Eugene, OR, USA) in PBS and were sectioned (200 μm) with a Vibratome HM650V (Microm, Walldorf, Germany). The vibratome sections were boiled 20 min in 0.1 M Tris-HCl, pH 8.5, followed by blocking overnight at 4°C with 0.5% bovine serum albumin (BSA, Life Technologies) diluted in Tris-buffered saline (TBST; 0.14 M NaCl, 2.5 mM KCl, 25 mM Tris pH 7.4) with 0.1% Triton X-100. Then sections were incubated overnight at 4°C with primary antibodies: rabbit anti-DDX4 (1:1000, ab13840, Abcam, Cambridge, UK) and rabbit anti-SYCP3 (1:500, NB300-232, Novus Biologicals Littleton, CO, USA) diluted in 0.5% BSA in TBST. The sections were washed with TBST at 4°C, followed by overnight incubation at 4°C with secondary antibodies: Alexa Fluor 568 goat anti-rabbit IgG (1:500, A-11011, Life Technologies) in 0.5% BSA in TBST, washed with TBST at 4°C and mounted with Vectashield Hard Set Mounting medium with 4',6-diamidino-2-phenylindole (DAPI) (Vector Laboratories, Burlingame, CA, USA).

Ethical approval for use of human material

Human fetal gonads (n=8 females; n=6 males) and adrenal glands (n=12 females; n=11 males) (S1 Table) were donated for research with informed consent from elective abortions without medical indication. The gestational age in weeks and days (for example W8.4 means 8 weeks and 4 days) was determined prior to the procedure by obstetric ultrasonography. To obtain 'weeks post conception' one needs to subtract two weeks from the given 'gestational age', determined by the last menstrual period (LMP). Both collection and use of human fetal tissues was approved by the Medical Ethical Committee of the Leiden University Medical Center (P08.087).

Sex genotyping, histology and immunofluorescence

The sex genotyping of the human fetal tissues, processing for histology and immunofluorescence were performed essentially as previously described [3]. All immunofluorescence staining was performed using 0.01 M citric buffer pH 6.0 for antigen retrieval. The primary antibodies used were goat anti-DDX4 (1:1000, AF2030, R&D Systems, Minneapolis, MN, USA), rabbit anti-DDX4 (1:500, ab13840, Abcam, Cambridge, UK), goat anti-POU5F1 (1:100, sc-8628, Santa Cruz Biotechnology, CA, USA), rabbit anti-SYCP3 (1:500, NB300-232, Novus Biologicals Littleton, CO, USA), mouse anti-H2AFX (Ser139) (1:500, 05-636, Millipore Temecula, CA, USA) and mouse anti-TUBB3 (1:500, ab78078, Abcam, Cambridge, UK). The secondary antibodies used were Alexa Fluor 594 donkey anti-goat (1:500, A11058, Life Technologies), Alexa Fluor 488 donkey anti-rabbit (1:500, A21206, Life Technologies), Alexa Fluor 594 donkey anti-mouse (1:500, A-21203, Life Technologies), Alexa Fluor 647 donkey anti-rabbit (1:500, A-31573, Life Technologies), Alexa Fluor 488 donkey

anti-goat (1:500, A-11055, Life Technologies), Alexa Fluor 555 donkey anti-rabbit (1:500, A-31572, Life Technologies) and Alexa Fluor 488 donkey anti-mouse (1:500, A21202 Life Technologies). Negative controls were performed by omitting the primary antibodies. TUNEL (terminal deoxynucleotidyl transferase dUTP nick end labeling) assay was performed using In Situ Cell Death Detection Kit (Roche Diagnostics, Mannheim, Germany). The sections were incubated at 37°C for 1 h. All slides were counterstained with a 1:1000 dilution of DAPI (Vector Laboratories, Peterborough, UK) in PBS for 1 min and mounted with ProLongGold antifade reagent (Life Technologies).

Imaging and quantification

After immunofluorescence, slides were analyzed and photographed on a Leica DMRA fluorescence microscope (Leica, Wetzlar, Germany) with the CoolSnap HQ2 camera (Photometrics, Tucson, USA) or on a Leica AF6000 fluorescence microscope equipped with a Hamamatsu EM-CCD C9100 digital Camera (Leica Microsystems, Wetzlar, Germany). The slides (consecutive for first trimester and every 5-10th for second trimester) were scanned on a Panoramic MIDI digital scanner (3DHISTECH Ltd., Budapest, Hungary) and analyzed with the software program 'Panoramic viewer' (3D HISTECH, Budapest, Hungary). Using this software, that allowed digital zooming and channel selection, we quantified the total number of germ cells per scanned section. Examples of POU5F1+DDX4–/low, POU5F1+DDX4+, DDX4+ germ cells are presented in Fig 4. To be considered a 'germ cell', POU5F1 was nuclear, DDX4 was cytoplasmic, DAPI (chromatin condensation) was adequate to the stage of development, both cell and nucleus had the typical germ cell shape and size; the immunostaining pattern was not observed in the negative controls.

Expression analysis

From online available single cell RNA sequencing data of human gonadal cells of first and second trimester (n=328 cells including somatic and germ cells), the expression data in fragments per kilobase of transcript per million (FPKM) of all the female germ cells (n=93) was downloaded from the Gene Expression Omnibus (GEO) database (GEO: GSE63818) [17]. For this analysis all male germ cells (n=149) and gonadal somatic cells (n=86) were excluded. Genes involved in neural crest cell development, migration and differentiation were obtained based on the GO_BP annotation (GO:0014033, GO:0001755, GO:0014033) from http://www.ensembl.org/biomart. The heatmap showing the log2(FPKM+1) was generated with the R package gplots.

Results

Germ cells were present in several ectopic locations in female mice embryos

First, we investigated the presence of germ cells at ectopic locations in mice at embryonic day (E)15.5 when basically all female gonadal germ cells have entered meiosis [18]. Using immunofluorescence for the late germ cell marker DDX4 (or VASA) and the meiotic marker

SYCP3, we observed the presence of DDX4-positive and SYCP3-positive germ cells in the E15.5 females analyzed (n=7) not only in the ovaries, but we also observed some germ cells in the mesonephros, sometimes in the abdominal mesentery, peri-aortic region, adrenal glands and a few in the proximity of the surface ectoderm, close to the external genital region and base of tail (Fig 1A-C).

Germ cells were present in human fetal male and female adrenals

Next, we investigated the presence of germ cells in human fetal adrenal glands in females and in males (S1 Table) by immunofluorescence for DDX4 and the early germ cell marker POU5F1 (or OCT4). We were able to detect single and double POU5F1/DDX4-positive germ cells, sometimes in small clusters, in all first trimester adrenal glands analyzed from W8.4-W13 (Fig 2A-B and S1 Fig). We quantified consecutive sections of several adrenals (n=3 females and n=3 males) and the majority of the sections contained 1 to 10 germ cells (Table 1). Moreover, POU5F1/DDX4-positive germ cells were never detected in the kidneys, when those were present in the slides.

To understand whether these 'adrenal' germ cells were entering meiosis, we used immunofluorescence for DDX4 and either (phosphorylated) H2AFX, a marker associated with DNA double-strand breaks both during meiosis entry, but also apoptosis [19-21] or SYCP3. Both in female and male first trimester adrenals, DDX4+ germ cells were never positive for

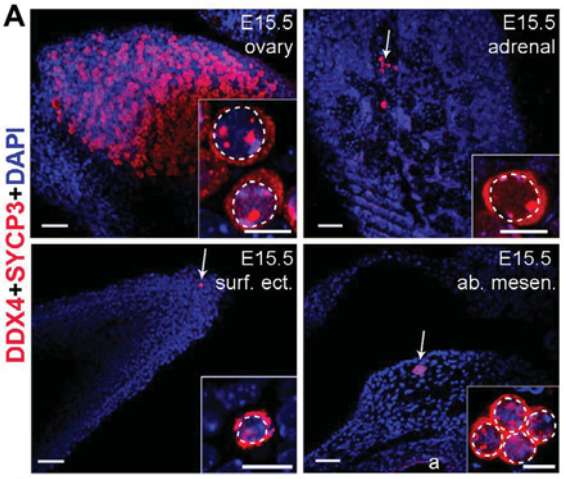

Fig 1. Ectopic germ cells in mice female embryos at E15.5.

(**A**) Transverse sections of E15.5 female embryos showing DDX4+/SYCP3+ germ cells (white arrows) at several anatomical locations (ovary, adrenal glands, surface ectoderm and abdominal mesentery). Magnified views show germ cells in more detail and dashed line depicts border between nucleus and cytoplasm. Abbreviations: a, aorta; surf. ect., surface ectoderm; ab. mesen., abdominal mesentery. Scale bars are 50 μm, and in the magnified inserts 5 μm. (**B**) Schematic of locations where ectopic germ cells were observed. (**C**) Table of the number of double DDX4+/SYCP3+ germ cells per ectopic location in each female E15.5 embryo analyzed (N=7).

H2AFX (Fig 2C-D and S1 Fig) or SYCP3 (S2 Fig). However, many H2AFX+ cells were observed in the adrenals and could correspond to adrenal cells undergoing apoptosis. To further investigate the fate of DDX4+ cells in the adrenals, we also performed TUNEL assay (Fig 2E-F and S1 Fig), but were unable to observe 'adrenal' DDX4+ germ cells in apoptosis. We conclude that during first trimester, pre-meiotic germ cells are relatively abundant in the adrenals (Fig 2).

We proceeded analyzing both female and male second trimester adrenals ranging from W14-W22, where we encountered germ cells at the periphery of the adrenal (Fig 3A-B, Table 1; S3 Fig), but we were unable to detect H2AFX+ germ cells (Fig 3C-D and S3 Fig) or SYCP3+ germ cells (S2 Fig). From the few germ cells encountered none were positive for TUNEL (Fig 3E-F and S3 Fig). Our results in human are in contrast with results in mice showing that germ cells observed in the adrenals were able to survive and mature [7, 9].

Developmental dynamics of human germ cells in first and second trimester

As we were unable to observe meiotic entry in the human 'adrenal' germ cells until W22, we investigated the spatial dynamics of meiotic entry in human ovaries, when possible from the same individual from which we had analyzed the adrenals (S1 Table). We discriminated firstly between POU5F1+ and DDX4+ germ cells (Fig 4A) and, secondly, we immunostained consecutive sections for two independent meiotic markers, H2AFX and SYCP3 (Fig 4B).

As previously observed by us and others [3, 22], in first trimester ovaries most germ cells were POU5F1+ and expressed either low (or no) DDX4, consisting of a relatively homogeneous

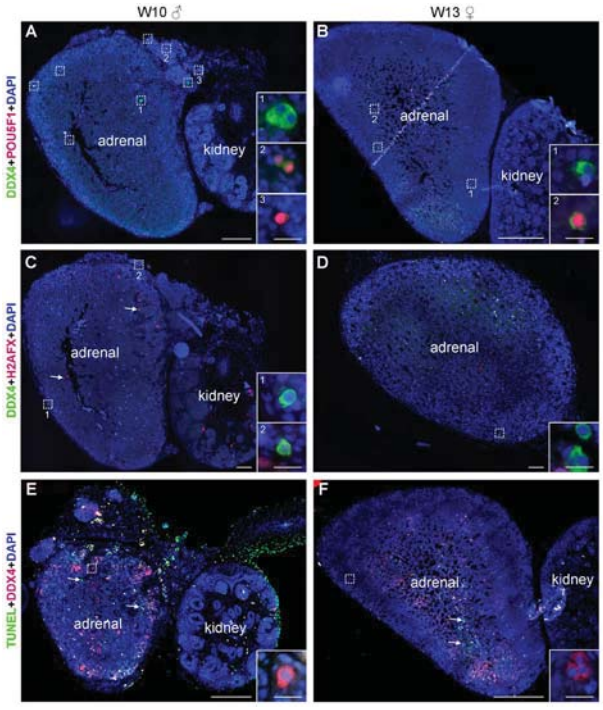

Fig 2. Germ cells in first trimester human fetal adrenals.

Histological sections of human adrenals (and adjacent kidney) in first trimester male (W10) and female (W13). (**A**,**B**) Germ cells were identified by expression of POU5F1 (in red) and/or DDX4 (in green). (**C**,**D**) DDX4+ (in green) germ cells do not express H2AFX (in red), however many H2AFX+ cells were present in the adrenals (white arrows). (**E**,**F**) DDX4+ (in red) germ cells were not TUNEL positive (in green), however many TUNEL+ cells were present in the adrenals (white arrows). Note the presence of autofluorescent red blood cells. Some germ cells are highlighted in dotted boxes. Magnified views of dotted boxes are shown as inserts and the insert number corresponds to its location. Scale bars are 200 μm in **A**-**B**, **E**-**F**, 100 μm in **C**-**D** and 20 μm in all inserts.

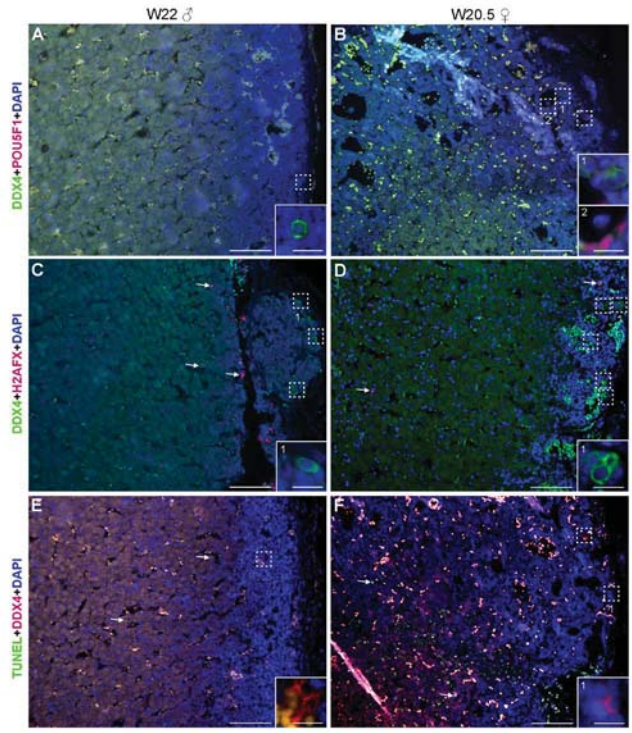

Fig 3. Germ cells in second trimester human fetal adrenals.

Histological sections of human adrenals of second trimester male (W22) and female (W20.5). (**A**,**B**) Germ cells were identified by expression of POU5F1 (in red) and/or DDX4 (in green). (**C**,**D**) DDX4+ (in green) germ cells do not express H2AFX (in red), however H2AFX+ cells were present in the adrenals (white arrows). (**E**,**F**) DDX4+ (in red) germ cells were not TUNEL positive (in green), however TUNEL+ cells were present in the adrenals (white arrows). Note the presence of autofluorescent red blood cells. Some germ cells are highlighted in dotted boxes. Magnified views of dotted boxes are shown as inserts and the insert number corresponds to its location. Scale bars are 100 μm in **A**-**F** and 20 μm in all inserts.

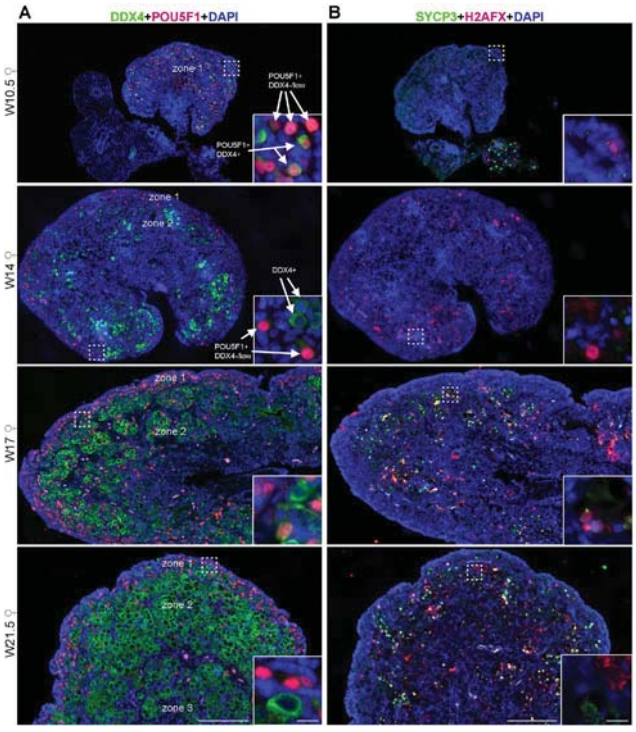

Fig 4. Dynamic expression of germ cell markers in human fetal ovaries.

(**A**) Histological sections of human ovaries at W10.5, W14, W17 and W21.5, immunostained for the early germ cell marker (nuclear) POU5F1 (in red) and late germ cell marker (cytoplasmic) DDX4 (in green). In zone 1, most germ cells are POU5F1+ DDX4-/low; in zone 2 and 3, most germ cells are DDX4+. Several germ cells in zone 3 have developed into primordial follicles. Inserts are magnifications of the dotted boxes. (**B**) Histological sections of human ovaries at W10.5, W14, W17 and W21.5, immunostained for the meiotic markers H2AFX (in red) and SYCP3 (in green). Inserts are magnifications of the dotted boxes. Note the presence of autofluorescent red blood cells. Scale bars are 200 μm and in the magnified inserts 20 μm.

population of germ cells (zone 1) (Fig 4A, Table 2; S4A Fig). During second trimester, we observed a shift towards DDX4+ germ cells interiorly (zone 2), whereas a pronounced peripheral layer of POU5F1+ cells remained (Fig 4A, Table 2; S4B Fig). At W21.5, the majority of germ cells in the ovary were DDX4+POU5F1– and localized interiorly. In addition, some of these DDX4+ cells were developing into primordial follicles (zone 3) (Fig 4A).

Germ cells in male gonads were also quantified and, as in females, a shift towards DDX4+POU5F1– germ cells was observed between the first and second trimesters (Fig 5A, Table 2; S5 Fig). Until W22, male germ cells expressed neither H2AFX nor SYCP3 (Fig 5B).

Asynchronous meiotic entry in human ovarian germ cells

In human ovaries, H2AFX was upregulated in many germ cells at W14 (Fig 4B). However, at W17, germ cells in zone 2 (where most DDX4+ germ cells were located) showed chromatin decondensation and interestingly either predominately H2AFX or SYCP3 filament-like expression (Fig 4B, Fig 6A,Ai), suggestive of meiotic entry. By contrast, cells in the peripheral area (zone 1), where most POU5F1+ germ cells located remained negative for both meiotic markers (Fig 4B). Later, at W21.5, as zone 1 becomes thinner, more peripheral germ cells started showing chromatin decondensation and a salt-and-pepper pattern expression of H2AFX, SYCP3 or both (Fig 4B; Fig 6B,Bi,C,Ci). In primary follicles in zone 3, the oocytes expressed neither H2AFX nor SYCP3 (Fig 6D,Di). However, it is clear that many germ cells in zone 1, most

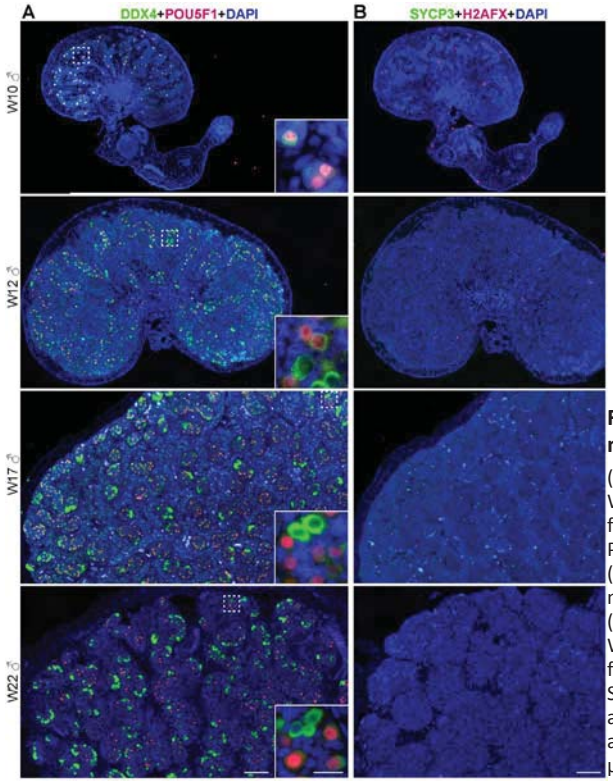

Fig 5. Dynamic expression of germ cell markers in human fetal testes.

(**A**) Histological sections of human testes at W10, W12, W17 and W22, immunostained for the early germ cell marker (nuclear) POU5F1 (in red) and late germ cell marker (cytoplasmic) DDX4 (in green). Inserts are magnifications of the dotted boxes.
(**B**) Histological sections of human ovaries at W10, W12, W17 and W22, immunostained for the meiotic markers H2AFX (in red) and SYCP3 (in green). Note the presence of autofluorescent red blood cells. Scale bars are 200 μm and in the magnified inserts 20 μm.

probably POU5F1+DDX4–/low germ cells, had not entered meiosis by W21.5. Comparing our data with that reported for spread human spermatocytes double-stained for H2AFX and SYCP3 [23], we conclude that H2AFX+SYCP3–/low germ cells were in (pre-)leptotene, germ cells containing patches of H2AFX and SYCP3 were in zygotene; SYCP3+H2AFX– germ cells were in pachytene and the SYCP3–H2AFX– oocytes in primordial follicles, as the synaptonemal complexes dissolve, have reached diplotene.

It has been reported that human germ cells show marked asynchrony regarding meiotic phases during fetal ovarian development [24] and this is in agreement with our data. However, even though we observed a maturation wave from peripheral POU5F1+ germ cells to the more inner-located primordial follicles, we have no evidence to support the idea that the different prophase meiotic phases occur in a wave-like manner in the ovary.

Association between human germ cells and neural crest derivatives

To further understand the relationship between the 'ovarian' and 'adrenal' germ cells, we studied the presence of neural crest derivatives in both adrenals and ovaries between W9 and W22. Neural crest derivatives, marked by class III beta-tubulin (TUBB3), have been described to guide human PGCs towards the gonadal primordia [2, 4] and perhaps inadvertently to other organs, including the adrenals.

Surprisingly, we observed that most POU5F1+ germ cells in the ovaries from both first and second trimester were strongly positive for TUBB3 (Fig 7A-B). However, most DDX4+ germ cells in the second trimester were TUBB3– (Fig 7B). This was interesting because it suggested that early human germ cells could have a 'neural crest' related expression signature, reminiscent of their migratory phase. We are aware that TUBB3 is not an exclusive marker for migratory neural crest cells, but is a general marker for the neural lineage [25]; and it is possible that this and many other genes are expressed in germ cells as a consequence of the global DNA

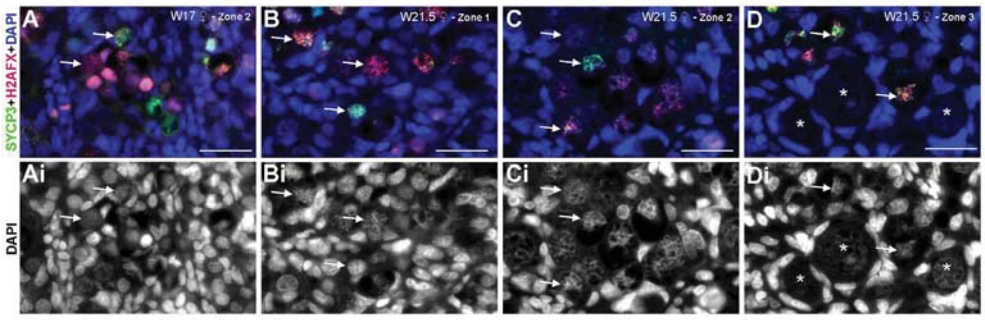

Fig 6. Meiosis in second trimester human fetal ovaries.

(**A**) High magnifications of histological sections of a human ovary at W17 immunostained for the meiotic markers H2AFX (in red) and SYCP3 (in green) showing zone 2. **Ai**, DAPI channel only. (**B**-**D**) High magnifications of histological sections of a human ovary at W21.5, immunostained for the meiotic markers H2AFX (in red) and SYCP3 (in green) showing zone 1, zone 2 and zone 3. **Bi**, **Ci**, **Di**, DAPI channel only. White arrows point to germ cells showing decondensed chromatin and various degrees of H2AFX and SYCP3 expression. Note that primordial follicles (indicated by white asterisks), characteristic of zone 3, were negative for both H2AFX and SYCP3. Scale bars are 30 μm.

demethylation that PGCs undergo during migration [17].

We investigated this further by interrogating an online available single cell transcriptomics dataset of human female germ cells from first and second trimester [17]. Using early (POU5F1, NANOG, KIT) and late markers (DAZL, DDX4, SYCP3, SYCP2, SYCP1, HORMAD2) to

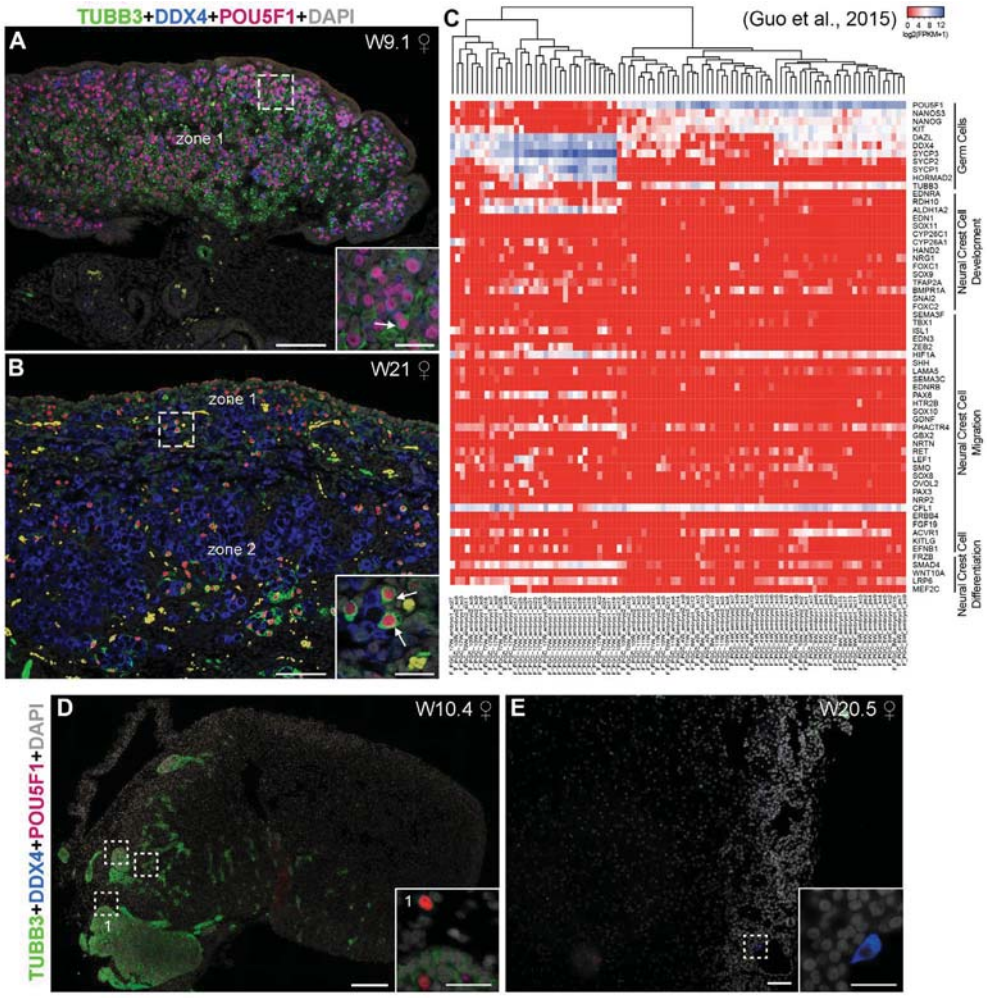

Fig 7. Expression of TUBB3 in human fetal female ovaries and adrenals.

(**A**-**B**) Histological section of human ovaries at W9.1 (**A**) and W21 (**B**) immunostained for the early germ cell marker POU5F1 (in red), late germ cell marker DDX4 (in blue), TUBB3 (in green) and DAPI (in grey). Inserts are magnifications of the dotted boxes. White arrows point to germ cells expressing POU5F1 and TUBB3. Note the presence of autofluorescent red blood cells. (**C**) Heatmap depicting the expression profile in fragments per kilobase of transcript per million (FPKM) of selected genes including early, late and meiotic germ cell markers as well as neural crest development, migration and differentiation markers early in a data set consisting of single-cell transcriptional profile of human female germ cells of first and second trimester [17]. (**D**-**E**) Histological section of human fetal female adrenals at W10.4 (**D**) and W20.5 (**E**) immunostained for the early germ cell marker POU5F1 (in red), late germ cell marker DDX4 (in blue), TUBB3 (in green) and DAPI (in grey). Inserts are magnifications of the dotted boxes. Scale bars are 100 μm in **A**,**B**,**E**; 200 μm in **D** and 20 μm in all inserts.

differentiate between early and late human female germ cells, we confirmed that the majority of early POU5F1+DDX4–/low germ cells (in zone 1) expressed TUBB3, whereas late DDX4+ germ cells (zone 2) did not. However, except for TUBB3 and perhaps ACVR1 (or ALK2), a receptor associated with germ cell development in mice [26], we did not find a clear association between early germ cells and markers of neural crest cell development, migration or differentiation (Fig 7C). Late DDX4+ germ cells were enriched for neural crest markers such as RDH10, ALDH1A2, PAX6, PHACTR4, SMAD4 and LRP6 (Fig 7C).

We were able to detect many TUBB3+ nerve bundles penetrating the first trimester adrenals (to form the adrenal medulla) and there we could also observe POU5F1+ and/or DDX4+ germ cells (Fig 7D), in agreement with others [4]. The few peripheral DDX4+ cells encountered in the second trimester expressed no (or low) levels of TUBB3 (Fig 7E), as in the ovary.

Discussion

How do the human germ cells end up in the adrenals?

We observed that 'ovarian' and 'adrenal' POU5F1+ germ cells expressed TUBB3. As these germ cells are still phenotypically immature, expression of TUBB3 is a reminiscence of the migratory phase of germ cells and a common characteristic with neural crest derivatives [2, 4]. Whether germ cells only share this characteristic with neural crest cell derivatives or effectively depend on structural support provided by neural crest derivatives to colonize the gonadal ridge (or the adrenals) remains to be elucidated. We could envisage that neural crest cells and PGCs could use (partly) common migratory routes, share common markers, or respond to similar chemo-attractant cues to colonize both the adrenal and genital primordia.

An alternative explanation to the presence of germ cells in the adrenals is the common origin of the human gonadal primordia and adrenal primordia, both initially expressing high levels of DAX1 (also known as NR0B1) and SF1 (also known as NR5A1) [6, 27, 28]. The colonization by the PGCs, at least in rats, is shown to occur before the physical separation of gonadal and adrenal primordia [29]. It is feasible that in humans this also occurs and that some germ cells reach the adrenal primordia and remain there after the two organs separate.

Do human 'adrenal' germ cells enter meiosis synchronously with 'ovarian' germ cells?

In mice, the meiotic wave (described from anterior to posterior) in females is of relatively short duration (from E11.5 to E12.5) and gametogenesis during mice embryonic development is further a rather synchronous process [30]. By contrast, the process of gametogenesis from PGCs to primordial follicle in female human germ cells is strongly asynchronous and clearly spatially regulated [3, 22]. Here, we show that in humans the time window for the start of meiosis in females is less defined than in mouse and we did not observe robust meiotic entry (by SYCP3) at least until W17 in ovaries. However, even at W21.5 in the female gonads there was still a large population of germ cells that had not entered meiosis, particularly in the periphery

of the ovary. It would be interesting to investigate the fate of these peripheral POU5F1+ germ cells at later developmental stages. They may perhaps still enter meiosis or alternatively they may have missed the time window to do so and enter apoptosis. In any case, due to the asynchrony of meiotic entry it is difficult to predict when the expression of the meiotic markers should be expected to occur in the 'adrenal' germ cells in humans and we cannot exclude the possibility that 'adrenal' germ cells enter meiosis after W22.

What happens to human 'adrenal' germ cells?

Ectopic human KIT+ and POU5F1+ germ cells have been described in the abdomen from W4 to W16 in the developing peripheral nervous system [2, 4]. Here, we show that ectopic germ cells at E15.5 in mice seem to be present in the adrenals, but also at other locations on their migratory path. In humans, although the number of adrenals analyzed was limited, 'adrenal' germ cells seemed to be able to downregulate POU5F1 and upregulate DDX4, as in the ovary, but were unable to enter meiosis at least until W21.5. The 'adrenal' POU5F1 and/or DDX4 germ cells were not apoptotic (TUNEL-positive). It remains unclear whether during further development, those germ cells remain in the adrenal or lose their germ cell identity by downregulating POU5F1 and DDX4.

Ectopic germ cells are thought to give rise to extragonadal germ cells tumors that occur in particular in midline structures [31, 32], if they fail to be eliminated by apoptosis, but develop instead malignant characteristics. Interestingly, genome-wide association studies (GWAS) have identified single-nucleotide polymorphisms (SNPs) in DDX4 as highly associated with neuroblastoma tumors [33]. Moreover, the origin of adrenal neuroblastoma tumors that occur mainly in children remains elusive, but has been associated with TUBB3-positive neural crest derivatives [34]. Because POU5F1+ germ cells both in ovaries and adrenals seem to express TUBB3 as well, it may be important to investigate the expression of additional markers to exclude a potential link between neuroblastoma and 'adrenal' germ cells.

Acknowledgements

We are grateful to the Centre for Contraception, Abortion and Sexuality (CASA) in Leiden and Den Haag for all the efforts to collect and provide the human fetal material; and Heiko Locher and Stafford Anjie both for technical advice and help with the isolation and histology of organs.

Funding

We acknowledge the China Scholarship Council (CSC) [NO.201307040026] to NH, the São Paulo research foundation (FAPESP) [BEPE 2014/26761-0] to AFdS, the Bontius Stichting [PANCREAS] to MSR, the Fundação para a Ciência e Tecnologia (FCT) [SFRH/BD/78689/2011] to MMGF and the Netherlands Organization of Scientific Research (NWO) [ASPASIA 015.007.037] and the Interuniversity Attraction Poles-Phase VII [IUAP/PAI P7/14] to SMCdSL.

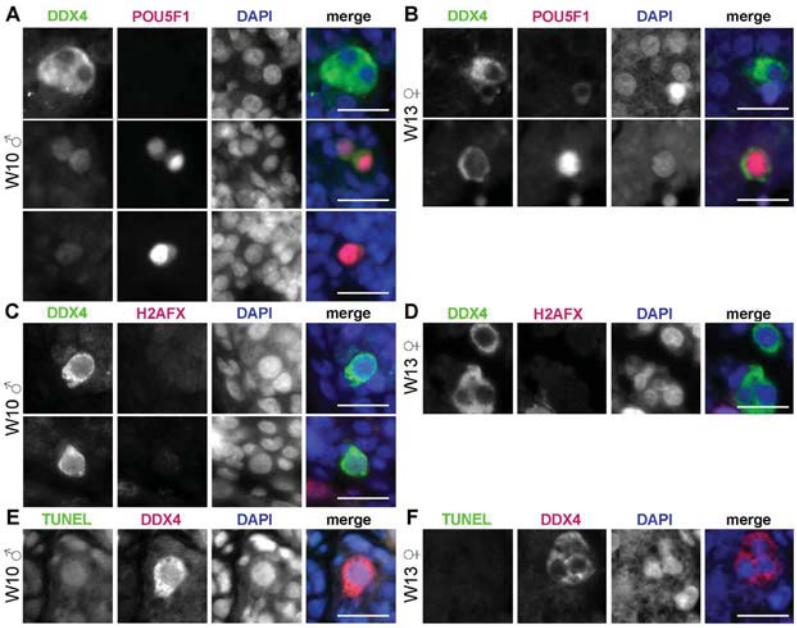

S1 Fig. Germ cells in first trimester human fetal adrenals.

High magnifications of histological sections of human W10 male and W13 female adrenals in first trimester showing (**A**,**B**) single channels for DDX4, POU5F1, DAPI and merged; (**C**,**D**) single channels for DDX4, H2AFX, DAPI and merged; (**E**,**F**) single channels for TUNEL, DDX4, DAPI and merged. Scale bars are 20 μm.

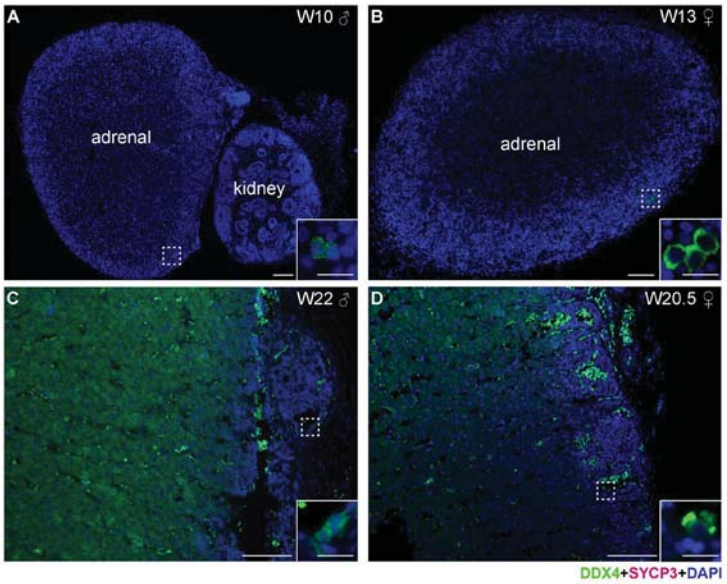

S2 Fig. No meiotic entry in germ cells in human fetal adrenals.

Histological sections of human adrenals first trimester W10 male (**A**) and W13 female (**B**) and second trimester W22 male (**C**) and W20.5 female (**D**). DDX4 (in green) germ cells do not express the meiotic marker SYCP3 (in red). Inserts are magnifications of the dotted boxes. Note the presence of autofluorescent red blood cells. Scale bar is 100 μm and in inserts 20 μm.

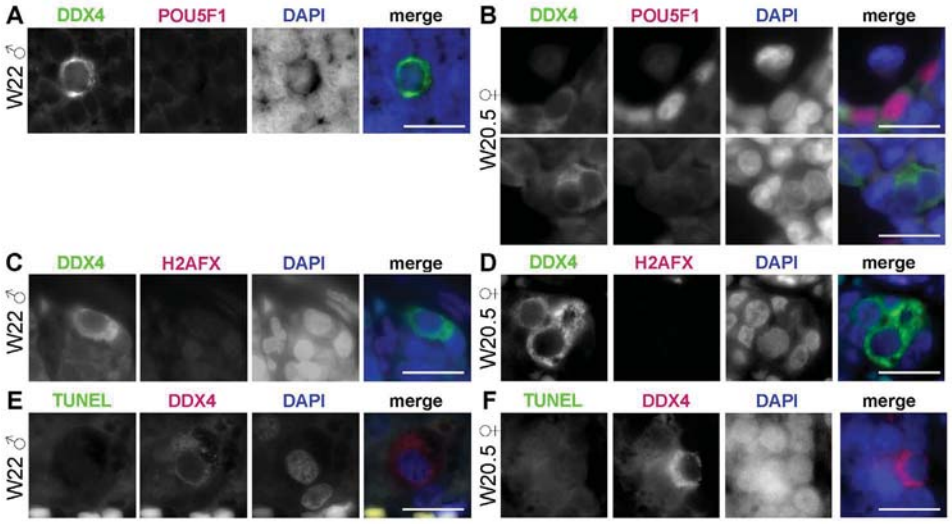

S3 Fig. Germ cells in second trimester human fetal adrenals.

High magnifications of histological sections of human W22 male and W20.5 female adrenals in second trimester showing (**A**,**B**) single channels for DDX4, POU5F1, DAPI and merged; (**C**,**D**) single channels for DDX4, H2AFX, DAPI and merged; (**E**,**F**) single channels for TUNEL, DDX4, DAPI and merged. Scale bars are 20 μm.

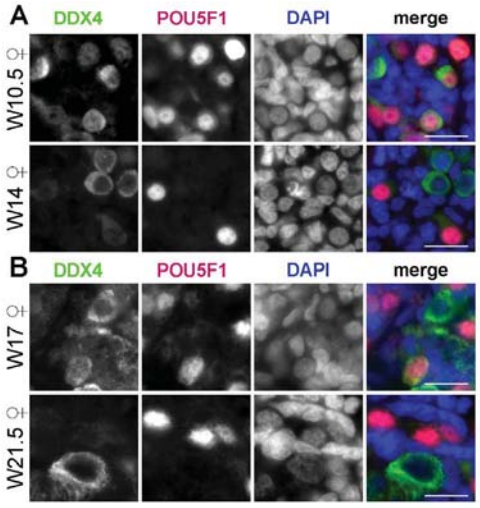

S4 Fig. Germ cells in human fetal ovaries.

High magnifications of histological sections of human W10.5 and W14 (**A**), W17 and W21.5 (**B**) female gonads showing single channels for DDX4, POU5F1, DAPI and merged. Scale bars are 20 μm.

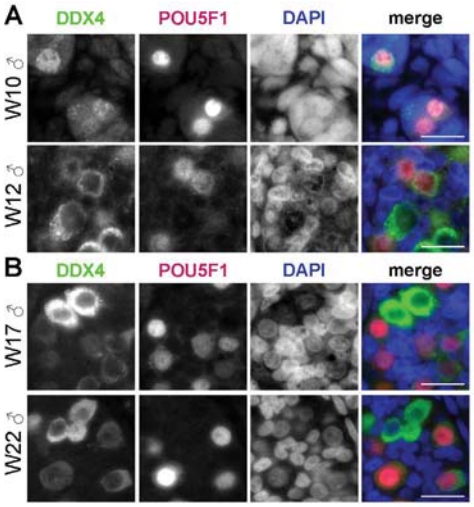

S5 Fig. Germ cells in human fetal testes.

High magnifications of histological sections of human W10 and W12 (**A**), W17 and W22 (**B**) male gonads showing single channels for DDX4, POU5F1, DAPI and merged. Scale bars are 20 μm.

References

1. Byskov AG: Differentiation of mammalian embryonic gonad. Physiol Rev 1986, 66:71-117.
2. Mollgard K, Jespersen A, Lutterodt MC, Yding Andersen C, Hoyer PE, Byskov AG: Human primordial germ cells migrate along nerve fibers and Schwann cells from the dorsal hind gut mesentery to the gonadal ridge. Mol Hum Reprod 2010, 16:621-631.
3. Heeren A, van Iperen L, Klootwijk DB, de Melo Bernardo A, Roost MS, Gomes Fernandes MM, Louwe LA, Hilders CG, Helmerhorst FM, van der Westerlaken LA, Chuva de Sousa Lopes SM: Development of the follicular basement membrane during human gametogenesis and early folliculogenesis. BMC Dev Biol 2015, 15:4.
4. Mamsen LS, Brochner CB, Byskov AG, Mollgard K: The migration and loss of human primordial germ stem cells from the hind gut epithelium towards the gonadal ridge. Int J Dev Biol 2012, 56:771-778.
5. Keegan CE, Hammer GD: Recent insights into organogenesis of the adrenal cortex. Trends Endocrinol Metab 2002, 13:200-208.
6. Morohashi K: The ontogenesis of the steroidogenic tissues. Genes Cells 1997, 2:95-106.
7. Upadhyay S, Zamboni L: Ectopic germ cells: natural model for the study of germ cell sexual differentiation. Proc Natl Acad Sci U S A 1982, 79:6584-6588.
8. Wrobel KH, Suss F: On the origin and prenatal development of the bovine adrenal gland. Anat Embryol (Berl) 1999, 199:301-318.
9. Zamboni L, Upadhyay S: Germ cell differentiation in mouse adrenal glands. J Exp Zool 1983, 228:173-193.
10. Runyan C, Gu Y, Shoemaker A, Looijenga L, Wylie C: The distribution and behavior of extragonadal primordial germ cells in Bax mutant mice suggest a novel origin for sacrococcygeal germ cell tumors. Int J Dev Biol 2008, 52:333-344.
11. Stallock J, Molyneaux K, Schaible K, Knudson CM, Wylie C: The pro-apoptotic gene Bax is required for the death of ectopic primordial germ cells during their migration in the mouse embryo. Development 2003, 130:6589-6597.
12. Bowles J, Knight D, Smith C, Wilhelm D, Richman J, Mamiya S, Yashiro K, Chawengsaksophak K, Wilson MJ, Rossant J, et al: Retinoid signaling determines germ cell fate in mice. Science 2006, 312:596-600.
13. Koubova J, Menke DB, Zhou Q, Capel B, Griswold MD, Page DC: Retinoic acid regulates sex-specific timing of meiotic initiation in mice. Proc Natl Acad Sci U S A 2006, 103:2474-2479.
14. Kumar S, Chatzi C, Brade T, Cunningham TJ, Zhao X, Duester G: Sex-specific timing of meiotic initiation is regulated by Cyp26b1 independent of retinoic acid signalling. Nat Commun 2011, 2:151-158.
15. Starz-Gaiano M, Lehmann R: Moving towards the next generation. Mech Dev 2001, 105:5-18.
16. De Melo Bernardo A, Sprenkels K, Rodrigues G, Noce T, Chuva De Sousa Lopes SM: Chicken primordial germ cells use the anterior vitelline veins to enter the embryonic circulation. Biol Open 2012, 1:1146-1152.
17. Guo F, Yan L, Guo H, Li L, Hu B, Zhao Y, Yong J, Hu Y, Wang X, Wei Y, et al: The Transcriptome and DNA Methylome Landscapes of Human Primordial Germ Cells. Cell 2015, 161:1437-1452.
18. Bullejos M, Koopman P: Germ cells enter meiosis in a rostro-caudal wave during development of the mouse ovary. Mol Reprod Dev 2004, 68:422-428.
19. Hunter N, Borner GV, Lichten M, Kleckner N: Gamma-H2AX illuminates meiosis. Nat Genet 2001, 27:236-238.
20. Ismail IH, Hendzel MJ: The gamma-H2A.X: is it just a surrogate marker of double-strand breaks or much more? Environ Mol Mutagen 2008, 49:73-82.
21. Rogakou EP, Boon C, Redon C, Bonner WM: Megabase chromatin domains involved in DNA double-strand breaks in vivo. J Cell Biol 1999, 146:905-916.
22. Anderson RA, Fulton N, Cowan G, Coutts S, Saunders PT: Conserved and divergent patterns of expression of DAZL, VASA and OCT4 in the germ cells of the human fetal ovary and testis. BMC Dev Biol 2007, 7:136.
23. Roig I, Liebe B, Egozcue J, Cabero L, Garcia M, Scherthan H: Female-specific features of recombinational double-stranded DNA repair in relation to synapsis and telomere dynamics in human oocytes. Chromosoma

2004, 113:22-33.

24. Kurilo LF: Oogenesis in antenatal development in man. Hum Genet 1981, 57:86-92.
25. Locher H, Frijns JH, Huisman MA, Chuva de Sousa Lopes SM: TUBB3: neuronal marker or melanocyte mimic? Cell Transplant 2014, 23:1471-1473.
26. de Sousa Lopes SM, Roelen BA, Monteiro RM, Emmens R, Lin HY, Li E, Lawson KA, Mummery CL: BMP signaling mediated by ALK2 in the visceral endoderm is necessary for the generation of primordial germ cells in the mouse embryo. Genes Dev 2004, 18:1838-1849.
27. Hanley NA, Ball SG, Clement-Jones M, Hagan DM, Strachan T, Lindsay S, Robson S, Ostrer H, Parker KL, Wilson DI: Expression of steroidogenic factor 1 and Wilms' tumour 1 during early human gonadal development and sex determination. Mech Dev 1999, 87:175-180.
28. Hanley NA, Rainey WE, Wilson DI, Ball SG, Parker KL: Expression profiles of SF-1, DAX1, and CYP17 in the human fetal adrenal gland: potential interactions in gene regulation. Mol Endocrinol 2001, 15:57-68.
29. Hatano O, Takakusu A, Nomura M, Morohashi K: Identical origin of adrenal cortex and gonad revealed by expression profiles of Ad4BP/SF-1. Genes Cells 1996, 1:663-671.
30. Bowles J, Koopman P: Retinoic acid, meiosis and germ cell fate in mammals. Development 2007, 134:3401-3411.
31. Looijenga LH, Van Agthoven T, Biermann K: Development of malignant germ cells - the genvironmental hypothesis. Int J Dev Biol 2013, 57:241-253.
32. Schneider DT, Schuster AE, Fritsch MK, Hu J, Olson T, Lauer S, Gobel U, Perlman EJ: Multipoint imprinting analysis indicates a common precursor cell for gonadal and nongonadal pediatric germ cell tumors. Cancer Res 2001, 61:7268-7276.
33. Nguyen le B, Diskin SJ, Capasso M, Wang K, Diamond MA, Glessner J, Kim C, Attiyeh EF, Mosse YP, Cole K, et al: Phenotype restricted genome-wide association study using a gene-centric approach identifies three low-risk neuroblastoma susceptibility Loci. PLoS Genet 2011, 7:e1002026.
34. De Preter K, Vandesompele J, Heimann P, Yigit N, Beckman S, Schramm A, Eggert A, Stallings RL, Benoit Y, Renard M, et al: Human fetal neuroblast and neuroblastoma transcriptome analysis confirms neuroblast origin and highlights neuroblastoma candidate genes. Genome Biol 2006, 7:R84.

Table 1. Quantification of germ cells in human adrenals

ID	sex	age (weeks.days)	sections (n)	POU5F1+DDX4-/low nr germ cells	%	POU5F1+DDX4+ nr germ cells	%	DDX4+ nr germ cells	%	total nr germ cells
AQ1	female	W8.6	10	56	74.7	18	24.0	1	1.3	75
AY1	female	W9.6	10	23	46.0	8	16.0	19	38.0	50
DR3	female	W13	9	1	2.6	12	31.6	25	65.8	38
DD2	female	W16	84	0	0.0	0	0.0	2	100.0	2
BQ1	female	W17.4	49	0	0.0	0	0.0	2	100.0	2
CC2	female	W18	73	0	0.0	0	0.0	14	100.0	14
BM2	female	W20	146	1	6.7	0	0.0	14	93.3	15
CD1	female	W20.5	69	0	0.0	10	13.0	67	87.0	77
AV1	male	W8.4	10	6	15.8	32	84.2	0	0.0	38
BG2	male	W10	10	22	23.7	51	54.8	20	21.5	93
AT1	male	W12	8	1	10.0	4	40.0	5	50.0	10
AZ1	male	W15.4	35	0	0.0	0	0.0	0	0.0	0
CV2	male	W16.5	91	0	0.0	0	0.0	6	100.0	6
CQ1	male	W17	129	0	0.0	1	25.0	3	75.0	4
CX1	male	W18	110	0	0.0	0	0.0	2	100.0	2
CR1	male	W22	121	0	0.0	0	0.0	236	100.0	236

Table 2. Quantification of germ cells in human gonads

ID	sex	age (weeks.days)	sections (n)	POU5F1+ DDX4-/low nr germ cells	%	POU5F1+ DDX4+ nr germ cells	%	DDX4+ nr germ cells	%	total nr germ cells
BA2	female	W10.5	2	459	94.3	14	2.9	14	2.9	487
CE1	female	W14	6	421	14.6	5	0.2	2456	85.2	2882
DK2	female	W16.3	9	3841	61.5	0	0.0	2409	38.5	6250
BE1	female	W17	7	2683	45.6	0	0.0	3203	54.4	5886
AL3	female	W20	4	238	53.6	0	0.0	206	46.4	444
DW3	female	W21.5	8	1004	19.2	0	0.0	4234	80.8	5238
BG2	male	W10	3	266	69.1	116	30.1	3	0.8	385
AT1	male	W12	7	1827	65.1	880	31.3	101	3.6	2808
AE2	male	W14.2	8	1608	56.2	66	2.3	1187	41.5	2861
CQ1	male	W17	10	5551	83.1	62	0.9	1068	16.0	6681
CT1	male	W20	10	2690	36.4	0	0.0	4710	63.6	7400
BW1	male	W22	4	720	41.1	0	0.0	1032	58.9	1752

Table S1. Number and sex of human organs anlysed.

Embryo ID	Sex	Age (weeks of gestation)	Adrenal	Gonad
AV1	male	W8.4	x	
AH1	male	W9.3	x	
BG2	male	W10	x	x
AC1	male	W11	x	
AT1	male	W12	x	x
V1	male	W12	x	
AE2	male	W14.2		x
AZ1	male	W15.4	x	
CV2	male	W16.5	x	
CQ1	male	W17	x	x
CX1	male	W18	x	
CT1	male	W20		x
BW1	male	W22		x
CR1	male	W22	x	
AQ1	female	W8.6	x	
AG1	female	W9.1	x	
AY1	female	W9.6	x	
AI3	female	W10.4	x	
BA2	female	W10.5	x	x
AQ2	female	W11.4	x	
DR3	female	W13	x	
CE1	female	W14		x
DD2	female	W16	x	
DK2	female	W16.3		x
BE1	female	W17		x
BQ1	female	W17.4	x	x
CC2	female	W18	x	
DJ2	female	W18		x
AL3	female	W20		x
CD1	female	W20.5	x	
BM2	female	W21	x	
DW3	female	W21.5		x
Total			23	14

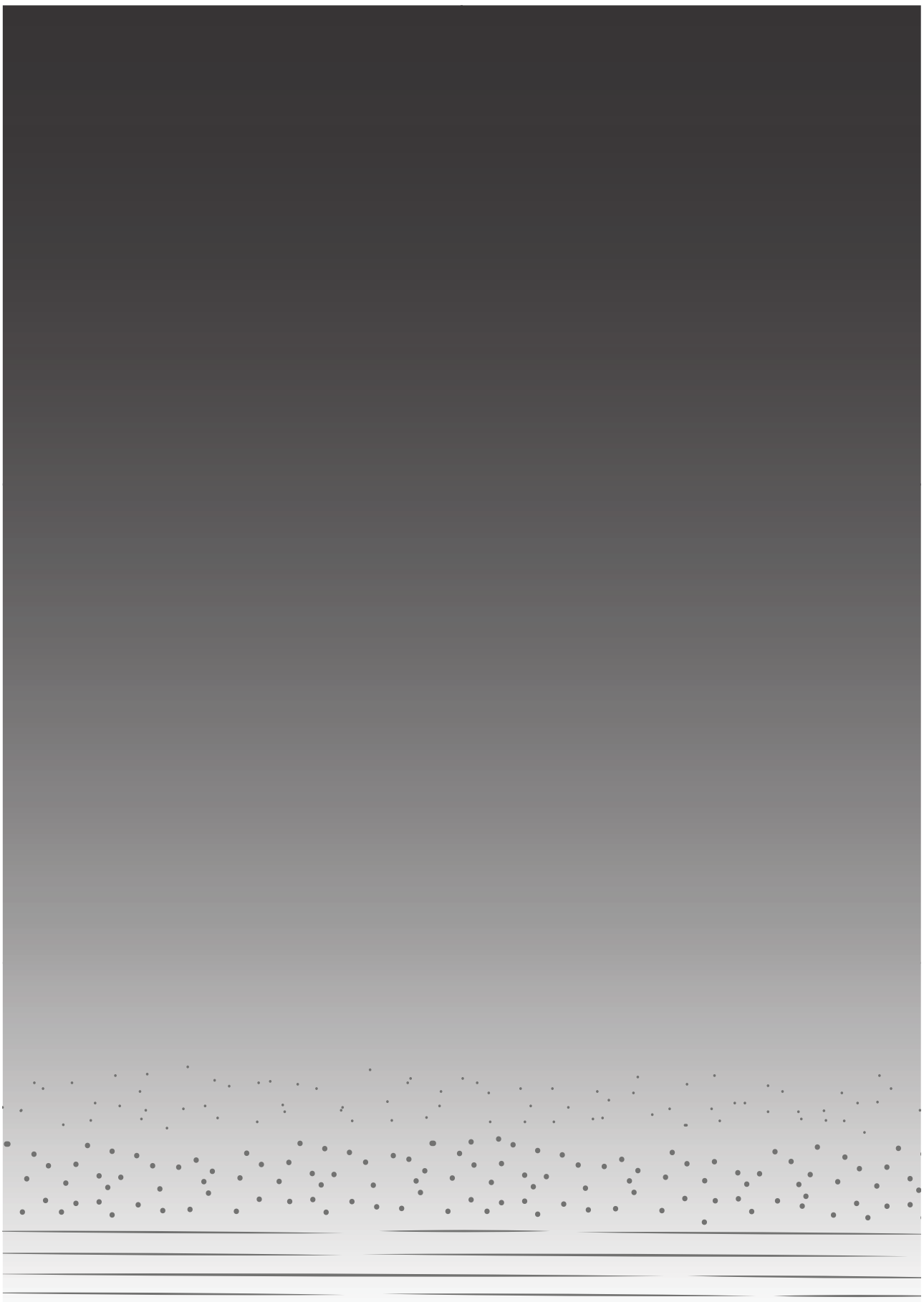

CHAPTER 3

Transcriptomic data analysis indicates X chromosome inactivation in human pre-implantation embryos

Nannan He[1], Ioannis Moustakas[2], Jelle J. Goeman[3,4], David van Bruggen[1,#], Szymon M. Kielbasa[3], Lucette A. J. van der Westerlaken[5], Hailiang Mei[2], Susana M. Chuva de Sousa Lopes[1,6]

[1]Department of Anatomy and Embryology, Leiden University Medical Center, Leiden, The Netherlands

[2]Sequence Analysis Support Core, Leiden University Medical Center, Leiden, The Netherlands

[3]Department of Medical Statistics and Bioinformatics, Leiden University Medical Center, Leiden, The Netherlands

[4]Department for Health Evidence, Radboud University Medical Center, Nijmegen, The Netherlands

[5]Department of Gynaecology, Division of Reproductive Medicine, Leiden University Medical Center, Leiden, The Netherlands

[6]Department for Reproductive Medicine, Ghent University Hospital, Ghent, Belgium

[#]Current address: Laboratory of Molecular Neurobiology, Department of Medical Biochemistry and Biophysics, Karolinska Institute, Stockholm, Sweden

Manuscript ready for submission.

Abstract

Previously, X chromosome dosage compensation in the human pre-implantation embryos (E3-E7) was thought to be accomplished by reducing the expression of both X chromosomes, without X chromosome inactivation (XCI). Here, we investigated the status of XCI in human pre-implantation embryos at single cell level, by analyzing online available RNA-seq data of human E3-E7 pre-implantation embryos. We separated X-linked genes into genes subject to X inactivation ("X-sub") and escapees ("X-esc"). Smaller proportion of biallelic expression in X-sub than in autosomal genes indicates one chromosome X is inactive in E4-E6 cells and E7 TE cells, whereas there is reactivation in E7 EPI and PE cells. Moreover, combined human androgen receptor gene (*AR*)/retinitis pigmentosa 2 (*RP2*)-based DNA methylation sensitive assay suggests non-imprinted X inactivation in human TE-derived cells, in contrast to mice.

Introduction

The mechanism to achieve dosage compensation of X-linked genes between mammalian females and males is X chromosome inactivation (XCI), in which one of the two X chromosomes in female somatic cells is silenced [1, 2]. XCI is triggered by the spread of *XIST* RNA along the whole X chromosome [3], while there is no *XIST* transcription on the active X chromosome (Xa). Epigenetic markers of the inactive X chromosome (Xi) include trimethylation of histone H3 at lysine 27 (H3K27me3) [4], hypoacetylation of histone H4 [5, 6] and DNA methylation at CpG-rich promoters [7, 8]. In female somatic cells, most X-linked genes are subject to X inactivation ("X-sub") and have monoallelic expression of either allele, whereas a fraction of genes escape X inactivation (known as escapees, "X-esc") and have expression of both alleles. The percentage of escapees along human chromosome (Chr)X is around 15%, higher than the percentage in mice (about 3%) [9, 10]. Many of the escapees are located in the pseudoautosomal regions [11], where genes are present on both X and Y chromosomes. Moreover, some escapee genes are revealed to be tissue-specific (variable escapees) [12].

X inactivation has been investigated by several methods including *XIST* gene expression [13], H3K27 trimethylation [14], allele-specific expression (ASE) analysis [15], human androgen receptor assay (HUMARA) [16] and retinitis pigmentosa 2 (*RP2*)-based assay [17]. In ASE analysis, the informative single-nucleotide polymorphisms (SNPs) are able to assign parental origin of the expressed alleles, based on embryonic RNA sequence, embryonic and parental genome sequence [18]. However, in the absence of parental genome sequence, alleles for a SNP site can only be assigned to reference allele or alternative allele based on reference genome. Healthy individuals carry highly polymorphic microsatellite CAG repeat sequence in the first exon of human X-linked androgen receptor gene (*AR*) and polymorphic microsatellite GAAA repeat sequence in the promoter region of X-linked *RP2* gene. The allele specific methylation of a 5'CpG island on *AR* locus and a CpG island in promoter of *RP2* is reported to be associated with XCI [16, 17].

In mice, the dynamic X inactivation status during early development has been more extensively studied than in humans [19-21]. In mouse pre-implantation embryos, two separate waves of XCI have been revealed [19, 20, 22]. The first XCI wave occurs at the two- to four-cell stage, leading to the imprinted paternal X chromosome (Xp) inactivation in all blastomeres of the embryo [18]. The Xp remains inactivated in the trophectoderm (TE) and primitive endoderm (PE) during the development, whereas it becomes reactivated in the epiblast (EPI) at embryonic day (E)3.5. Shortly afterwards, either the Xp or the maternal X-chromosome (Xm) gets inactivated during the second XCI wave, resulting in random XCI in the EPI [23]. This is followed by reactivation of the silent X in mouse female primordial germ cells (PGCs) between E8.5 and E12.5, but not in the female somatic cells [14].

In humans, the inactivated X chromosome in PGCs becomes reactivated in 4 week embryos [15], having biallelic expression of X-genes. On the contrary, fetal somatic cells maintain

random inactivation and show monoallelic expression of X-genes. During pre-implantation development at E3-E7, X-genes in cells of pre-lineage and all lineages are thought to maintain biallelic expression [13, 24].

A recent study reveals that lineage segregation of EPI, PE and TE occurs at E5 in humans, using single-cell RNA-seq of E3-E7 embryos [25]. Before segregation, E3, E4 and immature E5 cells are referred to as "pre-lineage" cells. Several genes are identified to be enriched in EPI (*PRDM14*, *GDF3*, *TDGF1*, *NODAL*, *SOX2*, *NANOG*), PE (*COL4A1*, *HNF1B*, *PDGFRA*, *GATA4*, *FN1*) and TE (*GATA2*, *GATA3*) lineages. The algorithm "KeyGenes" (http://www.keygenes.nl) [26] recently developed, as a tool to determine classifier genes for provided samples groups (training set), is able to identify genes either highly expressed or lowly expressed for pre-lineage cells and cells of three lineages. In addition, KeyGenes predicts the identities of queried samples (test set) based on identity scores of test set to training set.

Based on Ohno's hypothesis, X-genes are upregulated twofold in order to achieve the gene dose balance between ChrX and autosomes [27]. The ratio of median expression level of X-linked genes to that of autosomal genes (X:A median expression ratio) [28-30] has been used to investigate X chromosome dosage compensation in female somatic cells and PGCs, with results supporting [28, 29] or rejecting [30] Ohno's hypothesis. Additionally, the ratio of total expression level of X-linked genes to that of autosomal genes (X:A total expression ratio) [15] is another approach to investigate X chromosome dosage compensation.

In this study, we investigated whether there was X inactivation in human pre-implantation embryos and whether the inactivation was imprinted or random, by systematic analysis of online available single-cell RNA-seq data and combined *AR/RP2*-based assay on human TE-derived cells. Our results indicate X inactivation in E4-E6 cells and E7 TE cells. Moreover, the X inactivation in human TE-derived cells is random, in contrast to mice.

Methods

Data acquisition

From online available single-cell RNA-seq data of human E3-E7 pre-implantation cells (n=1519 cells from 87 embryos, karyotype 46,XX or 46,XY), FASTQ files of individual sequencing batches were accessed from the ArrayExpress database: E-MTAB-3929 [25], as well as the expression data in counts and Reads Per Kilobase Per Million (RPKM) files of all cells (n=1519). Previously published single-cell RNA-seq datasets of human gonadal cells of first and second trimesters (n=328 cells including somatic cells and PGCs) were obtained from the Gene Expression Omnibus (GEO) database (GEO: GSE63818) [15].

Expression levels and cells reassignment by KeyGenes

Transcriptomic data in RPKM were primarily analyzed in R (version 3.2.5) (https://cran.r-project.org/bin/windows/base/old/3.2.5/). Markers for pre-lineage, EPI, PE and TE, as well as epigenetic and pluripotency markers were used for multi-dimensional scaling (MDS) plot

exhibiting log2(RPKM+1), using R package "stats". KeyGenes algorithm [26] was used to identify classifier genes for each cell type between E3-E7 and to confirm cell identities by generating their identity scores to cells representative of four cell types (as training set in KeyGenes). Cells were reassigned when prediction score was above 0.8 to the other cell types. Reassignments were used in further analysis. The heatmap showing log2(RPKM+1) was generated with R package "gplots" [31] with the same gene set as for MDS.

Variant calling and annotation

All RNA-seq datasets were processed using the Gentrap pipeline developed at Leiden University Medical Center (http://biopet-docs.readthedocs.io/en/latest/pipelines/gentrap/). Gentrap pipeline consisted of FASTQ preprocessing (including quality control, quality trimming and adapter clipping), RNA-seq reads alignment to human reference genome, feature quantification at read or base level and variant calling. More specifically, FASTQ preprocessing was done using sickle (version 1.33) [32] ("sickle se -t sanger"). The RNA-seq reads were aligned to human reference genome GRCh38 [33] using GSNAP (version 2014-12-23) [34] (http://research-pub.gene.com/gmap/) ("gsnap --format sam --nthreads 8 --db GCA_000001405.15_GRCh38_no_alt_analysis_set --novelsplicing 1 --batch 4"). The sam to bam conversion, bam sorting and creation of mpileup files were performed using SAMtools (version 1.1) [35]. Varscan (version 2.3.7) [36] was then used on the mpileup output to call SNPs, with the following settings: min-coverage=8, min-reads2=2, min-avg-qual=15, min-var-freq=0.01, min-freq-for-hom=0.75. The final outputs of the Gentrap pipeline were multi-sample VCF files. In our study, genotypes in RNA-seq data were called on sites where common variants occur. R package "VariantAnnotation" [37] was used to acquire genotype (0=reference allele, 1=alternative allele), alternative allele and reference allele read counts from VCF files. The variants were annotated using the SeattleSeq Annotation [38], with GRCh38 as the source genome (http://snp.gs.washington.edu/SeattleSeqAnnotation144/).

Median expression and total expression of ChrX and autosomes

For each pre-implantation cell, median and total expression of autosomal genes, X-sub and X-esc genes was calculated by the median expression of all transcribed genes (RPKM>0) and by the sum of all the transcribed genes (in RPKM).

X:A median (and total) expression ratios between female and male cells of the same cell type at the same embryonic day were compared, using R packages "gdata" [39] and "lme4" [40]. Female-to-male median (and total) expression ratio was calculated by median value of female/male X:A median (and total) expression ratios.

Proportion of biallelic expression in X-linked and autosomal genes

Female pre-implantation cells and fetal cells were included for biallelic expression analysis. Genotypes were called at common SNP sites located in gene coding regions with high frequency in the general population. All SNP sites with minor allele frequency (MAF)≥5% in

the 1000 Genomes Project (https://www.ncbi.nlm.nih.gov/variation/docs/human_variation_vcf/#common_all) were selected. Then cells with genotype calls (including reference calls) at minimum 2000 SNP sites were included for further analysis. For these cells, biallelic expression proportion in each cell type at each embryonic day was shown in boxplots, using relevant R packages ("VariantAnnotation", "ggplot2" [41] and "plyr" [42]). Biallelic expression proportion between X-linked genes (X-sub and X-esc, separately) and autosomal genes was compared using the statistical approach of "Generalized linear mixed model fit by maximum likelihood (Laplace Approximation) [glmerMod])", using R packages "gdata" [39] and "lme4" [40].

Allele-specific expression analysis

X-SNP sites with expression of both reference and alternative alleles in individual embryos, were considered to be heterozygous in embryonic DNA and therefore were selected for ASE analysis. For these SNPs, read counts of reference and alternative alleles in each cell of individual embryos were plotted using R packages "VariantAnnotation", "ggplot2", "reshape2" [43], "plyr", "stringr" [44], "gridExtra" [45] and "dplyr" [46].

TE-derived cells collection from human blastocyst outgrowths

This work was approved by the Ghent University Hospital Ethical Committee (PROJECT #2009/281) and the Belgian Federal Ethical Committee on Embryo Research (PROJECT #ADV022). All embryos were obtained with written informed consent signed by the donor couples undergoing in vitro fertilization (IVF) at the Center for Reproductive Medicine of Ghent University. Day 3 cryopreserved embryos were thawed and cultured to E7 blastocyst stage at 37°C, 6% CO_2 and 5% O_2. After extra 6 days culture, TE-derived cells were isolated from the blastocyst outgrowths, half used for sex determination and the other half for DNA methylation assay.

Genomic DNA was extracted from the TE-derived cells. For this, we digested each sample by adding 80µl proteinase K buffer, 260µl of RNase free H_2O, 20µl of 10% SDS and 10µl of proteinase K (10 mg/µl) (Promega, catalog #V3021, Madison, WI, USA). Then the mixture was incubated on a thermal mixer at 55°C , 750 revolutions per minute (RPM) overnight. After enzyme inactivation (95°C, 10 minutes), we added 120µl 5M ice cold NaCl to the sample. The tube was repeatedly inverted to mix and then centrifuged at 0°C for 5 minutes at 13000 RPM. After centrifugation, 400µl of the supernatant was transferred to a clean tube, and 1ml of ice cold 95% ethanol was added. After incubation at -20°C for one hour, each sample was centrifuged at 0°C for 5 minutes at 13000 RPM and the supernatant was discarded. 1ml of ice cold 70% ethanol was added and each sample was centrifuged once more at 0°C for 5 minutes at 13000 RPM, after which the supernatant was discarded. Polymerase chain reaction (PCR) for AMELX/Y was performed to detect embryos gender as reported [47].

Human combined *AR* and *RP2*-based methylation assay

DNA digestion with CpG methylation sensitive restriction enzyme *Hpa*II (R0171S,

New England Biolabs, Ipswich, MA, USA) was carried out at 37°C overnight, followed by incubation at 65°C for 20 minutes to inactive the enzyme. Afterwards, fluorescent tagged primers for gene *AR* (FAM-5'-TCCAGAATCTGTTCCAGAGCGTGC-3' and anti-sense primer 5'-GCTGTGAAGGTTGCTGTTCCTCAT-3') and for gene *RP2* (FW-5'-TGACATAGCGAGACCCTGTG-3', RV-5'- TGGTGGGTTCTCTAGCTGGT-3') were used for DNA amplification, with a PCR cycle of 95°C for 3 minutes, 35 times 95°C for 45 seconds, 60°C for 30 seconds, 72°C for 30 seconds and a final extension step at 72°C for 10 minutes.

Fragment analysis was performed at the Leiden Genome Technology Centre (LGTC; http://www.lgtc.nl) using a 96-capillary ABI PRISM® 3730xl DNA analyzer (Applied Biosystems, Carlsbad, CA, USA). *AR* and *RP2* alleles were distinguished and quantified through capillary electrophoresis by exploiting the variable glutamine repeat present on the amplified region of the *AR* locus [16, 48], using Peak Scanner Software v2.0 (Applied Biosystems, Carlsbad, CA, USA).

Percentage of Xp methylation for the amplified *AR* and *RP2* region was calculated [49], meaning that 50% indicated a 1:1 ratio in which each parental allele was equally methylated. Exclusive inactivation of the maternal or paternal allele meant 0% or 100% of Xp methylation respectively. Skewed maternal or paternal XCI was considered present when the percentage of paternal methylation was ≤25% or ≥75% respectively.

Results

Cell identities in human pre-implantation embryos

We analyzed existing high-quality single-cell transcriptome dataset of 1519 cells from 87 human pre-implantation embryos (N=44, female; N=43, male) at E3 (n=81, N=13), E4 (n=190, N=16), E5 (n=367, N=23), E6 (n=415, N=18) and E7 (n=466, N=17) [25].

Based on expression profile in RPKM of all the 1519 E3-E7 cells, MDS with a set of carefully selected 126 genes (S1 Table) separated pre-lineage cells at E3-E5 from cells of three lineages (EPI, PE and TE) at E5-E7 in the first dimension (Dim1) (Fig 1A, S1A Fig). This gene set (S1 Table) included reported pre-lineage markers, markers for three lineages [25, 50] as well as known epigenetic and pluripotency markers. Along the second dimension (Dim2), TE cells were separated from inner cell mass (ICM; EPI+PE) cells at E5-E7 (S1A Fig). MDS on E7 cells separated TE cells from ICM cells in Dim1 and separated EPI from PE cells in Dim2 (S1A Fig).

With KeyGenes algorism, we first determined the identifier genes for pre-lineage and three lineages, and then confirmed identities of cells and also reassigned the mislabeled cells. Since lineage segregation was already complete at E7, we chose 26 E7 representative cells for EPI (n=9), PE (n=8) and TE (n=9) as training set 1 (cells marked by black circles in S1A Fig). The classifier genes were *INPP5D*, *NANOG*, *PRDM14*, *PSORS1C2* for E7 EPI lineage, *COL4A1*, *FN1*, *HNF1B*, *LGALS2* for E7 PE lineage and *GPRC5B*, *IL6R* for E7 TE lineage (S1A Fig). Identities of E6 (n=415) and E7 (n=466) cells, as test set 1, were predicted by KeyGenes based on training set 1. With prediction score above 0.8 as the cutoff, 10 E6 cells and 4 E7 cells were found to be mislabeled and subsequently reassigned by KeyGenes (S2 Table). Next, to determine

identifiers for pre-lineage and to predict identities of E5 cells, we combined training set 1 (n=26) with E4 cells (n=10) clustered closer to E5 cells in MDS as training set 2 (n=36, cells marked by black circles in S1B Fig). The identified classifier genes were *ETNPPL*, *HINT1*, *TPM4*, *VOM1* for E4 pre-lineage, *GDF3*, *NANOG*, *NODAL*, *VENTX* for E7 EPI lineage, *COL4A1*, *CTSE*, *HNF1B*, *LGALS2*, *RSPO3* for E7 PE lineage and *ALPL*, *CFLAR*, *GPR160*, *KLF4*, *POU5F1* for E7 TE lineage (S1B Fig). Identities of E5 cells (n=367), as test set 2, were predicted by KeyGenes based on training set 2. A total of 48 E5 cells were reassigned with prediction score>0.8 (S2 Table). With reassigned identities, cell components of all 87 embryos were shown in Fig 1B.

Compared to the original cell identities (S1B Fig), MDS on reassigned cells (Fig 1C, S2 Table) provided more clear segregation of pre-lineage cells and cells of three lineages in Dim1. Based on expression of the 126 genes of interest, heatmap on reassigned cells gave sub-clusters of E3 pre-lineage, E4 pre-lineage, E5 pre-lineage, E4-E5 pre-lineage, PE, EPI and TE lineages (S2 Fig).

X:Autosome expression ratio during human pre-implantation development

To study dosage compensation in females and males between E3-E7, we used both approaches (X:A median expression ratio and X:A total expression ratio) to compare X-linked genes and autosomal genes expression. Since escapees have biallelic expression and may potentially increase gene dose of X-genes in females, we separated X-linked genes into two categories: X-esc (92 genes, S3 Table) [11, 51-54] and X-sub.

First, for each of the 1519 cells between E3-E7, we calculated median expression of all genes with RPKM>0 for all 22 pairs of autosomes (~22280 genes), X-sub (~840 genes) and X-esc (~60 genes) (S3 Fig). Between E3-E7, X-sub:A median expression ratios ranged from 0.39 to 1.39 in females (median=0.86) and from 0.31 to 1.17 in male cells (median=0.71) (Fig 1D, left panel; S4 Table), while X-esc:A median expression ratios ranged from 0.46 to 6.21 in female cells (median=1.99) and from 0.50 to 3.01 in males (median=1.50) (Fig 1D, right panel; S4 Table). X-sub:A median expression ratios and X-esc:A median expression ratios in female and male cells of each type at each embryonic day were shown in S4 Table.

We compared the X:A median expression ratios between females and males of the same cell type at the same embryonic day. In most cases, female cells at E3-E7 showed significantly higher X-sub:A median expression ratios and X-esc:A median expression ratios than male cells (Fig 1D, S4 Table). While female cells of E7 EPI and E7 PE had comparable X-sub:A median expression ratios to male cells of EPI and PE at E7 (Fig 1D, S4 Table), we observed comparable X-esc:A median expression ratios between female and male cells of E5 PE, E5 TE, E6 EPI and E6 PE lineages (Fig 1D, S4 Table). To further study female-to-male X chromosome dosage, we calculated relative X-sub:A median expression ratio between females and males (Fig 1E). Female-to-male X-sub:A median expression ratios ranged from 1.09 (in E7 TE) to 1.42 (in E6 PE) (Fig 1E, S4 Table), being higher than 1 between E3-E7. Female-to-male X-esc:A median expression ratios ranged from 1.19 (in E6 PE) to 1.60 (in E7 PE) (Fig 1E, S4 Table), being higher than 1

between E3-E7.

Next, we summed the RPKM values of transcribed (RPKM>0) autosomal genes, X-sub and X-esc genes for each cell (S4A Fig). The X-sub:A total expression ratios ranged from 1.20% to 4.93% in female cells (median=2.77%) and from 0.77% to 2.84% in male cells (median=1.69%) (S4B Fig, left panel; S4 Table), whereas the X-esc:A total expression ratios ranged from 0.33% to 1.54% in female cells (median=0.77%) and from 0.17% to 1.08% in male cells (median=0.50%) (S4B Fig, right panel; S4 Table). Using the same statistic method as above, we compared females and males of the same cell type at the same day. We observed significantly higher X:A total expression ratios in females than males in all cases at E3-E7 (S4B Fig). Female-to-male X-sub:A total expression ratios ranged from 1.26 (in E7 TE) to 2.00 (in E5 pre-lineage) (S4C Fig, S4 Table), being higher than 1 between E3-E7. Female-to-male X-esc:A total expression ratios

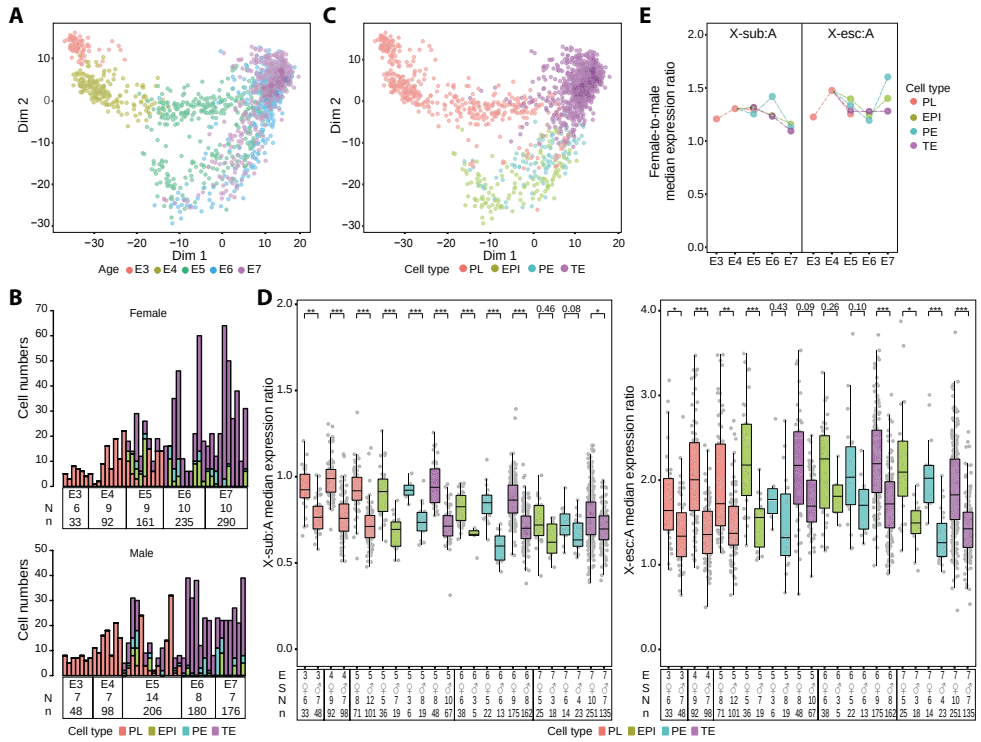

Fig 1. X:Autosome median expression ratios in human E3-E7 cells.

(**A**) Multidimensional scaling plot showing individual cells at E3-E7, color-coded by embryonic day, using 126 selected genes of interest including pre-lineage, epiblast, primitive endoderm, trophectoderm markers as well as epigenetic and pluripotency markers. (**B**) Histograms showing cell components in human female and male E3-E7 embryos, with reassigned cell identities by KeyGenes. (**C**) Multidimensional scaling plots showing individual cells with reassigned identities, color-coded by cell type using the same selected genes of interest as Fig 1A. (**D**) Boxplots showing X-sub:A median expression ratios (left panel) and X-esc:A median expression ratios (right panel) for individual cells of each type at each embryonic day. Outliers are not indicated. *P* values between females and males are indicated by * ($P<0.05$), ** ($P<0.01$) and *** ($P<0.001$). (**E**) Dot plots representing female-to-male X-sub:A median expression ratio and female-to-male X-esc:A median expression ratio in each cell type at each embryonic day. N: number of embryos; n: number of cells; E: embryonic day; S: sex; PL: pre-lineage.

ranged from 1.28 (in E3 pre-lineage) to 1.88 (in E7 EPI) (S4C Fig, S4 Table), being higher than 1 between E3-E7.

Smaller proportion of biallelic expression in X-sub than in autosomal genes at E4-E7

To investigate XCI in female pre-implantation embryos, especially the embryos with different cell types, we excluded embryos with less than 5 cells and/or with only TE cells, resulting in 692 cells from female embryos (N=30) at E3 (n=26, N=4), E4 (n=84, N=6), E5 (n=139, N=7), E6 (n=196, N=6) and E7 (n=247, N=7) (S5 Table). Moreover, from another publicly available single-cell RNA-seq dataset [15], we included female fetal PGCs (n=10, N=2) and fetal somatic cells (n=38, N=5) as XaXa controls (with biallelic expression of X-sub genes) and XaXi controls (with monoallelic expression of X-sub genes) respectively.

According to 1000 Genomes Project, each SNP of X-linked genes and autosomal genes has its own MAF in human population. In order to achieve similar possibilities of being heterozygous for SNPs on X-linked genes and autosomal genes, SNPs located in gene coding regions with MAF≥5% in global human population were included in the analysis, 2502 SNPs on ChrX and 11395 SNPs on autosomes.

Single cells with less than 2000 SNPs were excluded from further analysis. Cells included were 10 fetal PGCs (N=2) and 34 fetal somatic cells (N=5) and 513 pre-implantation cells [E3 (n=18, N=4), E4 (n=64, N=6), E5 (n=87, N=7), E6 (n=136, N=6), E7 (n=208, N=7)] (S5 Table).

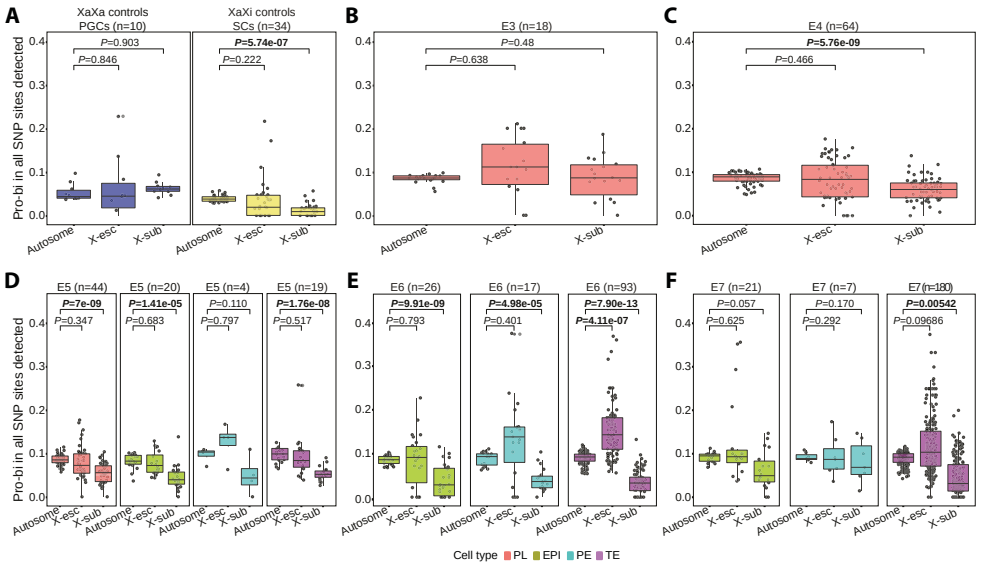

Fig 2. Proportion of biallelic expression in autosomal genes, X-esc and X-sub genes in human fetal cells and pre-implantation cells.

(**A**-**F**) Boxplots showing the proportion of biallelic expression in expressed SNPs with MAF≥5% in autosomal genes, X-esc and X-sub genes, in (**A**) primordial germ cells (PGCs), fetal somatic cells (SCs) and (**B**-**F**) pre-implantation cells at E3-E7. *P* values between autosomal genes and X-linked genes (X-esc and X-sub, separately) are indicated. PL: pre-lineage.

For each cell, we calculated the proportion of biallelic expression ("Pro-bi") in all the SNP sites detected in autosomal genes and X-linked genes (X-sub and X-esc, separately) (Fig 2). Then we compared the Pro-bi between autosomal genes and X-linked genes (X-sub and X-esc, separately) in fetal PGCs, fetal somatic cells and pre-implantation cells of each cell type at each embryonic day (Fig 2).

In fetal PGCs (XaXa controls) and somatic cells (XaXi controls), Pro-bi between X-esc and autosomal genes were comparable (Fig 2A). Nevertheless, when Pro-bi between X-sub and autosomal genes were comparable in fetal PGCs, Pro-bi in X-sub was significantly lower than in autosomal genes in fetal somatic cells (*P* values shown in Fig 2A). Results suggest that our method of comparing the Pro-bi between X-sub genes and autosomal genes is reliable to investigate XCI in female cells. Pro-bi between X-esc and autosomal genes were comparable in most cell categories at E3-E7 (Fig 2A-F) except in E6 TE (n=93) (Fig 2E). In E3 cells, no significant difference was detected in Pro-bi between X-sub and autosomal genes (Fig 2B). In contrast, E4 cells had significantly lower Pro-bi in X-sub than in autosomal genes (Fig 2C). This indicates X inactivation wave occurring between E3-E4 in human embryos. At E5, Pro-bi was significantly lower in X-sub than in autosomal genes in pre-lineage (n=44), EPI (n=20) and TE cells (n=19) (Fig 2D), suggesting X inactivation in these cell types at E5. Pro-bi in X-sub was found to be comparable to that in autosomal genes in E5 PE cells (n=4) (Fig 2D), where statistical comparison might not be powerful enough to get conclusion on E5 PE cells. In all three lineages at E6 (EPI, n=26; PE, n=17; TE, n=93), Pro-bi was significantly lower in X-sub than in autosomal genes (Fig 2E), suggesting X inactivation in E6 embryos. Pro-bi in X-sub stayed significantly lower than in autosomal genes in E7 TE cells (n=180) (Fig 2F), whereas in E7 EPI (n=21) and PE cells (n=7), Pro-bi in X-sub became comparable to that in autosomal genes (Fig 2F). Together, results indicate X inactivation in E4-E6 embryos and E7 TE cells, followed by reactivation in E7 EPI and PE cells.

Random X inactivation in TE-derived cells

To further study whether the XCI pattern in these pre-implantation embryos was imprinted or random, we performed allele-specific expression analysis of X-linked genes compared to autosomal genes in individual E3-E7 female embryos (Fig 3). The numbers of expressed genes on Chr8 and Chr14 were comparable to ChrX in all E3-E7 cells (S6 Table). While Chr8 and Chr14 had comparable numbers of SNP sites with biallelic expression in individual E3-E7 embryos, the SNP sites with biallelic expression on ChrX were around half as many as those on Chr8 and Chr14 in each embryo (Fig 3A). Within individual E3-E7 embryos, SNP sites of X-sub genes showed monoallelic expression in some cells, and not restricted in a certain lineage even in E7 embryos (Fig 3B), while SNP sites on autosomes had biallelic expression in almost all the cells, as well as the SNP sites of X-esc genes (Fig 3B). Without genome sequence of the embryos, we were not able to determine the XCI pattern in embryos by allele-specific expression analysis.

Therefore, we continued investigating XCI pattern by another approach of exploring DNA methylation at CpG island of X-linked genes. For this, we performed combined human

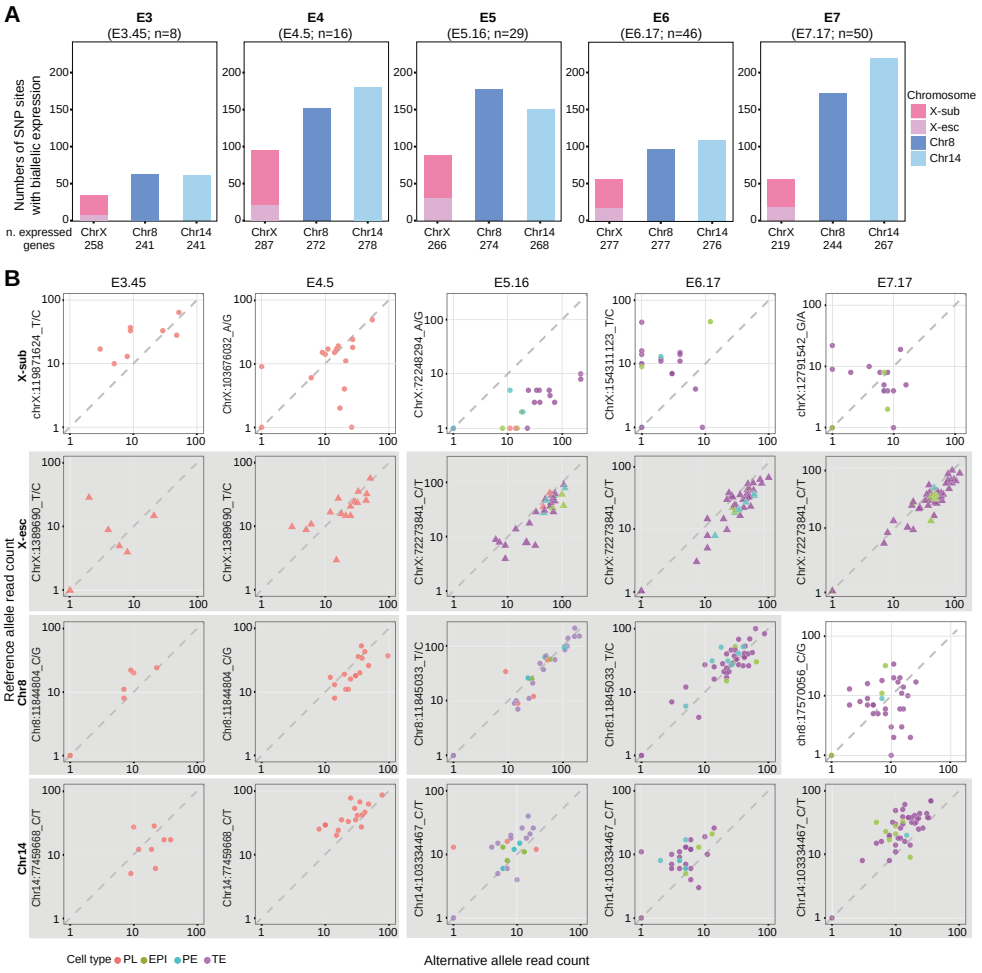

Fig 3. Allele-specific expression in E3-E7 embryos.

(**A**) Barplots showing numbers of SNP sites with biallelic expression on ChrX, Chr8 and Chr14 in individual embryos at E3-E7. Average number of expressed genes (with counts≥8) in all cells of an embryo is indicated below the corresponding chromosome. (**B**) Plots showing in individual E3-E7 embryos the expression of alternative and reference alleles for SNP sites on ChrX (X-sub and X-esc), Chr8 and Chr14, which were heterozygous in embryonic DNA. Plots were generated by lg[read counts of alternative allele (AD+1) and reference allele (RD+1)]. Plots in grey boxes are representing the same SNP sites. PL: pre-lineage.

AR/RP2-based assay on TE-derived cells of 8 male and 15 female human blastocyst outgrowths from 8 IVF cycles (S7 Table).

To determine the parental origin of *AR* and *RP2* alleles for female TE-derived cells, we first analyzed the maternal *AR* and *RP2* allele sizes in male TE-derived cells which held an unmethylated maternal allele but no paternal allele (Fig 4A). Female TE-derived cells with a single major peak in either *AR* or *RP2* gene in undigested DNA samples were considered as homozygous and therefore excluded from further analysis. Afterwards, for each female TE-derived cell sample, we calculated the percentage of paternal allele methylation as previously reported (Fig 4B) [49].

The percentage of paternal allele methylation for both genes in all female embryo outgrowth ranged from 33.3% - 68.6% (Fig 4B, S7 Table). Results showed equal methylation of each parental allele, suggesting random monoallelic expression of X-linked genes in these embryo outgrowth samples. Taking together with the observed smaller proportion of biallelic expression in X-sub than in autosomal genes in E7 TE cells, we conclude that human TE cells have random XCI, in contrast to mice.

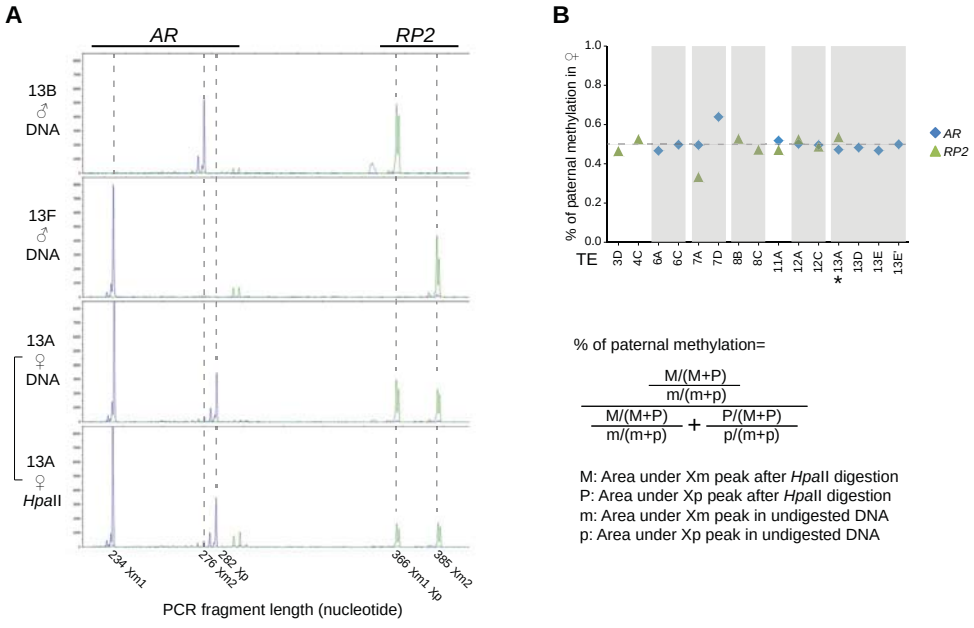

Fig 4. Equal methylation of paternal and maternal alleles in TE-derived cells.

(**A**) Electropherograms showing male and female sibling TE-derived cell samples with detected paternal (Xp) and maternal (Xm) alleles for *AR*/*RP2* genes in genomic DNA and DNA after *Hpa*II digestion. (**B**) Percentage of paternal methylation at CpG sites in *AR* locus and promoter of *RP2* gene in 15 female TE-derived cell samples. Samples from the same IVF cycle are put in individual grey boxes.

Discussion

Well-studied genetic substrains of mice made the allele-specific expression analysis of XCI in mouse pre-implantation embryos possible [18], whereas parental allelic origin is often not available for human embryos.

Analysis of RNA-seq data for human adult tissues showed that X-linked:A median expression ratio ranged from 0.34 to 0.70 in 6 male tissues (median=0.53) and from 0.42 to 0.47 in 4 female tissues (median=0.46) [30]. In another study on RNA-seq data for lymphoblastoid cell lines, X-linked:A median expression ratios were 0.64±0.07 in males (n=24) and 0.66±0.07 in females (n=17) [28] when all transcribed genes (RPKM>0) were included. Moreover, X-linked:A median expression ratios were revealed to increase depending on RPKM cutoffs (>0, ≥1, ≥2) of gene inclusion [28].

In our study, X-linked genes were separated into X-sub and X-esc categories since escapees might have increased dose in females than in males, even though some studies did not show significant differences in escapees expression level between sexes [30, 55]. Our results showed higher X-esc:A median expression ratios than X-sub:A median expression ratios in females and males at E3-E7 (Fig 1D), indicating upregulation of these escapee genes in females and males compared to X-sub genes. E7 EPI and E7 PE female cells had comparable X-sub:A median expression ratios to males (Fig 1D), indicating X chromosome dosage compensation in E7 cells of EPI and PE lineages. When dose of X-sub genes in female cells was normalized to males (Fig 1E), we observed lower female-to-male ratio at E7 compared to other embryonic days.

Without genome sequencing data, only the SNPs with biallelic expression or random monoallelic expression could be detected as informative SNPs. Therefore, SNPs having monoallelic expression within an embryo can be a result of homozygous SNPs in DNA or the imprinted inactivation in all the cells of this embryo. Our approach of comparing the Pro-bi between X-sub genes and autosomal genes was suggested to be reliable in XCI investigation by its performance in XaXa and XaXi controls (Fig 2A). Smaller Pro-bi in X-sub than in autosomes was detected in E4 cells, indicating X inactivation wave occurring between E3-E4 in human embryos. Then the Xi remains silent at E5-E6 until its reactivation in E7 EPI and E7 PE lineages. Here, we describe the dynamic XCI status during human pre-implantation development, in contrast to the previous reported biallelic expression in all cell types between E3-E7 [25]. Results strongly contrast with the previous hypothesis that both X chromosomes are active during human pre-implantation (E3-E7) development [25]. This is because in the allele-specific expression analysis of Petropoulos and colleagues [25], without genome sequencing data, only the SNPs with biallelic expression or random monoallelic expression could be detected as informative SNPs. Therefore, SNPs having imprinted monoallelic expression within an embryo would have been missed in the analysis. In addition, those genes with biallelic expression could be X-esc genes at human pre-implantation stage. In another study using RNA FISH for X-linked genes to detect XCI, *ATRX* gene shows biallelic expression in most cells of E5 female blastocysts

(without separation of ICM from TE) [13]; however, *ATRX* gene is an X-Y paired gene (thus an escapee) [54] which is supposed to have biallelic expression even on the inactive ChrX. The first XCI wave in mouse pre-implantation embryos occurs at the two- to four-cell stage [18] while in humans it happens between E3-E4. This difference is probably due to the different timing of zygotic genome activation (ZGA) in mice (at two cell stage [18]) and in humans (at E4 [25, 56]).

Combining X-sub:A median expression ratios in female cells (Fig 1D) and comparison results from Pro-bi between X-sub and autosomal genes (Fig 2B-F), we hereby conclude that two X chromosomes are Xa(non-upregulated)Xa(non-upregulated) in E3 cells, Xa(upregulated) Xi(inactive) in E4 cells, Xa(upregulated)Xi(inactive) in E5 pre-lineage, E5 EPI, E5 TE, E6 EPI, E6 PE and E6 TE cells, Xa(non-upregulated)Xa(non-upregulated) in E7 EPI and E7 PE cells, Xa(upregulated)Xi(inactive) in E7 TE cells (S4 Table).

The SNP sites with biallelic expression on autosomes (Chr8 and Chr14) were twice as many as those on ChrX in individual E3-E7 embryos (Fig 3A). This may be due to the silence of one X chromosome and monoallelic expression of X-genes. Moreover, in allele-specific expression analysis of X-sub genes, some cells had expression of both alleles whereas monoallelic expression was observed in other cells of the same embryo (Fig 3B). These genes could be escapees at human pre-implantation stage.

In combined *AR/RP2* methylation assay, bulk female TE-derived cells showed equal methylation of paternal and maternal alleles in both *AR* and *RP2* locus, indicating expression of both alleles and therefore random inactivation in human TE-derived cells, which is in contrast to the imprinted XCI in mouse TE cells.

In conclusion, we propose that in human pre-implantation embryos, both X chromosomes are active at E3 and one of them becomes inactive at E4. The Xi remains silent at E5-E6, followed by reactivation in EPI and PE at E7. In E7 TE, X inactivation stays and it is in a random pattern.

Funding

NH is funded by the China Scholarship Council (CSC) [NO.201307040026]; and SMCdSL by the Netherlands organization of Scientific Research, Netherlands [NWO ASPASIA 015.007.037] and Interuniversity Attraction Poles-Phase VII, Belgium [IUAP/PAI P7/14].

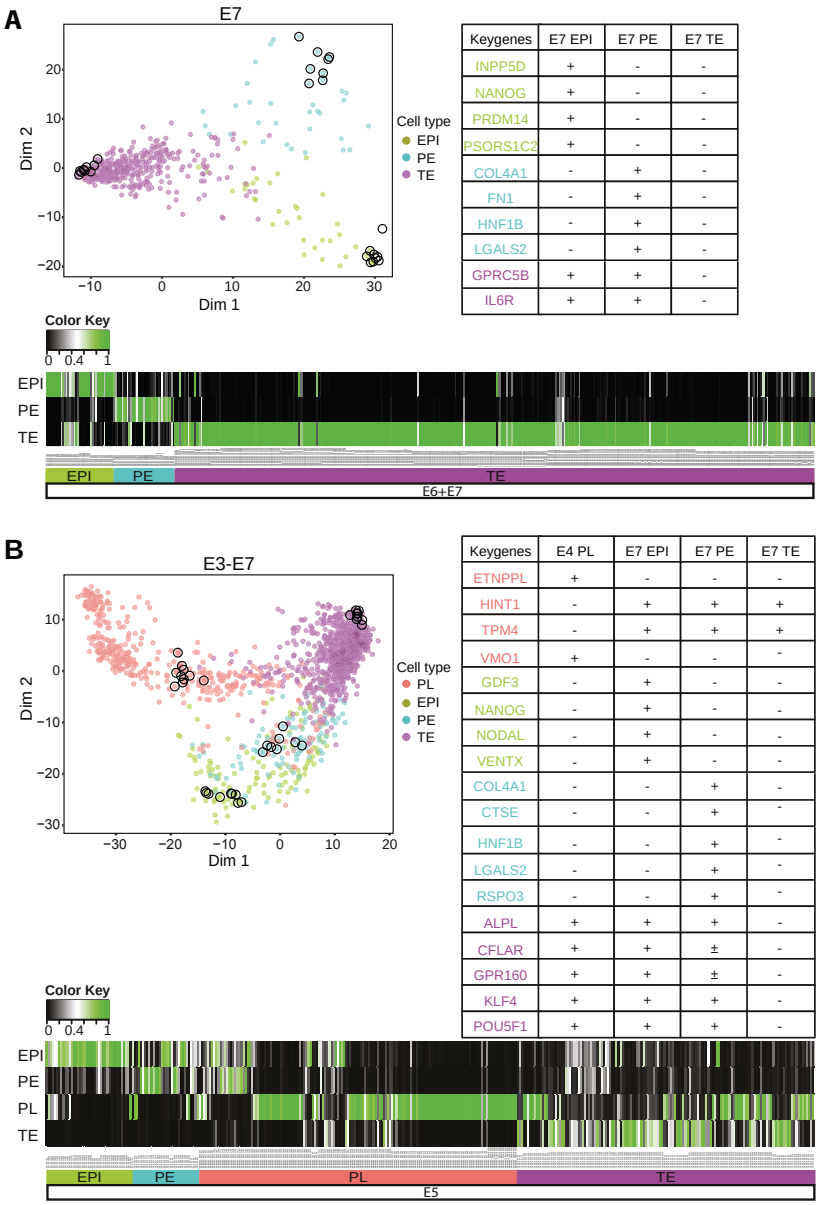

Keygenes	E7 EPI	E7 PE	E7 TE
INPP5D	+	-	-
NANOG	+	-	-
PRDM14	+	-	-
PSORS1C2	+	-	-
COL4A1	-	+	-
FN1	-	+	-
HNF1B	-	+	-
LGALS2	-	+	-
GPRC5B	+	+	-
IL6R	+	+	-

Keygenes	E4 PL	E7 EPI	E7 PE	E7 TE
ETNPPL	+	-	-	-
HINT1	-	+	+	+
TPM4	-	+	+	+
VMO1	+	-	-	-
GDF3	-	+	-	-
NANOG	-	+	-	-
NODAL	-	+	-	-
VENTX	-	+	-	-
COL4A1	-	-	+	-
CTSE	-	-	+	-
HNF1B	-	-	+	-
LGALS2	-	-	+	-
RSPO3	-	-	+	-
ALPL	+	+	+	-
CFLAR	+	+	±	-
GPR160	+	+	±	-
KLF4	+	+	+	-
POU5F1	+	+	+	-

S1 Fig. Training sets 1 and 2 in KeyGenes algorism.

(**A**) Multidimensional scaling plots showing separation of cells at E7 with their old identities, color-coded by cell type. Black circles in panels mark training set 1 used in KeyGenes. Cell type classifiers of training set are shown. KeyGenes heatmap shows the identity scores for the E6-E7 cells in the test set. The rows represent the three lineages from the training set and the columns depict the samples in the test set. The values of all identity scores are given in S2 Table. (**B**) Multidimensional scaling plots showing separation of all E3-E7 cells with their old identities, color-coded by cell type. Black circles in panels mark training set 2 used in KeyGenes. Cell type classifiers of training set are shown. KeyGenes heatmap shows the identity scores for the E5 cells in the test set. The rows represent pre-lineage and the three lineages from the training set and the columns depict the samples in the test set. The values of all identity scores are given in S2 Table. PL: pre-lineage.

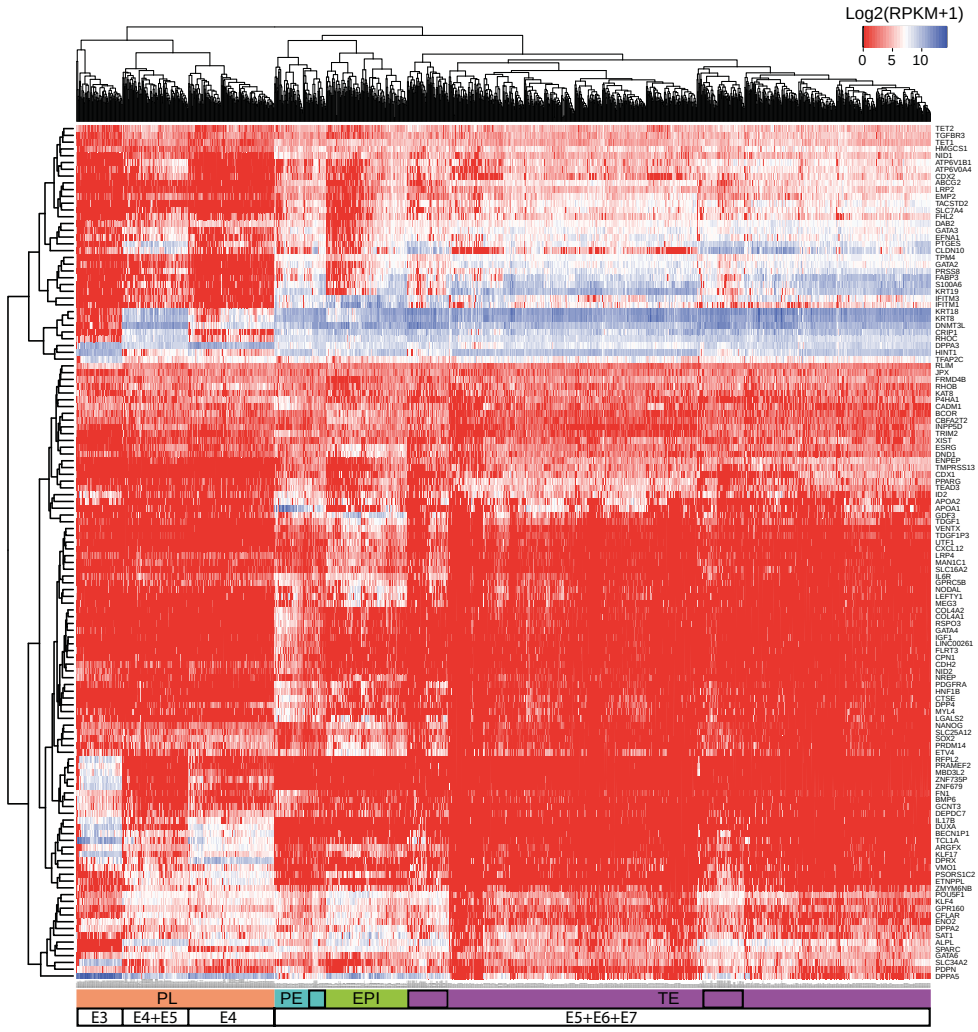

S2 Fig. Sub-clusters in human E3-E7 cells.

Heatmap depicting the expression profile in RPKM of the same genes of interest as in Fig 1A, in all 1519 human pre-implantation cells (with reassigned identities by KeyGenes) at E3-E7. Cell types and embryonic days are labeled. Black squares are cells with mixed identities. PL: pre-lineage.

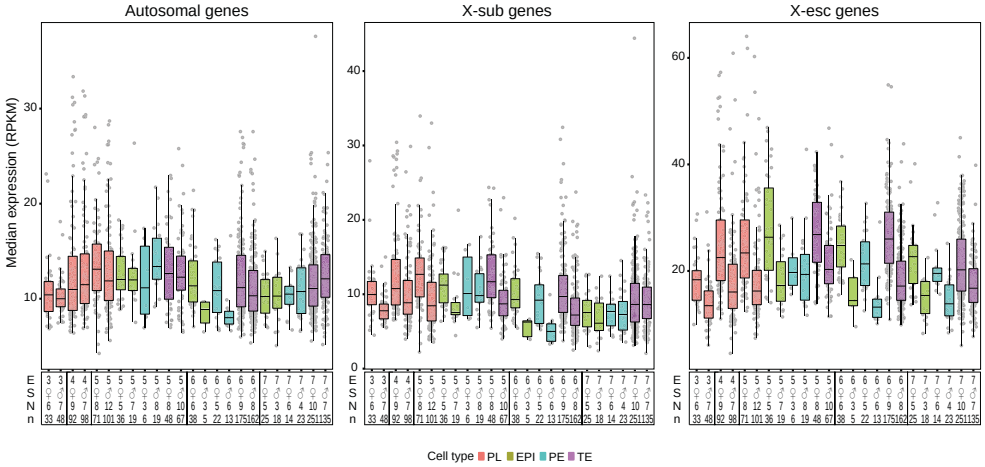

S3 Fig. Median expression of all transcribed (RPKM>0) autosomal genes, X-sub and X-esc genes.

Boxplots showing median expression of all transcribed (RPKM>0) autosomal genes, X-sub and X-esc genes in all female and male cells of each cell type at each embryonic day. E: embryonic day; S: sex; N: number of embryos; n: number of cells; PL: pre-lineage.

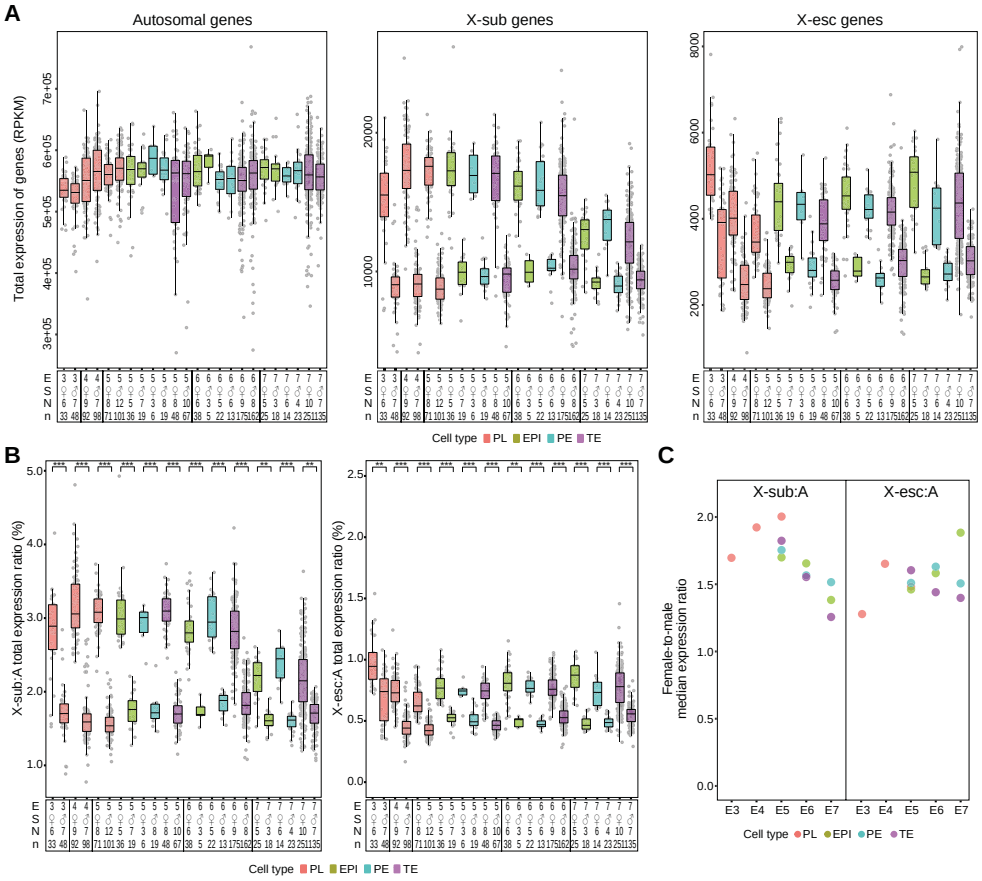

S4 Fig. X:Autosome total expression ratios in human E3-E7 cells.

(**A**) Boxplots showing total expression of all transcribed (RPKM>0) autosomal genes, X-sub and X-esc genes in all female and male cells of each cell type at each embryonic day. (**B**) Boxplots showing X-sub:A total expression ratios (left panel) and X-esc:A total expression ratios (right panel) for individual cells of each type at each embryonic day. Outliers are not indicated. *P* values between females and males are indicated by ** ($P<0.01$) and *** ($P<0.001$). (**C**) Dot plots representing female-to-male X-sub:A total expression ratio and female-to-male X-esc:A total expression ratio in each cell type at each embryonic day. E: embryonic day; S: sex; N: number of embryos; n: number of cells; PL: pre-lineage.

References

1. Inbar-Feigenberg M, Choufani S, Butcher DT, Roifman M, Weksberg R: Basic concepts of epigenetics. Fertil Steril 2013, 99:607-615.
2. Lyon MF: Gene action in the X-chromosome of the mouse (Mus musculus L.). Nature 1961, 190:372-373.
3. Clemson CM, McNeil JA, Willard HF, Lawrence JB: XIST RNA paints the inactive X chromosome at interphase: evidence for a novel RNA involved in nuclear/chromosome structure. Journal of Cell Biology 1996, 132:259-276.
4. Plath K, Fang J, Mlynarczyk-Evans SK, Cao R, Worringer KA, Wang H, Cecile C, Otte AP, Panning B, Zhang Y: Role of histone H3 lysine 27 methylation in X inactivation. Science 2003, 300:131-135.
5. Boggs BA, Cheung P, Heard E, Spector DL, Chinault AC, Allis CD: Differentially methylated forms of histone H3 show unique association patterns with inactive human X chromosomes. Nature genetics 2002, 30:73-76.
6. Jeppesen P, Turner BM: The inactive X chromosome in female mammals is distinguished by a lack of histone H4 acetylation, a cytogenetic marker for gene expression. Cell 1993, 74:281-289.
7. Mohandas T, Sparkes R, Shapiro L: Reactivation of an inactive human X chromosome: evidence for X inactivation by DNA methylation. Science 1981, 211:393-396.
8. Venolia L, Gartler S, Wassman E, Yen P, Mohandas T, Shapiro L: Transformation with DNA from 5-azacytidine-reactivated X chromosomes. Proceedings of the National Academy of Sciences 1982, 79:2352-2354.
9. Carrel L, Willard HF: X-inactivation profile reveals extensive variability in X-linked gene expression in females. Nature 2005, 434:400-404.
10. Berletch JB, Yang F, Disteche CM: Escape from X inactivation in mice and humans. Genome biology 2010, 11:213.
11. Gray KA, Yates B, Seal RL, Wright MW, Bruford EA: Genenames.org: the HGNC resources in 2015. Nucleic Acids Res 2015, 43:D1079-1085.
12. Berletch JB, Ma W, Yang F, Shendure J, Noble WS, Disteche CM, Deng X: Escape from X inactivation varies in mouse tissues. PLoS Genet 2015, 11:e1005079.
13. Okamoto I, Patrat C, Thepot D, Peynot N, Fauque P, Daniel N, Diabangouaya P, Wolf JP, Renard JP, Duranthon V, Heard E: Eutherian mammals use diverse strategies to initiate X-chromosome inactivation during development. Nature 2011, 472:370-374.
14. de Sousa Lopes SMC, Hayashi K, Shovlin TC, Mifsud W, Surani MA, McLaren A: X chromosome activity in mouse XX primordial germ cells. PLoS Genet 2008, 4:e30.
15. Guo F, Yan L, Guo H, Li L, Hu B, Zhao Y, Yong J, Hu Y, Wang X, Wei Y, et al: The Transcriptome and DNA Methylome Landscapes of Human Primordial Germ Cells. Cell 2015, 161:1437-1452.
16. Allen RC, Zoghbi HY, Moseley AB, Rosenblatt HM, Belmont JW: Methylation of HpaII and HhaI sites near the polymorphic CAG repeat in the human androgen-receptor gene correlates with X chromosome inactivation. Am J Hum Genet 1992, 51:1229-1239.
17. Machado FB, Machado FB, Faria MA, Lovatel VL, da Silva AFA, Radic CP, De Brasi CD, Rios ÁFL, de Sousa Lopes SMC, da Silveira LS: 5 me CpG Epigenetic Marks Neighboring a Primate-Conserved Core Promoter Short Tandem Repeat Indicate X-Chromosome Inactivation. PloS one 2014, 9:e103714.
18. Deng Q, Ramskold D, Reinius B, Sandberg R: Single-cell RNA-seq reveals dynamic, random monoallelic gene expression in mammalian cells. Science 2014, 343:193-196.
19. Okamoto I, Otte AP, Allis CD, Reinberg D, Heard E: Epigenetic dynamics of imprinted X inactivation during early mouse development. Science 2004, 303:644-649.
20. Payer B, Lee JT: X chromosome dosage compensation: how mammals keep the balance. Annu Rev Genet 2008, 42:733-772.
21. Reik W, Lewis A: Co-evolution of X-chromosome inactivation and imprinting in mammals. Nat Rev Genet 2005, 6:403-410.
22. Patrat C, Okamoto I, Diabangouaya P, Vialon V, Le Baccon P, Chow J, Heard E: Dynamic changes in paternal X-chromosome activity during imprinted X-chromosome inactivation in mice. Proc Natl Acad Sci U S A 2009, 106:5198-5203.

23. Silva J, Nichols J, Theunissen TW, Guo G, van Oosten AL, Barrandon O, Wray J, Yamanaka S, Chambers I, Smith A: Nanog is the gateway to the pluripotent ground state. Cell 2009, 138:722-737.
24. Sahakyan A, Plath K: Transcriptome Encyclopedia of Early Human Development. Cell 2016, 165:777-779.
25. Petropoulos S, Edsgard D, Reinius B, Deng Q, Panula SP, Codeluppi S, Plaza Reyes A, Linnarsson S, Sandberg R, Lanner F: Single-Cell RNA-Seq Reveals Lineage and X Chromosome Dynamics in Human Preimplantation Embryos. Cell 2016, 165:1012-1026.
26. Roost MS, van Iperen L, Ariyurek Y, Buermans HP, Arindrarto W, Devalla HD, Passier R, Mummery CL, Carlotti F, de Koning EJ, et al: KeyGenes, a Tool to Probe Tissue Differentiation Using a Human Fetal Transcriptional Atlas. Stem Cell Reports 2015, 4:1112-1124.
27. Ohno S: Sex chromosomes and sex-linked genes. Springer Science & Business Media; 2013.
28. Deng X, Hiatt JB, Ercan S, Sturgill D, Hillier LW, Schlesinger F, Davis CA, Reinke VJ, Gingeras TR, Shendure J: Evidence for compensatory upregulation of expressed X-linked genes in mammals, Caenorhabditis elegans and Drosophila melanogaster. Nature genetics 2011, 43:1179-1185.
29. Sangrithi MN, Royo H, Mahadevaiah SK, Ojarikre O, Bhaw L, Sesay A, Peters AH, Stadler M, Turner JM: Non-Canonical and Sexually Dimorphic X Dosage Compensation States in the Mouse and Human Germline. Developmental Cell 2017, 40:289-301. e283.
30. Xiong Y, Chen X, Chen Z, Wang X, Shi S, Wang X, Zhang J, He X: RNA sequencing shows no dosage compensation of the active X-chromosome. Nature genetics 2010, 42:1043-1047.
31. gplots: various R programming tools for plotting data
32. Joshi NA FJ: Sickle: A sliding-window, adaptive, quality-based trimming tool for FastQ files (Version 1.33) [Software]. Available at https://github.com/najoshi/sickle. 2011.
33. Rosenbloom KR, Armstrong J, Barber GP, Casper J, Clawson H, Diekhans M, Dreszer TR, Fujita PA, Guruvadoo L, Haeussler M, et al: The UCSC Genome Browser database: 2015 update. Nucleic Acids Res 2015, 43:D670-681.
34. Wu TD, Nacu S: Fast and SNP-tolerant detection of complex variants and splicing in short reads. Bioinformatics 2010, 26:873-881.
35. Li H, Handsaker B, Wysoker A, Fennell T, Ruan J, Homer N, Marth G, Abecasis G, Durbin R, Genome Project Data Processing S: The Sequence Alignment/Map format and SAMtools. Bioinformatics 2009, 25:2078-2079.
36. Koboldt DC, Zhang Q, Larson DE, Shen D, McLellan MD, Lin L, Miller CA, Mardis ER, Ding L, Wilson RK: VarScan 2: somatic mutation and copy number alteration discovery in cancer by exome sequencing. Genome Res 2012, 22:568-576.
37. Obenchain V, Lawrence M, Carey V, Gogarten S, Shannon P, Morgan M: VariantAnnotation: a Bioconductor package for exploration and annotation of genetic variants. Bioinformatics 2014, 30:2076-2078.
38. Ng SB, Turner EH, Robertson PD, Flygare SD, Bigham AW, Lee C, Shaffer T, Wong M, Bhattacharjee A, Eichler EE, et al: Targeted capture and massively parallel sequencing of 12 human exomes. Nature 2009, 461:272-276.
39. Warnes GR, Bolker B, Gorjanc G, Grothendieck G, Korosec A, Lumley T, MacQueen D, Magnusson A, Rogers J: gdata: Various R programming tools for data manipulation. R package version; 2014.
40. Bates D, Maechler M, Bolker B, Walker S: lme4: Linear mixed-effects models using Eigen and S4. R package version 2014, 1.
41. Wickham H: ggplot2: elegant graphics for data analysis. New York USA: Springer; 2009.
42. Wickham H: The split-apply-combine strategy for data analysis. Journal of Statistical Software 2011, 40: 1-29.
43. Wickham H: reshape2: Flexibly reshape data: a reboot of the reshape package. R package version 2012, 1.
44. Wickham H: stringr: modern, consistent string processing. The R Journal 2010, 2:38-40.
45. Auguie B: gridExtra: functions in Grid graphics. R package version 09 2012, 1.
46. Wickham H, Francois R: dplyr: A grammar of data manipulation. R package version 04 2015, 1:20.
47. Heeren AM, van Iperen L, Klootwijk DB, de Melo Bernardo A, Roost MS, Gomes Fernandes MM, Louwe LA, Hilders CG, Helmerhorst FM, van der Westerlaken LA, Chuva de Sousa Lopes SM: Development of the

follicular basement membrane during human gametogenesis and early folliculogenesis. BMC Dev Biol 2015, 15:4.

48. Goto T, Wright E, Monk M: Paternal X-chromosome inactivation in human trophoblastic cells. Mol Hum Reprod 1997, 3:77-80.

49. Bolduc V, Chagnon P, Provost S, Dubé M-P, Belisle C, Gingras M, Mollica L, Busque L: No evidence that skewing of X chromosome inactivation patterns is transmitted to offspring in humans. The Journal of clinical investigation 2008, 118:333-341.

50. Blakeley P, Fogarty NM, Del Valle I, Wamaitha SE, Hu TX, Elder K, Snell P, Christie L, Robson P, Niakan KK: Defining the three cell lineages of the human blastocyst by single-cell RNA-seq. Development 2015, 142:3613.

51. Zhang Y, Castillo-Morales A, Jiang M, Zhu Y, Hu L, Urrutia AO, Kong X, Hurst LD: Genes that escape X-inactivation in humans have high intraspecific variability in expression, are associated with mental impairment but are not slow evolving. Mol Biol Evol 2013, 30:2588-2601.

52. Park C, Carrel L, Makova KD: Strong purifying selection at genes escaping X chromosome inactivation. Mol Biol Evol 2010, 27:2446-2450.

53. Cotton AM, Ge B, Light N, Adoue V, Pastinen T, Brown CJ: Analysis of expressed SNPs identifies variable extents of expression from the human inactive X chromosome. Genome Biol 2013, 14:R122.

54. Bellott DW, Hughes JF, Skaletsky H, Brown LG, Pyntikova T, Cho TJ, Koutseva N, Zaghlul S, Graves T, Rock S, et al: Mammalian Y chromosomes retain widely expressed dosage-sensitive regulators. Nature 2014, 508:494-499.

55. Disteche CM: Dosage compensation of the active X chromosome in mammals. Nature genetics 2006, 38:47-53.

56. Yan L, Yang M, Guo H, Yang L, Wu J, Li R, Liu P, Lian Y, Zheng X, Yan J, et al: Single-cell RNA-Seq profiling of human preimplantation embryos and embryonic stem cells. Nat Struct Mol Biol 2013, 20:1131-1139.

Supporting information

S1 Table. 126 genes of interest to generate MDS and heatmap.

S2 Table. E5-E7 cells reassigned by KeyGenes.

S3 Table. List of escapee genes.

S4 Table. Median and total expression of chromosome X and autosomes.

S5 Table. Fetal gonadal cells included in the study.

S6 Table. Numbers of expressed genes in each E3-E7 cell.

S7 Table. The percentage of paternal allele methylation in combined human *AR/RP2*-based assays.

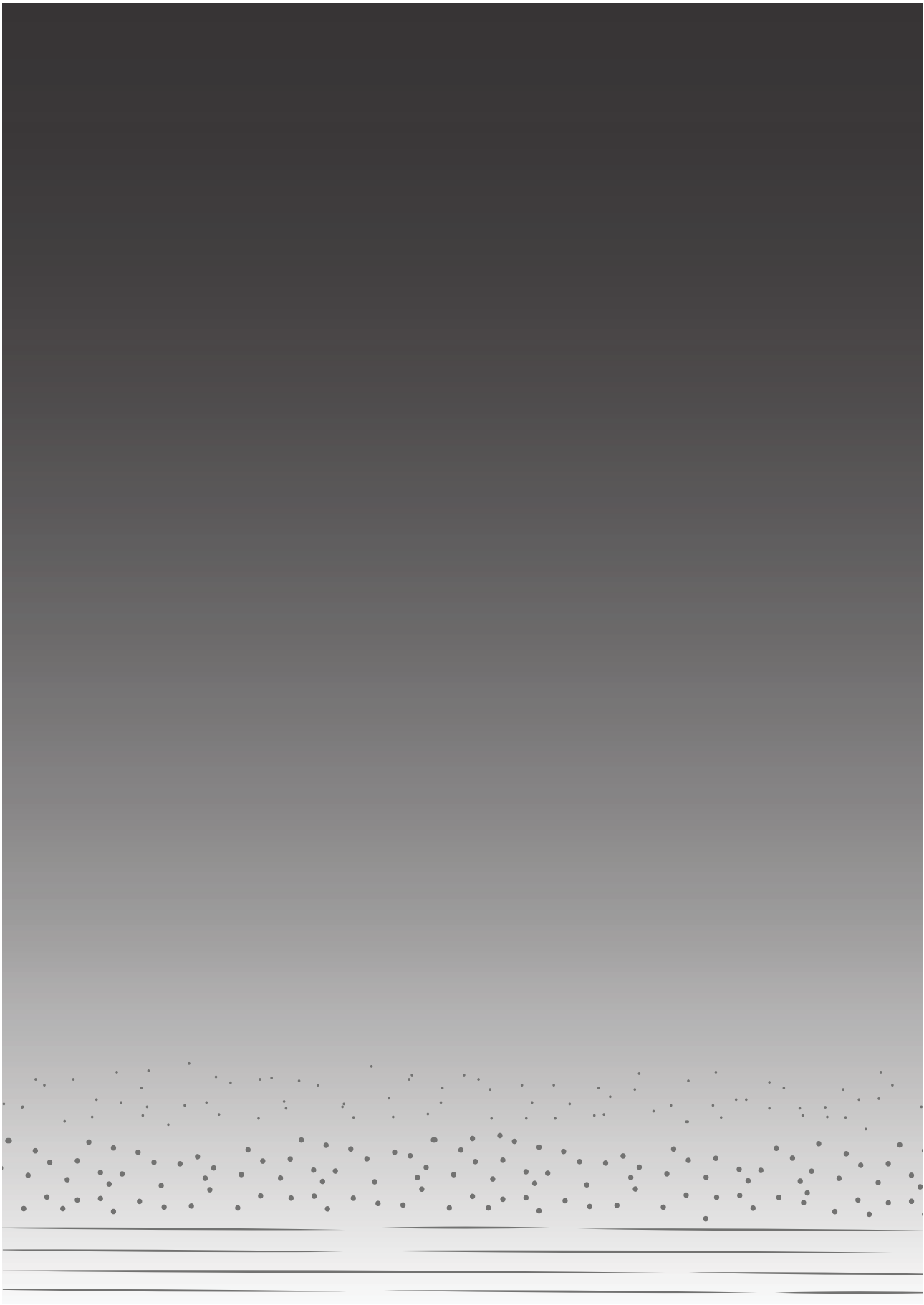

CHAPTER 4

Human extravillous trophoblasts penetrate decidual veins and lymphatics before remodeling spiral arteries during early pregnancy

Nannan He[1], Liesbeth van Iperen[1], Danielle de Jong[2], Karoly Szuhai[2], Frans M. Helmerhorst[3], Lucette A. J. van der Westerlaken[3], Susana M. Chuva de Sousa Lopes[1,4]

[1]Department of Anatomy and Embryology, Leiden University Medical Center, Leiden, The Netherlands

[2]Department of Molecular Cell Biology, Leiden University Medical Center, Leiden, The Netherlands

[3]Department of Gynaecology, Division of Reproductive Medicine, Leiden University Medical Center, Leiden, The Netherlands

[4]Department for Reproductive Medicine, Ghent University Hospital, Ghent, Belgium

PLOS ONE 2017, 12:e0169849.

Abstract

In humans, the defective invasion of the maternal endometrium by fetal extravillous trophoblasts (EVTs) can lead to insufficient perfusion of the placenta, resulting in pregnancy complications that can put both mother and baby at risk. To study the invasion of maternal endometrium between (W)5.5-12 weeks of gestation by EVTs, we combined fluorescence in situ hybridization, immunofluorescence and immunohistochemistry to determine the presence of (male) EVTs in the vasculature of the maternal decidua. We observed that interstitial mononuclear EVTs directly entered decidual veins and lymphatics from W5.5. This invasion of decidual veins and lymphatics occurred long before endovascular EVTs remodelled decidual spiral arteries. This unexpected early entrance of interstitial mononuclear EVTs in the maternal circulation does not seem to contribute to the materno-placental vascular connection directly, but rather to establish (and expand) the materno-fetal interface through an alternative vascular route.

Introduction

During human placental development, at the tips of the anchoring villi, cytotrophoblasts proliferate into cell columns and from there they can detach and invade the maternal decidualized endometrium (decidua) and even the myometrium [1, 2]. Those invading fetal cytotrophoblasts are known as extravillous trophoblasts (EVTs).

At term, there are several subtypes of EVTs present in the maternal decidua, depending on their localization: the interstitial mononuclear (as well as multinuclear) EVTs are dispersed in the decidual mesenchyme; the endovascular EVTs and intramural EVTs are both directly associated with remodeled spiral arteries and are present in their lumen (or replacing the endothelial cells) and in their tunica media [3] respectively and those EVTs migrate-colonize the spiral arteries in a retrograde fashion [4]; and a fourth category of 'epithelial' EVTs lines, together with maternal endothelial cells in a mosaic fashion, the basal plate of the maternal decidua basalis [5].

In humans, the defective invasion of the maternal decidua by fetal EVTs leads to insufficient perfusion of the placenta, resulting in pregnancy complications, such as intrauterine growth restriction, (recurrent) spontaneous abortion, (very) premature birth and preeclampsia [6, 7]. The unique vascular remodeling of the maternal decidua during pregnancy, whereby both fetal and maternal cells play complementary regulatory roles, is a fundamental process for a successful pregnancy [8, 9].

Endovascular EVTs are observed in spiral arteries from (W)8 weeks of gestation, 'plugging' (or blocking) the entrance of spiral arteries to the intervillous space preventing maternal blood flow until about W12 [10-12]. During this period (W8-W12), decidual veins become dilated in both decidua parietalis and basalis to give rise to decidual venous lakes [13]. By W12, both decidual veins and spiral arteries are in open connection with the intervillous space of the placenta allowing the maternal blood to circulate between the placental villi [10-12]. This materno-placental vascular connection provides efficient exchange of nutrients, waste products, hormones and gases between the maternal blood and the fetal blood and is crucial to ensure fetal growth.

After the materno-placental vascular connection is established, the constant maternal blood flow transports small tissue fragments (syncytial knots) that are shed from the outer layer of the placental villi of multinucleated (non-viable) syncytiotrophoblasts into the decidual venous where those knots become trapped and are subsequently cleared [13-15]. If the syncytial knots escape to enter the maternal circulation, they can cause trophoblastic embolism and even sudden death of the mother [16].

Interestingly, the presence of fetal cells [17], placental-derived particles and exosomes [18, 19] in the maternal blood from W6 has been described, but in the absence of robust materno-placental vascular connection this remains to be clarified. Therefore, we sought to systematically characterize the presence of EVTs in the endometrium in the period W5.5-W12. Our results indicate that between W5.5-W12, interstitial mononuclear EVTs efficiently enter the maternal (blood and lymph) circulation. This novel aspect of EVT invasion, enlarging materno-fetal

interface early during pregnancy, may shed new light in our understanding of pregnancy complications and maternal immune tolerance.

Materials and Methods

Ethics approval and human tissue collection

The Medical Ethics Committee of the Leiden University Medical Center (protocol P08.087) approved the collection and use of material for this study. Written informed consent was obtained from all patients (N=13). Tissue was obtained by vacuum aspiration from women undergoing voluntary pregnancy termination without medical indication and obtained anonymized. The gestational age (in weeks and days) was determined by obstetric ultrasonography and can be converted to weeks post conception by subtracting two weeks. Tissue samples (S1 Table) were collected in cold saline solution (0.9% NaCl). The decidua basalis and parietalis were identified retrospectively by the presence of scattered pKRT-positive EVTs in histological sections.

Sex genotyping and histochemistry

The material was sex genotyped by polymerase chain reaction (PCR) for AMELX/AMELY as previously described [20]. The decidua was fixed in 4% paraformaldehyde (PFA) overnight at 4ºC, paraffin embedded and sectioned as previously described [20]. For Azan staining, paraffin sections were deparaffinised using xylene and dehydrated by standard procedures. The sections were then treated with 0.1% Azocarmine B (Edward Gurr Ltd., London, UK) in 5% glacial acetic acid (Merck, Darmstadt, Germany) for 3 minutes, rinsed several times in water, treated with 5% phosphotungstic acid (Fluka, Sigma-Aldrich, St. Louis, USA) solution for 6 minutes, again rinsed several times in water and immersed in a 1:1 solution of water to 0.4% orange G (Merck, Darmstadt, Germany)/0.2% aniline blue (Nustain, Nottingham, UK) in 1% glacial acetic acid for 15 minutes, all at room temperature (RT). Sections were then rinsed in water, dehydrated through a series of ethanol solutions, xylene and mounted in Entellan (Merck, Darmstadt, Germany).

Immunofluorescence

Paraffin sections were deparaffinised using xylene and dehydrated by standard procedures and used for immunofluorescence as previously described [20]. Briefly, antigen retrieval was performed in citrate buffer, followed by treatment with blocking solution consisting of 1% bovine serum albumin (BSA; Sigma-Aldrich, St. Louis, USA) in 0.05% PBST [0.05% Tween-20 (Merck-Schuchardt, Hohenbrunn, Germany) in phosphate-buffered saline (PBS)] for 40 minutes at RT. Sections were then incubated with the primary antibodies diluted in blocking solution for 1 hour at RT, washed twice in PBST for 5 minutes and incubated with secondary antibodies diluted in blocking solution for 1 hour at RT. The primary antibodies used were mouse anti-pan-keratin (pKRT; 1:100; AE1/AE3, Dako, Heverlee, Belgium), rabbit anti-platelet/endothelial adhesion molecule 1 (PECAM1; 1:200; sc1506-R, Santa Cruz Biotechnology, Santa Cruz, CA,

USA), rabbit anti-alpha-smooth muscle actin (ACTA2; 1:200; ab5694, Abcam, Cambridge, UK), mouse anti-podoplanin (PDPN; 1:100; ab77854, Abcam, Cambridge, UK) and rat anti-PDPN (1:100; 12-9381-42, eBioscience, San Diego, CA, USA). The secondary antibodies used were Alexa Fluor 594 donkey anti-mouse IgG (1:500; A-21203), Alexa Fluor 488 goat anti-rabbit IgG (1:500; A-11034), Alexa Fluor 555 goat anti-rat IgG (1:500; A-21434), Alexa Fluor 488 donkey anti-mouse IgG (1:500; A-21202) and Alexa Fluor 647 donkey anti-rabbit IgG (1:500; A-31573) (all from Life Technologies, Eugene, OR, USA). Nuclei were stained with 4',6-diamidino-2-phenylindole (DAPI; Vector Laboratories Ltd., Peterborough, UK) and sections were mounted in Prolong Gold anti-fade reagent (Life technologies). As negative controls, slides were immunostained omitting the primary antibodies.

Fluorescence in situ hybridization (FISH) for chrX and chrY

FISH with probes of human chrX and chrY was carried out to distinguish fetal (male) cells from maternal (female) cells. After selected immunostained slides were imaged, they were incubated with 0.4% pepsin (pepsin from porcine gastric mucosa, P7000-100G, Sigma-Aldrich, St Louis, MO, USA) in 0.02M HCl for 5 minutes at 37°C. Centromere specific alphoid repeat probes used were pBamX5 and pDP97 of the human chrX and chrY, respectively [21, 22]. Both probes were labeled by nick translation with FITC (chrX probe) or Cy3 (chrY probe). Probe labeling and hybridization reaction were performed using previously published protocols [23, 24].

Image acquisition

Slides were either scanned on a Pannoramic 250 FLASH digital scanner (3D HISTECH Ltd., Budapest, Hungary) and representative areas selected for images using the software program 'Pannoramic viewer' (3D HISTECH Ltd., Budapest, Hungary); or photographed on a Leica DMRA fluorescence microscope (Leica, Wetzlar, Germany) equipped with a CoolSnap HQ2 camera (Photometrics, Tucson, USA). Figures were compiled using Photoshop CS6 (Adobe Systems Inc., San Jose, USA).

Quantification of veins being invaded by EVTs

The combination of Azan staining and immunofluorescence for ACTA2, PECAM1 and PDPN on serial sections from the decidua basalis enabled us to distinguish decidual veins from arteries and lymphatic vessels. Decidual veins were PECAM1-positive, ACTA2-negative and PDPN-negative vessels, with reduced amounts of extracellular matrix surrounding them. Veins were considered invaded when there were one or multiple (male) EVTs (KRT-positive, chrY-positive) penetrating the (maternal) vessel wall (chrY-negative, PECAM1-positive, ACTA2-negative and PDPN-negative). To quantify the percentage of decidual veins invaded by EVTs, we manually counted decidual veins (with and without EVTs invasion) in each paraffin section of decidua basalis of different individuals (N=9) between W5.5-W12. The number of paraffin sections (n) counted is shown. The results are shown as mean±standard deviation.

Results

Interstitial mononuclear EVTs invade decidual veins from W5.5-W7.5

We investigated the presence of (male) EVTs in the decidua in the period W5.5-W12 and have analyzed a total of n=19 samples of decidua basalis and n=20 decidua parietalis from N=13 women (S1 Table). Due to a paucity of markers to identify specifically EVTs, we used a combined approach of cytogenetics (FISH for sex chromosomes chrX and chrY) and immunofluorescence for pan-keratin (pKRT) to distinguish maternal glandular epithelial cells from the fetal (male) EVTs in the endometrium (S1 Fig). This staining-combination also allowed us to distinguish decidua parietalis from decidua basalis (S1 Fig). Combining cytochemistry (Azan staining) and immunofluorescence for the arterial-marker ACTA2, the endothelial-marker PECAM1 and the lymphatic-marker PDPN, we were able to differentiate between arteries, veins and lymphatic vessels.

Surprisingly, between W5.5-W7.5 in the decidua basalis, we detected invasion of (non-dilated) ACTA2-negative PECAM1-positive decidual (maternal) veins by (male) individual interstitial mononuclear EVTs (Fig 1A-E). These (male) EVTs were clearly observed penetrating the endothelial wall of decidual veins, often in consecutive sections (Fig 1B) in all the W5.5-W7.5 decidua basalis analyzed (n=9 from N=6 individuals). We counted decidual veins in paraffin sections (n=40) from different individuals between W5.5-W7.5 (N=4), and observed that on average 17% (147/856) of the decidual veins were invaded by EVTs (Fig 1E, orange bars).

By contrast, individual interstitial mononuclear EVTs were always observed outside the arterial smooth-muscle layer of the ACTA2-positive PECAM1-positive decidual spiral arteries, even in those arteries located close to the maternal basal plate and in the vicinity of EVTs (Fig 2).

From W8-W12, mononuclear EVTs invade spiral arteries as well as decidual veins

Between W8-W12 (N=7), interstitial mononuclear EVTs were still observed penetrating many decidual veins both close to the basal plate and more interiorly located (Fig 3A-B and S2 Fig). We counted decidual veins in paraffin sections (n=47) from different individuals between W8.1-W12 (N=5), and observed that on average 16% (165/1038) of the decidual veins were invaded by EVTs (Fig 1E, blue bars), comparable to what was observed between W5.5-W7.5. At this gestational age, many decidual spiral arteries located at the maternal basal plate were indeed being remodeled and contained endovascular and intramural EVTs in the lumen and tunica media, respectively (Fig 3C). However, we noticed that deeper located decidual spiral arteries remained unremodelled, whereas neighboring deeper located veins were consistently invaded by individual interstitial mononuclear EVTs in all decidua basalis analyzed (Fig 3B-C and S2 Fig).

From the decidual samples analyzed in this study, cytogenetic analysis revealed that one individual decidua was from a W8.4 conceptus with Klinefelter syndrome (mosaic 47,XXY and 46,XY) (Fig 4A), even though additional chromosomal abnormalities were not investigated.

Importantly, interstitial mononuclear XXY EVTs were observed entering decidual veins (Fig 4A), as in the other decidua of similar age, suggesting that this aspect of the establishment of the materno-fetal interface occurred normally.

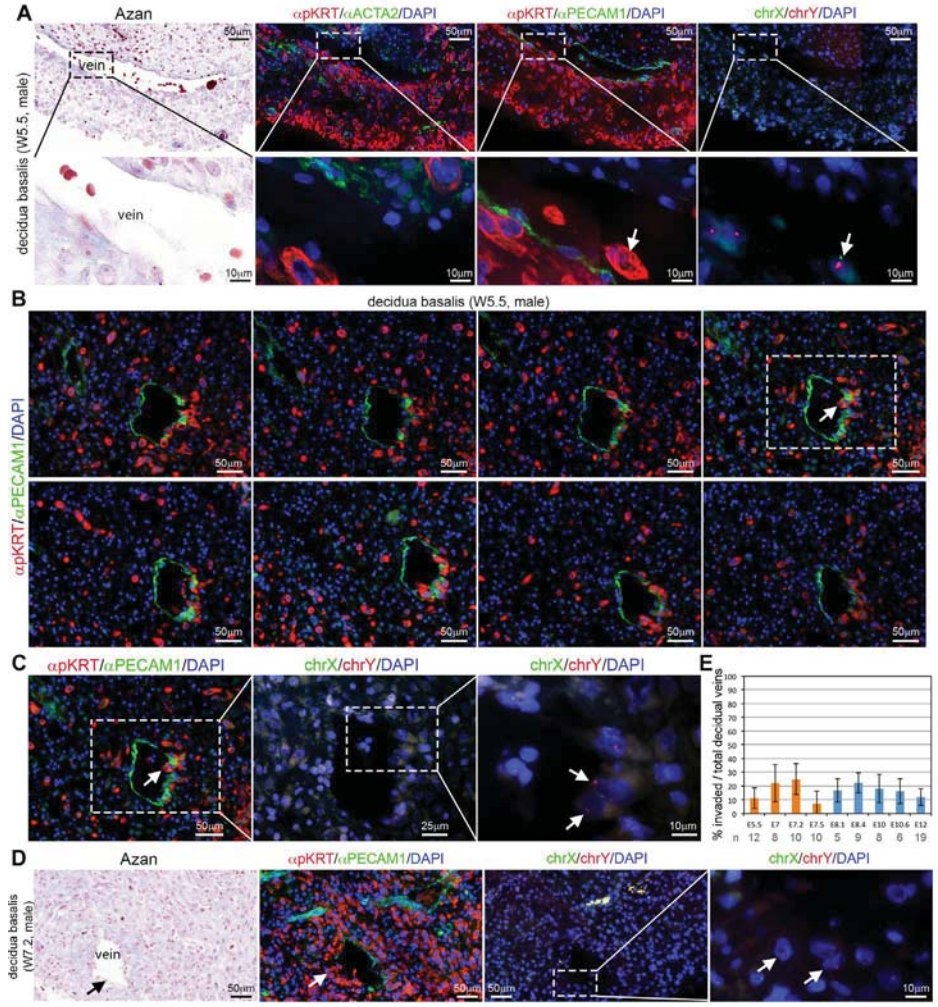

Fig 1. Human EVTs penetrate decidual veins early during first trimester (W5.5-W7.5).

(**A**) Histological sections of decidua basalis at W5.5 used for Azan staining (left panel), immunostained for pKRT and ACTA2 (left-middle panel) and immunostained for pKRT and PECAM1 (right-middle panel). FISH for chrX/chrY (right) was performed in the pKRT/PECAM1-stained sections. White arrows indicate male EVTs invading veins. The bottom row shows magnifications of the dashed boxes in the top row. (**B**) Consecutive sections of W5.5 decidua basalis were immunostained for pKRT/PECAM1. (**C**) FISH for chrX and chrY (right panels) magnifications are shown for the section in dashed box. White arrows point to male EVTs penetrating a decidual vein. (**D**) Histological sections of decidua basalis at W7.2 used for Azan staining (left panel), immunostained for pKRT and PECAM1 (left-middle panel). FISH for chrX/chrY (right panels) was performed in the pKRT/PECAM1-stained sections. The most right panel shows a magnification of the dashed box. White arrows indicate male EVTs invading veins. (**E**) Percentage of invaded decidual veins per total veins encountered per histological section (n) between W5.5-W12. Results are sown as mean ± standard deviation. All scale bars are depicted.

Interstitial mononuclear EVTs entered decidual lymphatics from W5.5-W12

To exclude that the PECAM1-positive ACTA2-negative vessels were lymphatic vessels instead of veins, we investigated the expression of PDPN in the decidua [25-27]. Notably, not only PDPN-negative PECAM1-positive decidual veins were being invaded by interstitial mononuclear EVTs, but also many PDPN-positive PECAM1-positive decidual lymphatic vessels were in fact being invaded by interstitial mononuclear EVTs between W5.5-W12 (N=11 out of 12 analyzed) (Fig 4B). We observed dilated PDPN-positive lymphatics encircling (or insulating) spiral arteries to create characteristic round structures (data not shown), confirming findings by Volchek and colleagues (2010) [27]. The biological significance of these characteristic structures remains to be investigated. We also report PDPN-positive mesenchymal stroma inside the placental villi (cyan arrow in S2 Fig, top right panel), as previously reported by Wang et al (2011) [28].

Aggregates of mononuclear EVTs were present in decidual veins from W5.5

At W5.5, we could already observe small aggregates of mononuclear EVTs in veins in the decidua basalis (Fig 5A). Those resembled syncytial knots, but were morphologically distinct. At later time points, from W7-W12 (N=6), bona fide syncytial knots (central area of multiple nuclei and large peripheral area of cytoplasm) were often present in dilated veins in both the decidua basalis (Fig 5A-B) and parietalis (Fig 5B), suggestive of the gradual establishment of materno-placental vascular connection.

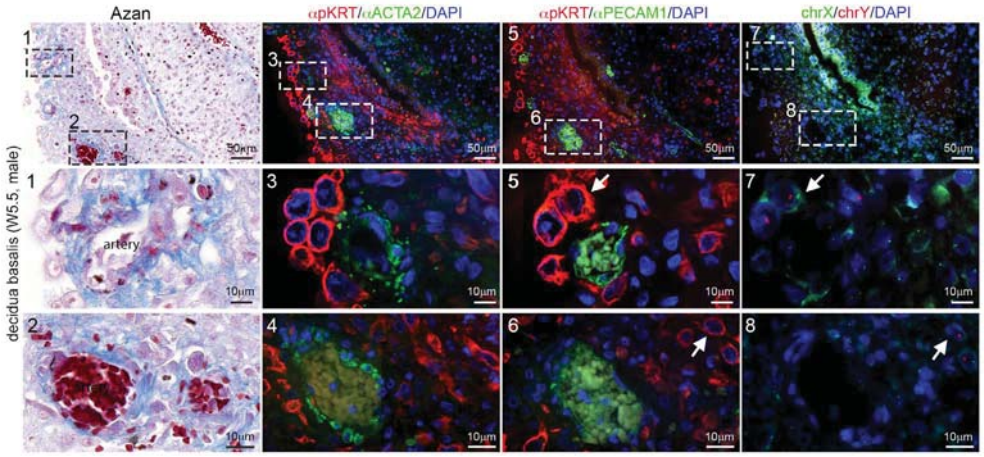

Fig 2. Human EVTs in the vicinity of arteries early during first trimester (W5.5).

Histological sections of W5.5 decidua basalis showing decidual arteries. Consecutive sections were used for Azan staining (left panel), immunostained for pKRT and ACTA2 (left-middle panel) and immunostained for pKRT and PECAM1 (right-middle panel). FISH for chrX and chrY (right panel) was performed in the pKRT/PECAM1-stained sections. The (middle and) bottom rows show magnifications of the (numbered) dashed boxes in the top rows. White arrows depict male EVTs. All scale bars are depicted.

Allo-epi-endothelium in the basal plate of first trimester decidua basalis

Finally, we report that the basal plate of the maternal decidua (between the anchoring villi) was lined by both (male) pKRT-positive EVTs and (female) PECAM1-positive maternal endothelial cells in the period analyzed (W5.5-W12) (Fig 6). This allo-epi-endothelium monolayer organization of 'epithelial' EVTs and maternal endothelial cells in a patchy-mosaic fashion has been described in term decidua [5] and we describe it now in the human decidua during the first trimester as well.

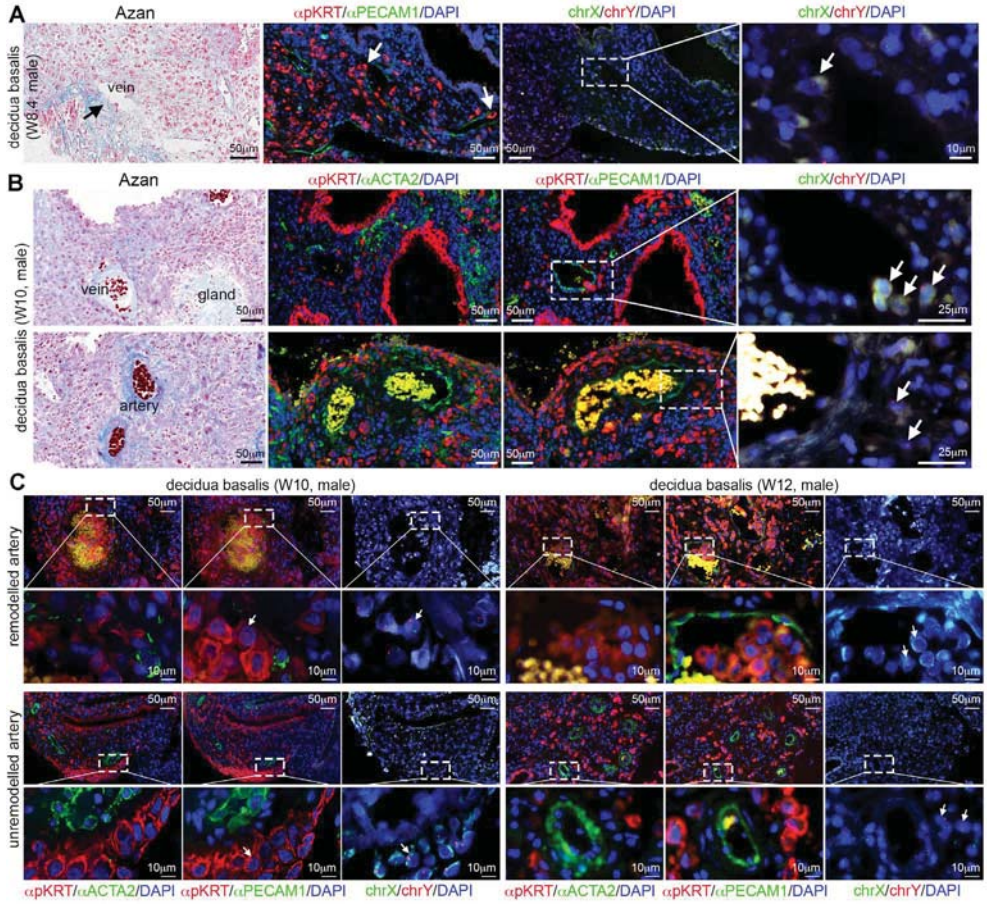

Fig 3. Human extravillous trophoblast cells in decidua between W8-W12.

(**A**) Histological sections of decidua basalis at W8.4 used for Azan staining (left panel), immunostained for pKRT and PECAM1 (left-middle panel). FISH for chrX/chrY (right panels) was performed in the pKRT/PECAM1-stained sections. The most right panel shows a magnification of the dashed box. White arrows indicate male EVTs invading veins. (**B**) Histological sections of decidua basalis at W10 used for Azan staining (left panel), immunostained for pKRT and ACTA2 (left-middle panel) and immunostained for pKRT and PECAM1 (right-middle panel). FISH for chrX/chrY (right) was performed in the pKRT/PECAM1-stained sections. White arrows indicate male EVTs. Low magnifications are shown in S2 Fig. (**C**) Histological sections of W10 and W12 decidua basalis showing remodeled and unremodelled arteries. Consecutive sections were immunostained for pKRT and ACTA2 (left panels) and immunostained for pKRT and PECAM1 (middle panels). FISH for chrX and chrY (right panels) was performed in the pKRT/PECAM1-stained sections. The bottom rows show magnifications of the dashed boxes in the top rows. All scale bars are depicted.

Discussion

Interstitial mononuclear EVTs enter the maternal circulation via veins and lymphatics

Our systematic analysis of first trimester decidua using a combination of immunofluorescence and FISH to distinguish between the types of vasculature and identify the EVTs unambiguously allowed us to reveal for the first time the direct invasion by interstitial

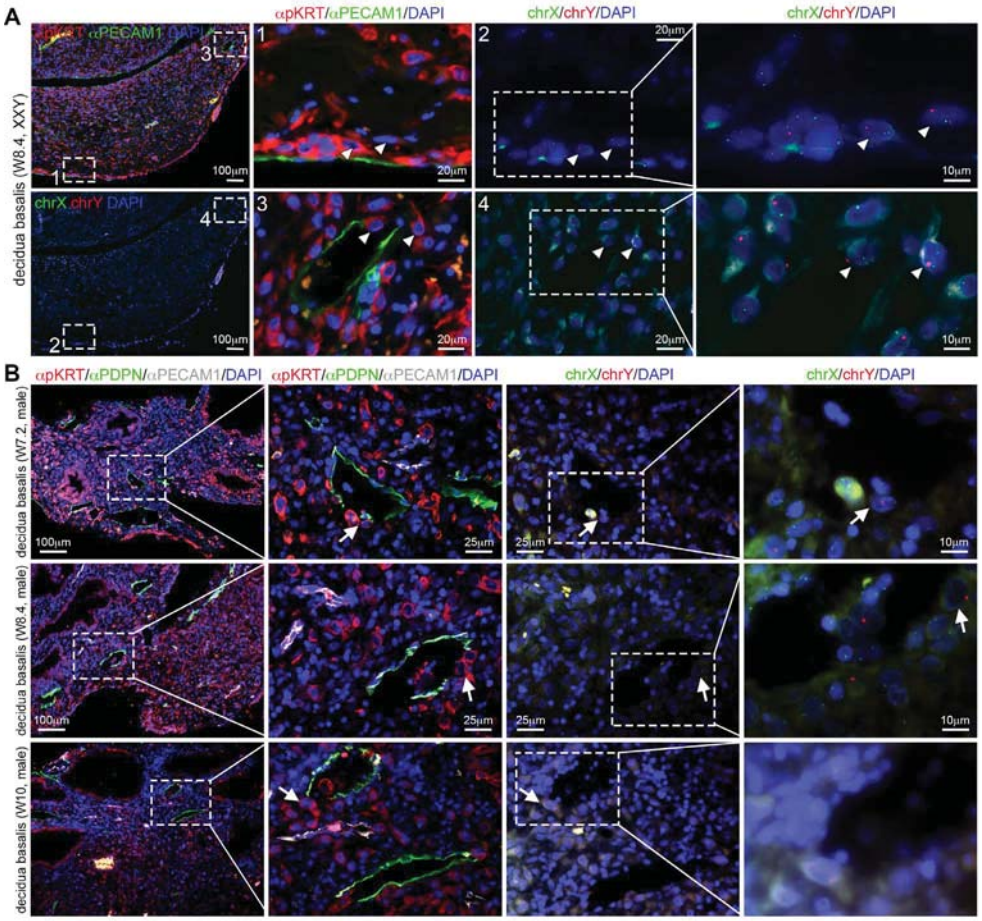

Fig 4. Human extravillous trophoblast cells invade decidual veins and lymphatics early during first trimester.

(**A**) Histological sections of decidua basalis from a (mosaic) Klinefelter syndrome (47,XXY and 46,XY) pregnancy at W8.4. Left panels show low magnifications of same section immunostained for pKRT and PECAM1 (top) and chrX/chrY FISH (bottom). Middle-left and middle-right panels are magnifications of the (numbered) dashed boxes in the left panels. Right panels are magnifications of the dashed boxes in the middle-right panels. White arrowheads point to XXY fetal EVTs. (**B**) Histological sections of decidua basalis at W7.2, W8.4 and W10 immunostained for pKRT, PDPN and PECAM1 (left panels). FISH for chrX and chrY (right) was performed in the in the pKRT/PDPN/PECAM1-stained sections. White arrows point to EVTs invading the lymphatic vessels. All scale bars are depicted.

mononuclear EVTs of decidual veins and lymphatics in the maternal decidua basalis by W5.5. This suggests an efficient entry of interstitial mononuclear EVTs into the maternal (blood and lymph) circulation in the absence of robust materno-placental vascular connection [10-12].

Consistent with our findings, very recently the group of Huppertz has also showed evidence for EVTs invasion of uterine veins [29], using an antibody against human leukocyte antigen (HLA)-G, often used as specific EVT marker [30]. However, caution should be taken when using only HLA-G to identify EVTs, due to the different HLA-G isoforms [31]. In addition, using HLA-G immunostaining as means to identify EVTs, the same group has also reported that EVTs (coined "endoglandular") also invaded uterine glands [32, 33]. In our study, using a combination of immunofluorescence and FISH, we were unable to detect (male) EVTs in maternal uterine glands between W5.5 and W12.

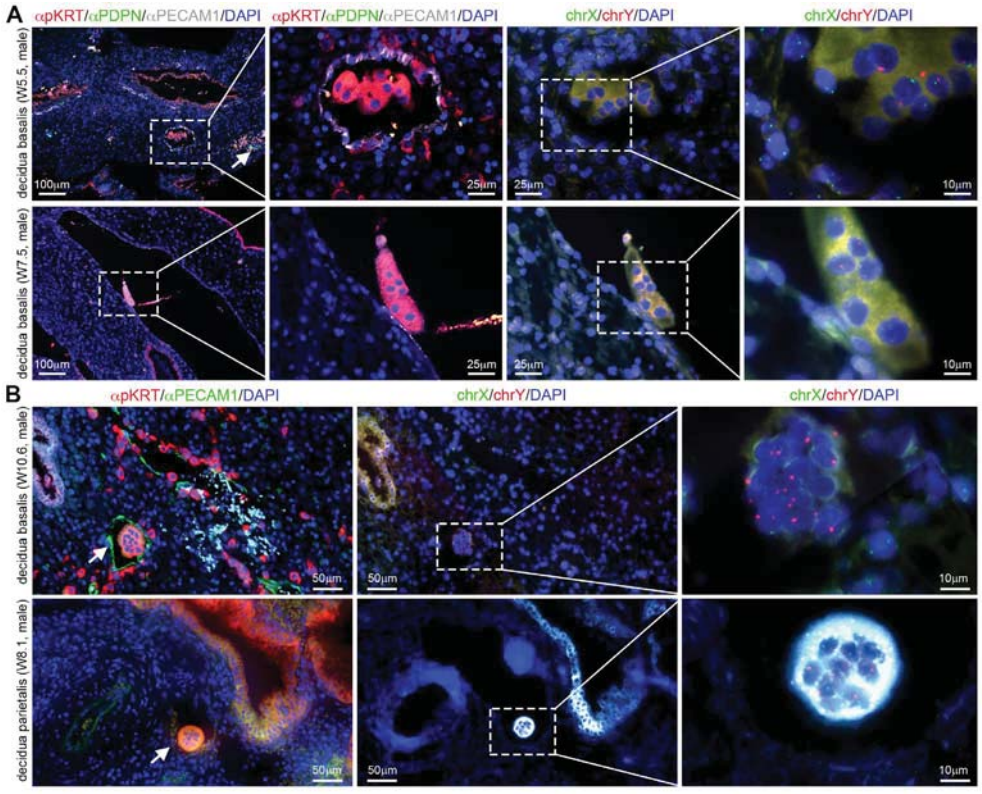

Fig 5. EVT aggregates and syncytial knots in the decidua basalis and parietalis.

(**A**) Histological sections of decidua basalis at W5.5 and W7.5 immunostained for pKRT, PDPN and PECAM1 (lefts panels) showing the presence of mononuclear EVT aggregates (top row) and syncytial knots (bottom row). FISH for chrX and chrY (right panels) was performed in pKRT/PDPN/PECAM1-stained sections. White arrow indicates PDPN-positive lymphatics. (**B**) Histological sections of W10.6 decidua basalis (top row) and W8.1 decidua parietalis (bottom row) immunostained for pKRT and PECAM1 showing the presence of syncytial knots in veins. FISH for chrX and chrY (right panels) was performed in pKRT/PECAM1-stained sections. All scale bars are depicted.

The timing of the venous invasion process (by the EVTs) is different from the passive deportation of (non-viable) syncytial knots detaching directly from placental villi to the intervillous space and being then transported to the decidual venous lakes once the materno-placental vascular connection has been established [13-15, 34].

Materno-fetal interface: EVTs stepping out of the uterus

The materno-fetal interface encompasses three main processes: the establishment of immune tolerance, regulation of decidual invasion by EVTs and uterine vascular remodeling [35], all taking place primarily in the uterus. Our results are in agreement with the timing of vascular remodeling as well as with the invasion of the decidua by interstitial and endovascular EVTs. Moreover, we observed the formation of the allo-epi-endothelium in the basal plate of the decidua basalis and therefore acknowledge the existence of epithelial EVTs [5].

Here, we propose that when interstitial mononuclear EVTs enter the maternal circulation they are not only substantially enlarging the materno-fetal interface, but they are also doing so earlier than previously accepted [via placental debris after materno-placental vascular connection [18]] and via an alternatively vascular route (decidual lymphatics and veins).

This novel venue of materno-fetal interface (taking place outside the uterus) may contribute significantly to trigger the maternal immune system to perhaps confer recognition to prevent rejection of the fetus while in the uterus. The EVTs have developed several strategies to ensure immune tolerance while in the maternal environment. This includes the expression of HLA-G, instead of HLA-A and HLA-B, in this way avoiding clearance by maternal natural killer cells [36]. In the uterus, the EVTs encounter and crosstalk with uterine macrophages, uterine

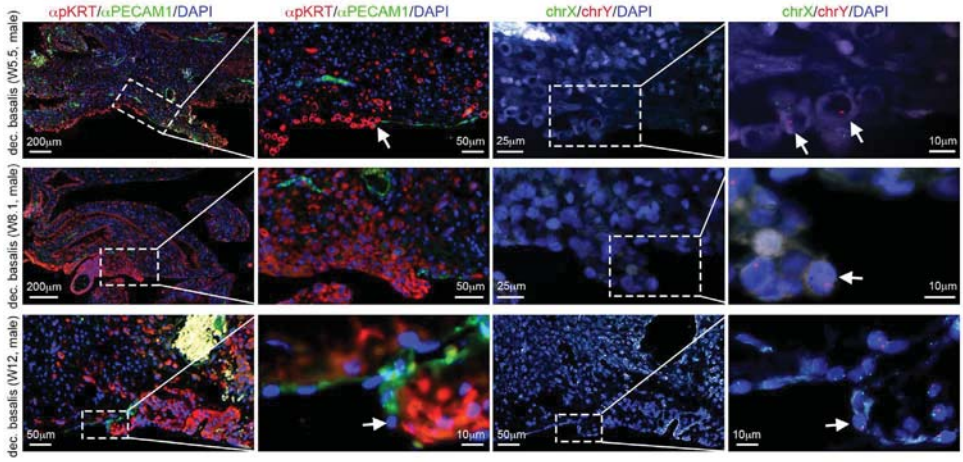

Fig 6. Allo-epi-endothelial surface of the decidua basalis during first trimester.

Histological sections of decidua basalis containing the basal plate of the decidua basalis immunostained for pKRT and PECAM1 at W5.5, W8.1 and W12. FISH for chrX/chrY was also performed on the pKRT/PECAM1-stained sections. Magnifications of the dashed boxes are shown. White arrows point to EVTs bordering with maternal PECAM1-positive endothelial cells in the basal plate of the maternal decidua basalis. All scale bars are depicted.

natural killer cells and T lymphocytes, modulating locally the maternal innate and adaptive immune response [35, 36]. The EVTs that enter the maternal circulation may have a primary role contributing to the adaptive and innate immune response, but through the recruitment of maternal cells to the uterus subsequently also contribute to successful vascular remodeling [4].

Materno-fetal interface and pregnancy complications

Sex chromosomal aneuploidy disorders, including Klinefelter syndrome, often produce small-for-gestational age fetuses [37]. We describe here the decidua basalis of one W8.4 pregnancy with Klinefelter syndrome (mosaic 47,XXY and 46,XY) and show interstitial mononuclear EVTs entering the maternal circulation via decidual veins. We were unable to detect "plugged" of remodeled arteries colonized by endovascular EVTs, probably due to the young age of the fetus.

Our understanding of placental complications in humans is rather limited due to the lack of in vitro assays and suitable animal models. However it is clear that the materno-fetal interface in all its facets is indispensable for a successful pregnancy [38, 39]. We speculate that pregnancy complications such as preeclampsia and intrauterine growth restriction that are closely associated to defects in vascular remodeling [3, 7, 40], as well as recurrent abortion, may correlate with defective presence of EVTs in the maternal circulation.

Acknowledgements

We would like to thank the Centre for Contraception Sexuality and Abortion (CASA) from Leiden and The Hague for the collection of human fetal material.

Funding

SMCdSL is funded by the Netherlands organization of Scientific Research, Netherlands [NWO ASPASIA 015.007.037] and Interuniversity Attraction Poles-Phase VII, Belgium [IUAP/PAI P7/14]; and NH by the China Scholarship Council (CSC) [NO.201307040026].

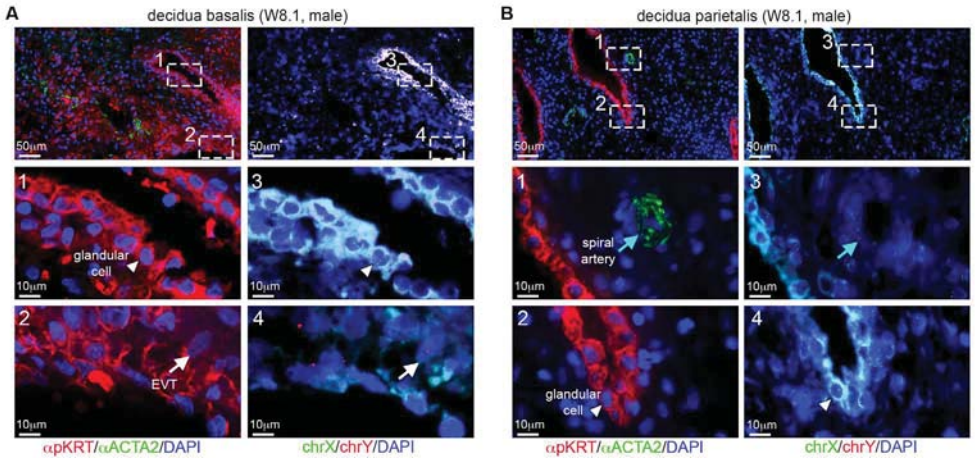

S1 Fig. Distinguishing male embryonic EVTs from female maternal glandular epithelial cells.

(**A**-**B**) Decidua basalis (A) and parietalis (B) immunostained for pKRT and ACTA2, followed by FISH for chromosome (chr) X and chrY in the pKRT/ACTA2-stained sections. The middle and bottom rows show magnifications of the (numbered) dashed boxes in the top row. White arrowheads depict female maternal glandular epithelial cells (gland cells), white arrows depict male EVTs and cyan arrows depict an unremodelled artery containing no (male) EVTs. All scale bars are depicted.

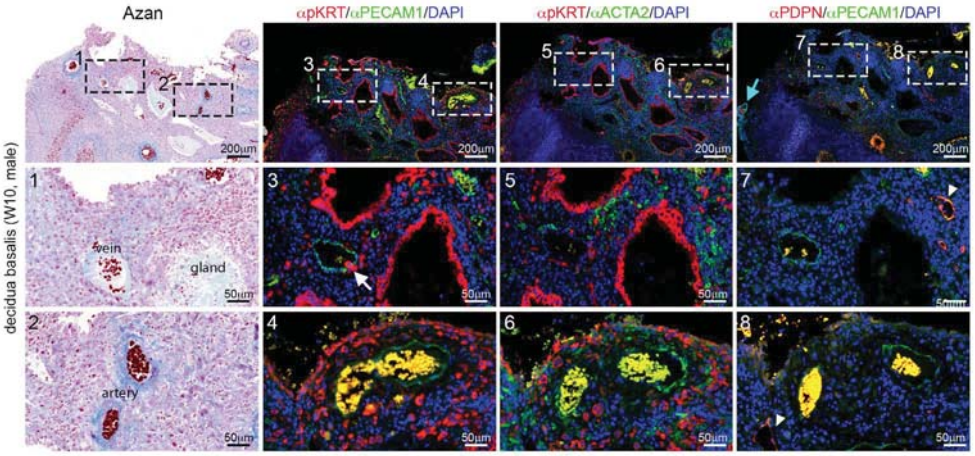

S2 Fig. Human extravillous trophoblast cells in decidua at W10.

Histological sections of W10 decidua basalis showing decidual veins, arteries and lymphatic vessels. Consecutive sections were used for Azan staining (left panels), immunostained for pKRT and PECAM1 (left-middle panels), immunostained for pKRT and ACTA2 (right-middle panels) and immunostained for PDPN and PECAM1 (right panels). The middle and bottom rows show magnifications of the (numbered) dashed boxes in the top rows. White arrow depicts EVTs invading a vein; cyan arrow points to an attached placental villus; white arrowheads point to a PDPN-positive lymphatic vessel. FISH for chrX and chrY is shown in Fig 3. All scale bars are depicted.

References

1. Brosens JJ, Pijnenborg R, Brosens IA: The myometrial junctional zone spiral arteries in normal and abnormal pregnancies: a review of the literature. Am J Obstet Gynecol 2002, 187:1416-1423.
2. Knofler M: Critical growth factors and signalling pathways controlling human trophoblast invasion. Int J Dev Biol 2010, 54:269-280.
3. Lyall F, Robson SC, Bulmer JN: Spiral artery remodeling and trophoblast invasion in preeclampsia and fetal growth restriction: relationship to clinical outcome. Hypertension 2013, 62:1046-1054.
4. Harris LK: Review: Trophoblast-vascular cell interactions in early pregnancy: how to remodel a vessel. Placenta 2010, 31 Suppl:S93-98.
5. Byrne S, Challis E, Williams JL, Pringle JH, Hennessy JM, Ockleford CD: A mosaic cell layer in human pregnancy. Placenta 2010, 31:373-379.
6. Burke SD, Karumanchi SA: Spiral artery remodeling in preeclampsia revisited. Hypertension 2013, 62:1013-1014.
7. Fisher SJ: Why is placentation abnormal in preeclampsia? Am J Obstet Gynecol 2015, 213:S115-122.
8. Plaisier M, Dennert I, Rost E, Koolwijk P, van Hinsbergh VW, Helmerhorst FM: Decidual vascularization and the expression of angiogenic growth factors and proteases in first trimester spontaneous abortions. Hum Reprod 2009, 24:185-197.
9. Plaisier M, Rodrigues S, Willems F, Koolwijk P, van Hinsbergh VW, Helmerhorst FM: Different degrees of vascularization and their relationship to the expression of vascular endothelial growth factor, placental growth factor, angiopoietins, and their receptors in first-trimester decidual tissues. Fertil Steril 2007, 88:176-187.
10. Burton GJ, Jauniaux E, Watson AL: Maternal arterial connections to the placental intervillous space during the first trimester of human pregnancy: the Boyd collection revisited. Am J Obstet Gynecol 1999, 181:718-724.
11. Pijnenborg R, Vercruysse L, Hanssens M: The uterine spiral arteries in human pregnancy: facts and controversies. Placenta 2006, 27:939-958.
12. Jauniaux E, Watson AL, Hempstock J, Bao YP, Skepper JN, Burton GJ: Onset of maternal arterial blood flow and placental oxidative stress. A possible factor in human early pregnancy failure. Am J Pathol 2000, 157:2111-2122.
13. Craven CM, Ward K: Syncytiotrophoblastic fragments in first-trimester decidual veins: evidence of placental perfusion by the maternal circulation early in pregnancy. Am J Obstet Gynecol 1999, 181:455-459.
14. Craven CM, Chedwick LR, Ward K: Placental basal plate formation is associated with fibrin deposition in decidual veins at sites of trophoblast cell invasion. Am J Obstet Gynecol 2002, 186:291-296.
15. Craven CM, Zhao L, Ward K: Lateral placental growth occurs by trophoblast cell invasion of decidual veins. Placenta 2000, 21:160-169.
16. Delmis J, Pfeifer D, Ivanisevic M, Forko JI, Hlupic L: Sudden death from trophoblastic embolism in pregnancy. Eur J Obstet Gynecol Reprod Biol 2000, 92:225-227.
17. Merviel P, Aractingi S, Uzan S: [Detection of fetal cells in maternal blood: myth or reality?]. Gynecol Obstet Fertil 2001, 29:371-376.
18. Chamley LW, Holland OJ, Chen Q, Viall CA, Stone PR, Abumaree M: Review: where is the maternofetal interface? Placenta 2014, 35 Suppl:S74-80.
19. Sarker S, Scholz-Romero K, Perez A, Illanes SE, Mitchell MD, Rice GE, Salomon C: Placenta-derived exosomes continuously increase in maternal circulation over the first trimester of pregnancy. J Transl Med 2014, 12:204.
20. Heeren A, van Iperen L, Klootwijk DB, de Melo Bernardo A, Roost MS, Gomes Fernandes MM, Louwe LA, Hilders CG, Helmerhorst FM, van der Westerlaken LA, Chuva de Sousa Lopes SM: Development of the follicular basement membrane during human gametogenesis and early folliculogenesis. BMC Dev Biol 2015, 15:4.
21. Cooke HJ, Schmidtke J, Gosden JR: Characterisation of a human Y chromosome repeated sequence and related sequences in higher primates. Chromosoma 1982, 87:491-502.
22. Willard HF, Smith KD, Sutherland J: Isolation and characterization of a major tandem repeat family from the human X chromosome. Nucleic Acids Res 1983, 11:2017-2033.

23. Szuhai K, Bezrookove V, Wiegant J, Vrolijk J, Dirks RW, Rosenberg C, Raap AK, Tanke HJ: Simultaneous molecular karyotyping and mapping of viral DNA integration sites by 25-color COBRA-FISH. Genes Chromosomes Cancer 2000, 28:92-97.

24. Szuhai K, Tanke HJ: COBRA: combined binary ratio labeling of nucleic-acid probes for multi-color fluorescence in situ hybridization karyotyping. Nat Protoc 2006, 1:264-275.

25. Red-Horse K: Lymphatic vessel dynamics in the uterine wall. Placenta 2008, 29 Suppl A:S55-59.

26. Red-Horse K, Rivera J, Schanz A, Zhou Y, Winn V, Kapidzic M, Maltepe E, Okazaki K, Kochman R, Vo KC, et al: Cytotrophoblast induction of arterial apoptosis and lymphangiogenesis in an in vivo model of human placentation. J Clin Invest 2006, 116:2643-2652.

27. Volchek M, Girling JE, Lash GE, Cann L, Kumar B, Robson SC, Bulmer JN, Rogers PA: Lymphatics in the human endometrium disappear during decidualization. Hum Reprod 2010, 25:2455-2464.

28. Wang Y, Sun J, Gu Y, Zhao S, Groome LJ, Alexander JS: D2-40/podoplanin expression in the human placenta. Placenta 2011, 32:27-32.

29. Moser G, Weiss G, Sundl M, Gauster M, Siwetz M, Lang-Olip I, Huppertz B: Extravillous trophoblasts invade more than uterine arteries: evidence for the invasion of uterine veins. Histochem Cell Biol 2016.

30. Apps R, Gardner L, Moffett A: A critical look at HLA-G. Trends Immunol 2008, 29:313-321.

31. James JL, Chamley LW: A caution on the use of HLA-G isoforms as markers of extravillous trophoblasts. Placenta 2008, 29:305-306; author reply 307.

32. Moser G, Weiss G, Gauster M, Sundl M, Huppertz B: Evidence from the very beginning: endoglandular trophoblasts penetrate and replace uterine glands in situ and in vitro. Hum Reprod 2015, 30:2747-2757.

33. Moser G, Gauster M, Orendi K, Glasner A, Theuerkauf R, Huppertz B: Endoglandular trophoblast, an alternative route of trophoblast invasion? Analysis with novel confrontation co-culture models. Hum Reprod 2010, 25:1127-1136.

34. Chamley LW, Chen Q, Ding J, Stone PR, Abumaree M: Trophoblast deportation: just a waste disposal system or antigen sharing? J Reprod Immunol 2011, 88:99-105.

35. Lash GE: Molecular Cross-Talk at the Feto-Maternal Interface. Cold Spring Harb Perspect Med 2015, 5.

36. Gregori S, Amodio G, Quattrone F, Panina-Bordignon P: HLA-G Orchestrates the Early Interaction of Human Trophoblasts with the Maternal Niche. Front Immunol 2015, 6:128.

37. Oelberg DG: Consultation with the specialist: prenatal growth: the sum of maternal, placental, and fetal contributions. Pediatr Rev 2006, 27:224-229.

38. Redman CW, Tannetta DS, Dragovic RA, Gardiner C, Southcombe JH, Collett GP, Sargent IL: Review: Does size matter? Placental debris and the pathophysiology of pre-eclampsia. Placenta 2012, 33 Suppl:S48-54.

39. Southcombe J, Redman C, Sargent I: Peripheral blood invariant natural killer T cells throughout pregnancy and in preeclamptic women. J Reprod Immunol 2010, 87:52-59.

40. Kaufmann P, Black S, Huppertz B: Endovascular trophoblast invasion: implications for the pathogenesis of intrauterine growth retardation and preeclampsia. Biol Reprod 2003, 69:1-7.

S1 Table. Characteristics of the human decidua samples.

Embryo ID	Sex	Age (weeks and days of gestation)	Decidua basalis (No. samples)	Decidua parietalis (No. samples)
EB3	XY	W5.5	2	1
EI1	XY	W6.2	2	4
EJ2	XY	W7	2	4
EM3	XY	W7.2	1	1
GP4	XY	W7.2	1	-
EL1	XY	W7.5	1	-
EC2	XY	W8.1	2	1
ED2	XXY	W8.4	1	1
FH1	XY	W8.4	1	1
GS1	XY	W8.5	1	1
EO3	XY	W10	1	1
FQ4	XY	W10.6	1	3
EG2	XY	W12	3	2
Total	-	-	**19**	**20**

CHAPTER 5

Spatial pattern of methylation in *IGF2/H19* ICR1 in human first-trimester placenta

Cristiana Libardi Miranda-Furtado[1,2,#,*], **Nannan He**[1,*], Matthias S. Roost[1], Maria M. Gomes Fernandes[1], Murilo Racy Soares[1,2], Liesbeth van Iperen[1], Ester Silveira Ramos[2,3,¶], Susana M. Chuva de Sousa Lopes[1,4,¶]

[1]Department of Anatomy and Embryology, Leiden University Medical Center, Leiden, the Netherlands

[2]Department of Genetics, Ribeirao Preto Medical School, University of Sao Paulo, Sao Paulo, Brazil

[3]Department of Gynecology and Obstetrics, Ribeirao Preto Medical School, University of Sao Paulo, Sao Paulo, Brazil

[4]Department of Reproductive Medicine, Ghent University Hospital, Ghent, Belgium

[#]Current address: Department of Gynecology and Obstetrics, Ribeirao Preto Medical School, University of Sao Paulo, Sao Paulo, Brazil

[*]Equal first authorship contribution

[¶]Equal senior authorship contribution

Manuscript ready for submission.

Abstract

Allele-specific DNA methylation is an important tool in studies of genomic imprinting. The *IGF2/H19* imprinting control region (ICR1) is essential for normal fetal and placental growth and development. Its pattern of methylation during human early pregnancy is poorly understood. We aimed to search for possible non-CpG single nucleotide polymorphisms (SNPs) on ICR1 and to investigate the pattern of methylation of in different placental villi of first trimester human placenta and embryonic tissue using bisulfite DNA sequencing. We were able to select two informative non-CpG SNPs, rs2071094:G>T and rs2107425:C>T in two first-trimester pregnancies, which allowed us to discriminate the paternal and maternal alleles. Our results indicate a normal imprint pattern in methylation of the *IGF2/H19* ICR1in first trimester embryos and placental villi.

Introduction

The imprinted *IGF2/H19* cluster domain, controlled by the *IGF2/H19* imprinting control region (ICR1), plays an essential role in growth and development of placental mammals [1, 2]. In humans, the *IGF2/H19* ICR1, located on the 11p15.5 chromosomal region, controls the paternally expressed *IGF2* and maternally expressed long non-coding RNA *H19*. One hypothesis for the regulation of this imprinting cluster is the insulator model for imprinting expression (reviewed in [3]), whereby the *IGF2/H19* ICR1 unmethylated maternal allele allows the CCCTC-binding factor (CTCF) to bind to its (seven) insulator consensus sequences, whereas CTCF cannot bind to CTCF-binding sites in the methylated paternal allele.

In humans, *H19* has been reported to be biallelically expressed in cytotrophoblasts until 10 weeks of gestation (W10), but to become monoallelically expressed in placenta at term, even though this could be due to the increased amount of mesodermal tissue in the placental villi [4-7]. In agreement, term placentas seem to show a normal imprinted or slightly hypomethylated *IGF2/H19* ICR1 [5, 8-11]. However, of those studies, only Turan and colleagues used informative single nucleotide polymorphisms (SNPs) (in that case rs10732516 present in the 6th CTCF binding site) to discriminate the parental origin of DNA methylation and reported not only variation between individual placentas but also pronounced spatial variation in the same term placenta [11].

Buckberry and colleagues compared the methylation status of the *IGF2/H19* ICR1 between term placentas and first-trimester placentas (W6-W12) and found no differences in average methylation levels in the 6th CTCF binding site (53.5%±7.2% versus 54.8%±6.9%, respectively) [5]. However, those authors used only one site of collection in the placentas and might have missed spatial variation in methylation. Moreover, although they discriminated allelic-specific expression, no discrimination was made between the parental alleles regarding the DNA methylation of the *IGF2/H19* ICR1 and only global DNA methylation levels were reported. Villous cytotrophoblast proliferate and generate trophoblastic columns, from the tips of which extravillous trophoblast cells (EVTs) detach and invade the maternal decidua [12]. Here, we have investigated for the first time the spatial pattern of methylation of the *IGF2/H19* ICR1 in first-trimester placental villi, using informative SNPs to discriminate between the parental alleles. We report a normal imprinted pattern for *IGF2/H19* ICR1 in all investigated placental villi samples, as well as in the respective embryos.

Materials and Methods

Tissue samples and sex genotyping

The collection and use of the material for this study was approved by the Human Ethics Committee of the Leiden University Medical Center, Netherlands (P08.087). Informed consent was obtained on the basis of Helsinki Declaration by the World Medical Association (WMA). Tissues were collected from elective abortion of uncomplicated pregnancies, without medical indication. The embryonic tissue was sex genotyped as previously described, using polymerase

chain reaction (PCR) for AMELX/AMELY [13]. Endometrium and embryonic tissue from first trimester was used for genotyping analysis to identify informative SNPs in *IGF2/H19* ICR1 region. In addition, four intact placental villi from different parts of the same placenta (V1 to V4) were cut at the basal connection with the placental plate and individually stored at -80°C for DNA methylation analysis.

Detection of genomic SNPs in the *IGF2/H19* ICR1 region

To identify genomic SNPs in the *IGF2/H19* ICR1 region flanking the 6th binding site for CTCF (Table 1), genomic DNA of decidua and embryo was purified [14] and used for PCR (FW 5'-GTA TTT CTG GAG GCT TCT CCT TC-3' and RV 5'-GAT CAT CAC ATA AGT AGG CGT GAC -3') with conditions 95°C 5 minutes, 35 cycles (95°C 30 seconds, 56°C 30 seconds, 72°C 30 seconds), and 72°C 5 minutes. The DNA fragments were sequenced by LGTC (www.lgtc.nl) and their sequence was aligned to identify SNPs (Table 1).

Bisulfite DNA sequencing

Genomic DNA from four different placental villi was modified and purified using the EpiTec Bisulfite Kit (Qiagen, Hilden, Germany) according to the manufacturer's instructions. On bisulfite-treated DNA, PCR was performed using previously described bisulfite primers for the *IGF2/H19* ICR1 region flanking the 6th binding site for CTCF [15] (FW 5'-TATGGGTATTTTTGGAGGTTTTTT-3' and RV 5'-AATCCCAAACCATAACACTAAAAC-3'), using AmplitaqTaq Gold DNA Polymerase (Applied Biosystems, CA, USA). PCR conditions were 95°C 5 minutes, 50 cycles (94°C 45 seconds, 59°C 45 seconds, 72°C 45 seconds) and 72°C 10 minutes. The resulting amplicons were cloned using pENTR 5'-TOPO TA Cloning kit (Invitrogen, Carlsbad, CA) according to manufacturer's instructions. The bacterial transformation was carried out in *E. coli* TOP10 (Invitrogen, Carlsbad, CA). The obtained colonies were screened by PCR and positive clones were sequenced as above.

Results

We have investigated first the presence of informative genomic SNPs in the *IGF2/H19* ICR1 in six aborted pregnancies from first trimester (Table 1). Three SNPs (rs10732516:G>A, rs2071094:G>T, rs2107425:C>T) were heterozygous in Pregnancy 1 embryonic DNA and homozygous in corresponding maternal DNA (Table 1). Pregnancy 5 showed one SNP (rs2107425:C>T) to be heterozygous in embryonic DNA and homozygous in maternal DNA. However, the other four pregnancies (Pregnancies 2, 3, 4 and 6) showed same homozygous or heterozygous SNPs in both embryonic and maternal DNA. Therefore, only Pregnancies 1 and 5 were included in further analysis.

The *IGF2/H19* ICR1 region analyzed contains 23 CpG sites (Fig 1). Interestingly, one of three identified informative genomic SNPs, rs10732516:G>A, is located on a CpG (CpG7 in Fig 1). For CpG7 (rs10732516) in Pregnancy 1, maternal alleles were AA (or TT in the reverse

strand) in DNA while embryonic alleles were AG (or TC). After bisulfite treatment, maternal T and methylated paternal C stay as T and C respectively, whereas unmethylated paternal C will be converted into T. Consequently, in bisulfite sequence of embryo, we could not tell whether the "T" in CpG7 is from maternal allele "T" or is from conversion of the unmethylated paternal allele "C". Therefore, CpG7 was not taken into account in the analysis of methylation of *IGF2/H19* ICR1. We investigated the spatial pattern of methylation of the *IGF2/H19* ICR1 in 4 different placental villi (and embryo) from Pregnancy 1. The density of methylation in the placental villi (excluding CpG7) was 124/147 (84.4%) in V1, 107/142 (75.4%) in V2, 128/149 (85.9%) in V3, 108/112 (96.4%) in V4 and 68/86 (79.1%) in the embryo (Fig 1A). From the presence of two informative SNPs (rs2071094:G>T, rs2107425:C>T), the general hypermethylated pattern of DNA resulted from a technical bias and that in each of the placental villi (and embryo) analyzed

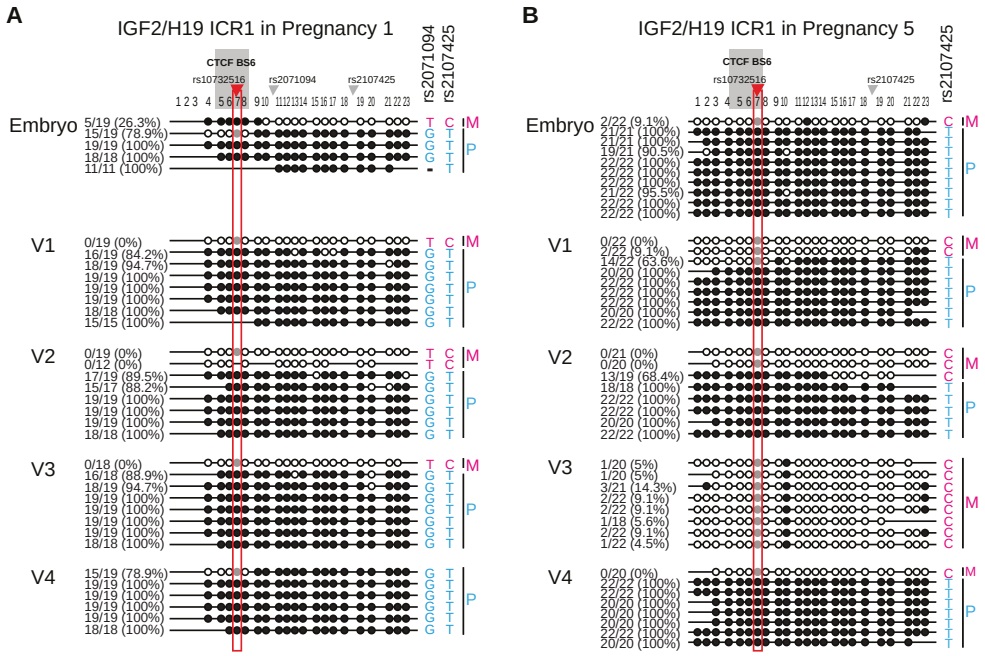

Fig 1. *IGF2/H19* ICR1 methylation profile in two pregnancies.

(**A**,**B**) The individual methylation sequence of the IGF2/H19 ICR1 as determined by bisulfite sequencing of the individual placenta villi V1, V2, V3 and V4 and the embryo tissue in Pregnancy 1 (**A**) and Pregnancy 5 (**B**). A black circle indicates a methylated CpG site and an open circle represents an unmethylated CpG site. A grey circle indicates the allele "T" in CpG7 of bisulfite sequence. The percentage of methylated CpG is given as well as the number of methylated CpG sites and total number of sequenced CpG sites. The nucleotides of the informative SNP sites rs2071094 and rs2107425 in *IGF2/H19* ICR1 are depicted in pink (maternal) and blue (paternal) for the different alleles. In the analyzed DNA stretch, the position of the 6th CTCF binding site includes CpG 5-8, the informative SNP rs2071094 is present between CpG 10 and CpG 11 and the informative SNP rs2107425 is present between CpG 18 and CpG 19.

the maternal allele (rs2071094:T, rs2107425:C) was demethylated, whereas the paternal allele (rs2071094:G, rs2107425:T) was methylated.

Next, we investigated the spatial pattern of methylation of the *IGF2/H19* ICR1 in 4 different placental villi (and embryo) in Pregnancy 5. The density of methylation in the placental villi (excluding CpG7) was 144/194 (74.2%) in V1, 116/164 (70.7%) in V2, 12/167 (7.8%) in V3, 146/166 (88.0%) in V4 and 194/217 (89.4%) in the embryo (Fig 1B). In each of the placental villi (and embryo) analyzed, the maternal allele (rs2107425:C) was demethylated, whereas the paternal allele (rs2107425:T) was methylated.

Discussion

In humans, *H19*, but not *IGF2*, has been reported to be biallelically expressed at least in cytotrophoblasts before W10, but to become monoallelically expressed in placentas at term [4-6, 16]. In agreement, several studies have reported that the *IGF2/H19* ICR1 is normally imprinted, or slightly hypomethylated, in term placentas [5, 8-11, 17, 18]. However, of those studies only Turan and colleagues used a methylation sensitive restriction enzyme (*Mlu*I) in combination with the restriction enzyme *Cfo*I (GCGC) to identify an informative SNP rs10732516 present in the 6th CTCF binding site, being able to identify allele-specific DNA methylation and reported a spatial variation in some term placentas [11]. In a recent study, Buckberry and colleagues compared the methylation status of the *IGF2/H19* ICR1 between term placentas and first trimester placentas (W6-W12) and found no differences in mean methylation levels in the 6th CTCF binding site [5]. However, those authors used only one site of collection and although they discriminated between allele-specific expression, they were unable to discriminate between the parental alleles regarding the methylation of the *IGF2/H19* ICR1, reporting only global DNA methylation levels.

Here, we have investigated for the first time the spatial pattern of methylation of the *IGF2/H19* ICR1 in first-trimester placental villi of two pregnancies. In the placenta analyzed here, two non-CpG SNPs were informative for identification of allele-specific DNA methylation. The SNP rs2071094:G>T was previously described [2, 19] and a novel one, the SNP rs2107425:C>T which identified both paternal and maternal alleles, one methylated and the other unmethylated and therefore a normal imprint pattern in the *IGF2/H19* ICR1 in the different placental villi and embryo, in contrast to some variability encountered between villi at term [11].

It is important to report a technical bias in bisulfite sequencing data towards hypermethylation that could have resulted from one allele being preferentially amplified or cloned over the other. Therefore, we suggest the combined use of the SNPs rs2071094:G>T and rs2107425:C>T as an important tool in allele-specific DNA methylation studies because it allows discrimination of both alleles and identifying a possible bias of bisulfite sequencing data for imprinting analysis.

The *IGF2/H19* ICR1 is an important region that controls key genes for placental and embryo growth and development. The genomic imprinting in first trimester of pregnancies is

poorly understood and our results represent ongoing steps in understanding the role of epigenetic regulation during human gestation and the identification of a novel informative non-CpG SNP at *IGF2/H19* ICR1, an essential feature for determining allele-specific DNA methylation.

Acknowledgements

We would like to thank N. Benabdallah and F. Brum Machado for help with SNP locations, primer analysis and discussions, and D. van Bruggen for discussions. We thank the Centre for Contraception Sexuality and Abortion (CASA; Leiden and The Hague, the Netherlands) for the human maternal and fetal material.

Funding

NH is funded by the China Scholarship Council (CSC) [NO.201307040026]; SMCdSL is funded by the Interuniversity Attraction Poles-Phase VII, Belgium [IUAP/PAI P7/14].

References

1. Frost JM, Moore GE: The importance of imprinting in the human placenta. PLoS Genet 2010, 6:e1001015.
2. Demars J, Shmela ME, Rossignol S, Okabe J, Netchine I, Azzi S, Cabrol S, Le Caignec C, David A, Le Bouc Y, et al: Analysis of the IGF2/H19 imprinting control region uncovers new genetic defects, including mutations of OCT-binding sequences, in patients with 11p15 fetal growth disorders. Hum Mol Genet 2010, 19:803-814.
3. Ideraabdullah FY, Vigneau S, Bartolomei MS: Genomic imprinting mechanisms in mammals. Mutat Res 2008, 647:77-85.
4. Adam GI, Cui H, Miller SJ, Flam F, Ohlsson R: Allele-specific in situ hybridization (ASISH) analysis: a novel technique which resolves differential allelic usage of H19 within the same cell lineage during human placental development. Development 1996, 122:839-847.
5. Buckberry S, Bianco-Miotto T, Hiendleder S, Roberts CT: Quantitative allele-specific expression and DNA methylation analysis of H19, IGF2 and IGF2R in the human placenta across gestation reveals H19 imprinting plasticity. PLoS One 2012, 7:e51210.
6. Jinno Y, Ikeda Y, Yun K, Maw M, Masuzaki H, Fukuda H, Inuzuka K, Fujishita A, Ohtani Y, Okimoto T, et al.: Establishment of functional imprinting of the H19 gene in human developing placentae. Nat Genet 1995, 10:318-324.
7. Pozharny Y, Lambertini L, Ma Y, Ferrara L, Litton CG, Diplas A, Jacobs AR, Chen J, Stone JL, Wetmur J, Lee MJ: Genomic loss of imprinting in first-trimester human placenta. Am J Obstet Gynecol 2010, 202:391 e391-398.
8. Bourque DK, Avila L, Penaherrera M, von Dadelszen P, Robinson WP: Decreased placental methylation at the H19/IGF2 imprinting control region is associated with normotensive intrauterine growth restriction but not preeclampsia. Placenta 2010, 31:197-202.
9. Penaherrera MS, Jiang R, Avila L, Yuen RK, Brown CJ, Robinson WP: Patterns of placental development evaluated by X chromosome inactivation profiling provide a basis to evaluate the origin of epigenetic variation. Hum Reprod 2012, 27:1745-1753.
10. Rancourt RC, Harris HR, Barault L, Michels KB: The prevalence of loss of imprinting of H19 and IGF2 at birth. FASEB J 2013, 27:3335-3343.
11. Turan N, Katari S, Gerson LF, Chalian R, Foster MW, Gaughan JP, Coutifaris C, Sapienza C: Inter- and intra-individual variation in allele-specific DNA methylation and gene expression in children conceived using assisted reproductive technology. PLoS Genet 2010, 6:e1001033.
12. Oefner CM, Sharkey A, Gardner L, Critchley H, Oyen M, Moffett A: Collagen type IV at the fetal-maternal interface. Placenta 2015, 36:59-68.
13. Heeren AM, Van Iperen L, Klootwijk DB, de Melo Bernardo A, Roost MS, Fernandes MMG, Louwe LA, Hilders CG, Helmerhorst FM, Van der Westerlaken LA: Development of the follicular basement membrane during human gametogenesis and early folliculogenesis. BMC developmental biology 2015, 15:4.
14. Olerup O, Zetterquist H: HLA-DR typing by PCR amplification with sequence-specific primers (PCR-SSP) in 2 hours: an alternative to serological DR typing in clinical practice including donor-recipient matching in cadaveric transplantation. Tissue Antigens 1992, 39:225-235.
15. Kim KP, Thurston A, Mummery C, Ward-van Oostwaard D, Priddle H, Allegrucci C, Denning C, Young L: Gene-specific vulnerability to imprinting variability in human embryonic stem cell lines. Genome Res 2007, 17:1731-1742.
16. Monk D, Arnaud P, Apostolidou S, Hills FA, Kelsey G, Stanier P, Feil R, Moore GE: Limited evolutionary conservation of imprinting in the human placenta. Proc Natl Acad Sci U S A 2006, 103:6623-6628.
17. Guo L, Choufani S, Ferreira J, Smith A, Chitayat D, Shuman C, Uxa R, Keating S, Kingdom J, Weksberg R: Altered gene expression and methylation of the human chromosome 11 imprinted region in small for gestational age (SGA) placentae. Dev Biol 2008, 320:79-91.
18. Rancourt RC, Harris HR, Michels KB: Methylation levels at imprinting control regions are not altered with ovulation induction or in vitro fertilization in a birth cohort. Hum Reprod 2012, 27:2208-2216.
19. Ibala-Romdhane S, Al-Khtib M, Khoueiry R, Blachere T, Guerin JF, Lefevre A: Analysis of H19 methylation in control and abnormal human embryos, sperm and oocytes. Eur J Hum Genet 2011, 19:1138-1143.

Table 1. SNPs present in *IGF2/H19* ICR1 and pregnancy genotypes.

SNPs	Pregnancy 1		Pregnancy 2		Pregnancy 3		Pregnancy 4		Pregnancy 5		Pregnancy 6	
	Embryo	Mother	Embryo	Mother	Embryo	Mother	Embryo	Mother	Embryo	Mother	Embryo	Mother
rs10732516: G>A*	**GA**	**AA**	GG	GG	GG	GG	**GA**	**GA**	**GA**	**GA**	**GA**	nd
rs112620988: T>A	TT	TT	TT	TT	TT	TT	TT	TT	TT	TT	TT	nd
rs34610866: G>-	GG	GG	GG	GG	GG	GG	GG	GG	GG	GG	GG	GG
rs2071094: G>T	**GT**	**TT**	GG	GG	GG	GG	**GT**	**GT**	GG	GG	**GT**	**GT**
rs35678657: G>T	GG	GG	GG	GG	GG	GG	GG	GG	GG	GG	GG	GG
rs373018220: T>A	TT	TT	TT	TT	TT	TT	TT	TT	TT	TT	TT	TT
rs113480908: G>A*	GG	GG	GG	GG	GG	GG	GG	GG	GG	GG	GG	GG
rs56125822: C>T	CC	CC	CC	CC	CC	CC	CC	CC	CC	CC	CC	CC
rs2107425: C>T	**CT**	**CC**	TT	TT	**CT**	**CT**	CC	CC	**CT**	**CC**	CC	CC
rs76162918: C>A*	CC	CC	CC	CC	CC	CC	CC	CC	CC	CC	CC	CC

*Informative SNPs present on a CpG; Bold, heterozygous SNP in embryo; Red bold, heterozygous SNP in embryo and homozygous in mother; nd, not determined.

CHAPTER 6

At term, XmO and XpO mouse placentas show differences in glucose metabolism in the trophectoderm-derived outer zone

Nannan He[1], Shujing Jane Lim[1,#], Joana C. Moreira de Mello[2], Injerreau Navarro[1], Monika Bialecka[1], Daniela C. F. Salvatori[1,3], Lucette A. J. van der Westerlaken[4], Lygia V. Pereira[2,¶], Susana M. Chuva de Sousa Lopes[1,5,¶]

[1]Department of Anatomy and Embryology, Leiden University Medical Center, Leiden, The Netherlands

[2]Department of Genetics and Evolutionary Biology, University of São Paulo, São Paulo, Brazil

[3]Central Laboratory Animal Facility, Leiden University Medical Center, Leiden, The Netherlands

[4]Department of Gynaecology, Leiden University Medical Center, Leiden, The Netherlands

[5]Department for Reproductive Medicine, Ghent University Hospital, Ghent, Belgium

[#]Current address: University of Edinburgh, College of Medicine and Veterinary Medicine, Edinburgh, United Kingdom

[¶]Equal senior authorship contribution

Frontiers in Cell and Developmental Biology 2017, 5(63).

Abstract

Genetic mouse model (39,XO) for human Turner syndrome (45,XO) harboring either a single maternally inherited (Xm) or paternally inherited (Xp) chromosome show a pronounced difference in survival rate at term. However, a detailed comparison of XmO and XpO placentas to explain this difference is lacking. We aimed to investigate the morphological and molecular differences between XmO and XpO term mouse placentas. We observed that XpO placentas at term contained a significantly larger area of glycogen cells (GCs) in their outer zone, compared to XmO, XX and XY placentas. In addition, the outer zone of XpO placentas showed higher expression levels of lactate dehydrogenase (*Ldha*) than XmO, XX and XY placentas, suggestive of increased anaerobic glycolysis. In the labyrinth, we detected significantly lower expression level of trophectoderm (TE)-marker keratin 19 (*Krt19*) in XpO placentas than in XX placentas. The expression of other TE-markers was comparable as well as the area of TE-derived cells between XO and wild-type labyrinths. XpO placentas exhibited specific defects in the amount of GCs and glucose metabolism in the outer zone, suggestive of increased anaerobic glycolysis, as a consequence of having inherited a single Xp chromosome. In conclusion, the XpO genotype results in a more severe placental phenotype at term, with distinct abnormalities regarding glucose metabolism in the outer zone.

Introduction

Turner syndrome is the most common sex chromosome disorder affecting 1 in 2000 live births. It is caused by the loss of genetic material from one of the sex chromosomes and the retained single X chromosome can be inherited either from the mother (Xm) or the father (Xp) [1]. In humans, 99% of the XO fetuses are lost during pregnancy [2, 3]. By contrast, in mice, 90% of embryos with a single Xm survive to term, whereas 40% of embryos with a single Xp are resorbed due to severe placental abnormalities [4-6]. This suggests that the transcription of a single Xm or Xp in mouse placentas is not equivalent and influences development differently, reflecting either a different genome-wide epigenetic landscape between Xp and Xm or the existence of certain paternally imprinted X-linked genes in the mouse placenta.

X chromosome inactivation (XCI) is better understood in mice than in humans [7-11] due to the existence of well-studied genetic substrains of mice. In mice, in female (XX) late blastocysts, the trophectoderm (TE) and primitive endoderm (PE) show imprinted XCI (with an obligatory active Xm) and the epiblast (EPI) shows random XCI (in each cell either the Xm or Xp is active) [7, 10, 12]. In the placenta, the TE-derived cells [trophoblast giant cells (TGCs), spongiotrophoblasts and glycogen cells (GCs) in the outer zone; mononuclear trophoblast cells and syncytiotrophoblast cells in the labyrinth] maintain imprinted XCI (active Xm). By contrast, the chorionic plate and the embryonic endothelial cells of the labyrinth are derived from EPI, therefore showing random XCI.

In humans, there may not be imprinted XCI in the placenta [13-15]. In agreement, by the end of the first trimester, the placental volume between XO and control placenta seemed comparable [16] and the birth weight of XmO and XpO new-born babies was similar [17]. Nevertheless, there is a higher incidence of XpO human fetuses lost during pregnancy [18] and the percentage of patients retaining the XmO is 60%-80% [19-23].

The placenta is a crucial organ during mammalian development, ensuring the selective and directional transport of gases, nutrients and waste products between the maternal blood and the embryonic blood [24]. In mice, the GCs may serve as a potential additional energy source, due to their high glycogen content and sensitivity to glucagon signaling [25]. The placenta is a highly regulative organ that adapts constantly to the maternal environment, for example oxygen tension and hypoxia [26, 27], availability of nutrients or calorie restriction [28] and exposure to maternal hormones [29, 30] to sustain optimal embryonic growth throughout pregnancy.

Interestingly, (epi)genetic abnormalities that affect placental development trigger an adaptive response in the placenta to suppress the decreased efficiency to support embryonic growth [31-34]. In the case of XO embryos, embryonic day (E)8.5 XpO embryos had been shown to have small ectoplacental cones [35]. However, by E14, XpO placentas had caught up in size and some showed a larger outer zone [36]. At E18.5, XpO placentas were significantly heavier than XX controls [5]. But in a later study, XmO, XpO and XY placentas were found heavier than XX placentas [37].

To date, a detailed comparison of XmO and XpO term placentas, in particular the TE-derived part of the placenta, is missing. Here, we show that E18.5 XpO placentas exhibited significantly larger area occupied by GCs in outer zone when compared to XmO, XX and XY placentas. Moreover, the expression of *Ldha*, coding for the enzyme that converts lactate to pyruvate through anaerobic glycolysis, was significantly higher in outer zone of XpO placentas than the XmO, XX and XY placentas, suggesting increased anaerobic glycolysis and underlying possible defects in oxygen availability in XpO placentas. In conclusion, the XpO genotype results in a more severe placental phenotype at term, with distinct abnormalities regarding glucose metabolism in the outer zone.

Materials and Methods

Mice and genotyping

All animal tissues used in this work were a generous gift from P. Burgoyne in accordance with the United Kingdom Animals Scientific Procedures Act 1986 and approved by the local ethical committee of the National Institute of Medical Research, London. MF1 mice bearing XX and XY embryos were from XX x XY crossings. XmO and XpO mice were generated as previously described [37]. Briefly, XmO animals were produced by crossing XX females with XYO males, and identified by visual detection of female genitalia; the XYO males were generated by crossing XPafO females with XY* males. The XpO animals were generated by crossing In(X) Paf/X females with XY males. All females (In(X)/X, XXPaf and XpO) were karyotyped with trypsin-Giemsa banding using fresh liver to identify the XpO embryos (with 39 chromosomes as opposed to 40 chromosomes).

Placenta collection and histology

From a total of 12 litters, E18.5 embryos were isolated in phosphate buffer saline (PBS) and separated into males and females by morphology and genotyped as above. The placentas were dissected into quarters and some quarters were collected for RNA isolation after removal of the outer zone (Jz, TGCs and decidua), whereas others were fixed in 4% paraformaldehyde (PFA, Merck, Darmstadt, Germany) at 4°C overnight (o/n), washed in PBS and dehydrated through increasing concentrations of ethanol and finally xylene, embedded in paraffin and serially sectioned (5 μm) in the sagittal plane using a microtome (Leica RM2055, Nussloch, Germany) in the medial-to-lateral direction (N=3 XX, N=3 XY, N=5 XmO, N=4 XpO).

Prior to Periodic acid-Shiff (PAS) staining, sections were deparaffinised in xylene, rehydrated through a series of ethanol solutions and incubated 30 minutes at 56°C in pre-heated 1% periodic acid (Sigma-Aldrich, St. Louis, USA), rinsed in water, immersed in Schiff's reagent (Klinipath, Duiven, The Netherlands) 30 minutes at room temperature (RT), rinsed in water and counterstained with Mayer's haematoxylin (Merck, Darmstadt, Germany). Congo red, Masson's trichrome and Hematoxylin-eosin staining were performed using standard histological procedures. Stained sections were washed in water, dehydrated through a series of ethanol, xylene and mounted in Entellan (Merck, Darmstadt, Germany).

Quantitative reverse-transcription polymerase chain reaction (QPCR)

QPCR was performed on placental quarters after removal of the outer zone and analyzed as described [38]; or on RNA material isolated from 5x paraffin sections of the outer zone using RecoverAll total nucleic acid isolation kit (AM1975, Ambion, Carlsbad, CA, USA) following the manufacturer's protocol. For normalization, the ΔΔCt method was used with the reference genes *Ubc* and *B2m*, stably expressed in mouse placenta [39]. All individual placentas were analysed in technical triplicates. The fold change in expression was calculated relative to the XX1 placenta. Briefly, the average ΔCt value from the technical triplicates of the XX1 (Ave ΔCt XX1) was calculated. Next, we subtracted Ave ΔCt XX1 from each ΔCt (ΔΔCt) and the relative fold change (2^-(ΔΔCt)) calculated. The fold change of each of the triplicate values per placenta was then averaged (mean) and the standard deviation was calculated. The primers used are listed in S1 Table.

Immunofluorescence

Paraffin sections were deparaffinised and used for immunofluorescence as previously described [40]. Primary antibodies used were rabbit anti-KRT19 (or keratin 19) (1:250; ab52625, Abcam, Cambridge, UK) and rat anti-EMCN (or endomucin) (1:150; sc-65495, Santa Cruz Biotechnology, Santa Cruz, CA, USA). Afterwards, sections were washed in 0.05% Tween-20/PBS, treated with 0.3% Sudan Black B (Edward Gurr Ltd, London, UK) in 70% ethanol for 5 minutes to eliminate background autofluorescence from red blood cells [41] and incubated with secondary antibodies diluted in blocking solution for 1 hour at RT. Secondary antibodies were Alexa Fluor 488 goat anti-rabbit (1:500; A-11034, Life Technologies, Eugene, OR, USA) and Alexa Fluor 555 goat anti-rat (1:500; A-21434, Life Technologies, Eugene, OR, USA). Nuclei were stained with 4',6-diamidino-2-phenylindole (DAPI) (Vector Laboratories, Peterborough, UK) and sections were mounted in Prolong Gold anti-fade reagent (Life technologies, Eugene, OR, USA). Slides used for isotype controls were treated as above using rabbit immunoglobulin fraction (1:250; X0903, Dako, Heverlee, Belgium) and rat IgG2a (1:150, MAB006, R&D Systems, Minneapolis, MN, USA) instead of the primary antibodies.

Imaging and quantification

Bright-field images were taken on an Olympus AX70 microscope (Olympus, Zoeterwoude, Netherlands) equipped with a digital camera (Olympus XC50, Tokyo, Japan). Fluorescence images were acquired on a Leica DMRA fluorescence microscope (Leica, Wetzlar, Germany) with a CoolSnap HQ2 camera (Photometrics, Tucson, USA) or a Leica AF6000 fluorescence microscope with a Hamamatsu EM-CCD C9100 camera (Leica Microsystems, Wetzlar, Germany). Quantification was performed in ImageJ 1.48 (http://imagej.nih.gov/ij).

Statistical analysis

The statistical analyses of the proportion of glycogen cells area in the outer zone of the placentas, the percentage of fetal vascular space, the area occupied by TE-derived cells in the

labyrinth and differential gene expression per genotype were performed using one-way ANOVA with the Tukey-HSD applied for post hoc testing, using statistical software package SPSS 20.0 (SPSS Inc., Chicago, IL, USA). $P<0.05$ was considered significant.

Results

At term, XpO placentas showed larger area occupied by GCs in the outer zone

We investigated the placental morphology of the four genotypes (N=3 XX, N=3 XY, N=5 XmO, N=3 XpO) at E18.5 using PAS-staining. This allowed us to distinguish the outer zone from the labyrinth (Fig 1A). We observed the presence of a broader outer zone in the lateral part of XmO (N=2 in 5, 40%) and XpO (N=3 in 3, 100%) placentas (Fig 1A). To quantify the area occupied by GCs in the outer zone, the ratio of the area occupied by GCs in the outer zone was calculated on individual placental sections (n=3-5 medial sections per placenta, containing a visible connection to the umbilical cord) (Fig 1B-C). The XpO placentas contained a significantly larger area occupied by GCs in the outer zone when compared to XX, XY and XmO placentas (P=0.004, 0.008 and 0.045 respectively, Fig 1C). In contrast, the area occupied by GCs in the outer zone of XmO placentas was comparable to that of XX and XY placentas (Fig 1C).

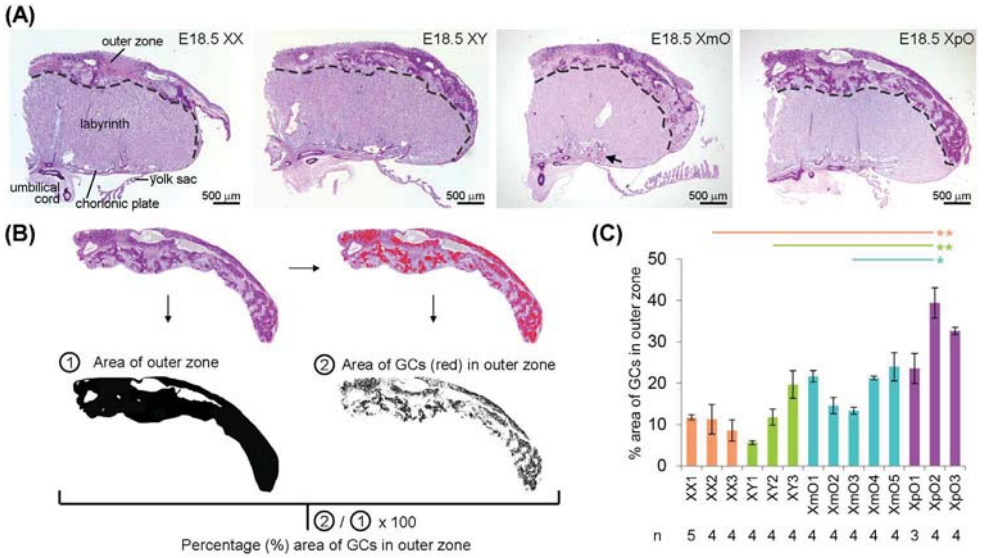

Fig 1. XpO placentas have a larger area occupied by glycogen cells in the outer zone.

(**A**) Representative PAS-stained medial placental sections of the different genotypes (XX, XY, XmO, XpO). (**B**) From the images acquired by microscopy, the outer zone of the placenta is digitally selected, then converted to black-and-white on ImageJ to provide the total area of the outer zone. From the selected outer zone of the placenta, the dark PAS-stained glycogen cells (GCs) are identified digitally (red cells) by selecting a threshold on Image J. The percentage of the GCs in the outer zone of each placenta section is obtained by using the ratio of the area of GCs ②/total area of the outer zone ①. (**C**) Graph depicting the percentage (%) area of outer zone occupied by GCs in the different genotypes (XX, XY, XmO, XpO). Significant P values between XpO placentas and the other genotypes are indicated by * (P<0.05) and ** (P<0.01).

At term, XpO placentas showed increased *Ldha* expression in the outer zone

The larger area of GCs in outer zone of XpO placentas led us to investigate defects in gene expression related to glucagon signaling and glucose metabolism (Fig 2A) in the outer zone. The expression level of glucagon receptor (*Gcgr*) as well as of glucose transporter *Slc2a1*, which mediate passive glucose uptake in cells [42] was similar between XmO, XpO and XX placentas (Fig 2B, S2 Table).

Two X-linked genes, *G6pdx* and *Pgk1*, encode essential enzymes in the conversion of glucose to pyruvate [43, 44]. In the outer zone, *G6pdx* showed significantly lower expression in both XmO and XpO placentas compared to the XX placentas (XmO versus XX: *P*=0.028; XpO versus XX: *P*=0.007; Fig 2B, S2 Table). However, expression of *Pgk1* was significantly higher in XpO placentas than in XmO placentas (*P*=0.009, Fig 2B, S2 Table).

Under normal oxygen supply (aerobic glycolysis), pyruvate is catabolized into acetyl-CoA to be used in the tricarboxylic acid (TCA) cycle to produce energy efficiently (Fig 2A). One of the enzymes of the TCA cycle, encoded by X-linked gene *Idh3g*, showed similar expression between XO and wild-type placentas (Fig 2B, S2 Table). However, if oxygen supply is low, pyruvate is metabolized to lactate (anaerobic glycolysis). In anaerobic glycolysis, the key

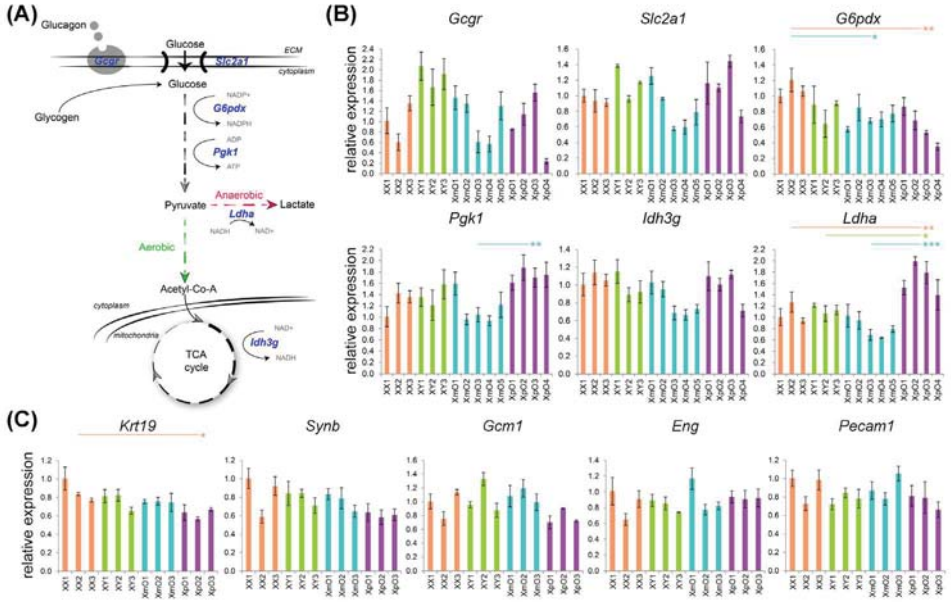

Fig 2. Expression of genes related to glucose metabolism in the outer zone and expression of genes related to TE and vasculature in the labyrinth.

(**A**) Scheme of glucose metabolism cascade, with the genes analyzed in blue. (**B**) Relative expression of the depicted genes in the outer zone of XX, XY, XmO, XpO placentas. Each bar represents mean ± standard deviation of technical triplicates of a different placenta. Significant *P* values between genotypes are indicated by * (*P*<0.05), ** (*P*<0.01) and *** (*P*<0.001). (**C**) Relative expression of the depicted genes in the labyrinth of XX, XY, XmO, XpO placentas. Each bar represents mean ± standard deviation of technical triplicates of a different placenta. Significant *P* value between XX and XpO is indicated by * (*P*<0.05).

enzyme that converts pyruvate into lactate is encoded by the *Ldha* gene. The expression levels of *Ldha* in the outer zone of XpO placentas were significantly higher than in the other placentas (XpO versus XX: P=0.007; XpO versus XY: P=0.015; XpO versus XmO: P<0.001; Fig 2B, S2 Table), suggesting higher levels of anaerobic respiration specifically in the outer zone of the XpO placentas, where a higher incidence of GCs was found.

The labyrinths of XO and wild-type placentas were comparable

Next, we determined the relative expression of TE markers [keratin 19 (*Krt19*), syncytin b (*Synb*), glial cells missing homolog 1 (*Gcm1*)] and endothelial markers [endoglin (*Eng*), platelet/endothelial cell adhesion molecule 1 (*Pecam1*)] in the labyrinth of the four types of placentas.

The expression levels of TE-marker *Krt19* in the labyrinth of XpO placenta were significantly lower than that in XX placenta (P=0.024, Fig 2C, S2 Table). However, the TE-markers *Synb* and *Gcm1* were similarly expressed in the four types of placentas (Fig 2C, S2 Table). There was also no difference in the expression of endothelial-markers *Eng* and *Pecam1* in the labyrinth (Fig 2C, S2 Table). Together, the data suggests that the labyrinth of XO placentas may be similar to wild-type placentas.

To further confirm that, we quantified the area occupied by (EMCN-positive) fetal capillaries and (KRT19-positive) TE-derived cells in the labyrinth (n=3-5 sections per individual placenta; N=3 XX, N=3 XY, N=5 XmO, N=4 XpO) (Fig 3). For the quantification, single channel images of the labyrinth zone from medial placental sections immunostained for anti-EMCN (red) and anti-KRT19 (green) and DAPI (details shown in Fig 3B,D,E) were used. The area of the fetal vasculature (Fig 3B), considered the area occupied by the EMCN-positive fetal capillaries, was similar between XO and wild-type labyrinths (Fig 3C, left panel). Moreover, the vascular density, calculated as the number of fetal capillaries per image, was also comparable between XO and wild-type labyrinths (Fig 3C, right panel).

To quantify the area of occupied by TE-derived cells, the nuclei area (DAPI-positive) was merged with the KRT19-positive cytoplasmic staining of the TE derived cells. However, to exclude the nuclear area of the fetal vasculature, we subtracted the fetal vascular area (Fig 3B,D,E). In this way, we obtained the area occupied solely by TE-derived cells (cytoplasm and nuclei). We concluded that the area occupied by TE-derived cells in labyrinth was similar between XO and wild-type placentas (Fig 3E).

At term, XpO placentas showed decreased *Xlr4b/4c* in the labyrinth zone

The X-linked *Xlr3b* has previously been identified as differentially expressed in XmO and XpO brains, but not in the placentas [45]. In addition to *Xlr3b*, *Xlr4b/4c* were also reported to be differentially expressed between XmO and XpO brains, but at least *Xlr4c* not in placentas [46]. However, whole placentas were used for analysis and a possible regional regulation could have been missed. We therefore investigated the expression of *Xlr3b* and *Xlr4b/4c* separately in outer zone and labyrinth zone of term placenta.

We did not observe significantly differential expression of *Xlr3b* and *Xlr4b/4c* in the XpO and XmO outer zones (Fig 4A, S2 Table), even though XpO outer zones had significantly lower *Xlr3b* than XY outer zones (*P*=0.030; Fig 4A, S2 Table). In the labyrinth zone, the expression levels of *Xlr3b* were comparable between genotypes (Fig 4B, S2 Table), but surprisingly XpO labyrinth zone had significantly lower expression levels of *Xlr4b/4c* than the other placentas (XpO versus XX: *P*=0.006; XpO versus XY: *P*<0.001; XpO versus XmO: *P*=0.003; Fig 4B, S2 Table).

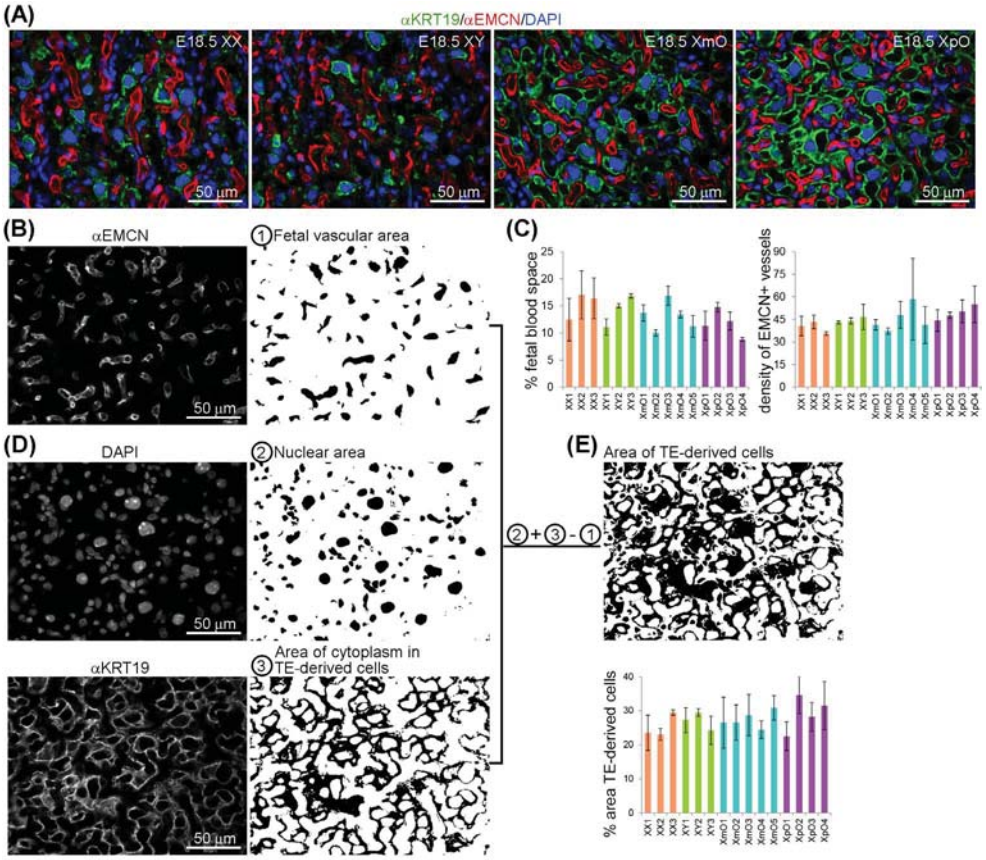

Fig 3. XO placentas show comparable fetal vascular area and TE-derived cell area in the labyrinth.

(**A**) Representative medial placental sections from the different genotypes (XX, XY, XmO, XpO) immunostained for KRT19 and EMCN show the organization of the fetal vasculature and maternal blood space in the labyrinth. (**B**) To quantify the fetal vascular area and density, single channel images for EMCN-positive fetal capillaries are filled with black area ① and either the number of vessels counted (density of fetal vessels in that area) or the percentage of fetal vascular area is quantified (sum of the area of EMCN-positive blood vessels/total area of the image x 100). (**C**) Graph depicting the percentage (%) of area occupied by fetal vasculature and the density of EMCN-positive fetal blood vessels in the different genotypes analyzed (XX, XY, XmO, XpO). (**D**) To calculate the percentage of area occupied by TE-derived cells, the single channel images for DAPI ② and KRT19 ③ are converted to black-and-white, added digitally and finally from that area (②+③) the fetal capillary area is subtracted (②+③-①) (sum of the resulting black area/total area of the image x 100). (**E**) Graph depicts the percentage (%) of area occupied by TE-derived cells in the different genotypes analyzed (XX, XY, XmO, XpO).

At term, XmO placentas contained higher incidence of fibrin nodules in the maternal arterial sinuses adjacent to the chorionic plate

Interestingly, the XmO placentas contained small nodules, partially occluding some maternal arterial sinuses proximal of the chorionic plate (black arrow in Fig 1A). After Congo red, Masson's trichrome and Hematoxylin-eosin staining, we concluded that those were fibrin deposits (Fig 5A).

To quantify the incidence of fibrin nodules in the different placentas (N=3 XX, N=3 XY, N=5 XmO, N=4 XpO), we manually counted the number of fibrin nodules present in medial placental sections. All XmO placentas contain fibrin deposits in most sections analyzed, whereas the nodules were not observed in most of the other placentas (XmO versus XX: P=0.0007; XmO versus XY: P=0.0007; XmO versus XpO: P=0.0019; Fig 5B). On average, per section one or two nodules were observed (Fig 5A,C).

Discussion

The lack of a second sex chromosome in XO mouse embryos leads to the development of smaller trophectoderm ectoplacental cones and, in some cases, pregnancy loss [5, 6, 35, 37, 47]. Our study on XO placental abnormalities in mice shows that inheriting the single X chromosome from the paternal or maternal side leads to different placental phenotypes: E18.5 XpO placentas contained a larger area of GCs in the outer zone with a possible consequent increase in anaerobic glycolysis and/or oxygen availability. This does not seem to be the case in XmO placentas. By contrast, XmO placentas show increased incidence of small fibrin nodules in maternal arterial sinuses proximal of the chorionic plate.

The placenta is sensitive to defects in epigenetic regulation, such as regulation of imprinted genes and imprinted X inactivation [31-33]. As such, it is not surprising that many imprinted and X-linked genes are expressed in the placenta and regulate metabolism and growth [31, 33, 34]. Defects in the epigenetic regulation of imprinted regions/genes often result in expansion

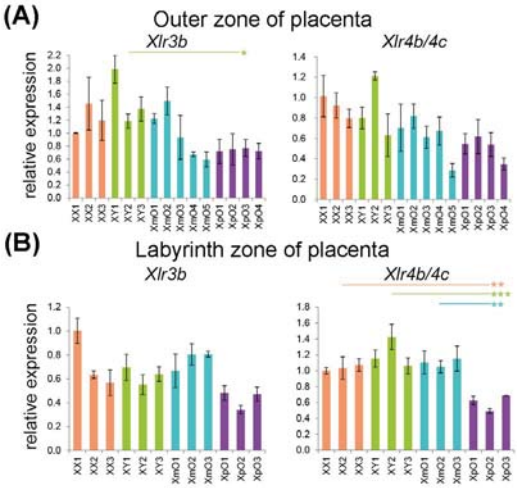

Fig 4. *Xlr* genes expression in the outer zone and labyrinth zone of term placentas.

(**A**-**B**) Relative expression of Xlr3b and Xlr4b/4c in the outer zone (**A**) and labyrinth zone (**B**) of XX, XY, XmO, XpO placentas. Each bar represents mean ± standard deviation of technical triplicates of a single placenta. Significant *P* values between genotypes are indicated by * (P<0.05), ** (P<0.01) and *** (P<0.001).

of the outer zone of the placenta [31, 33, 34]. The higher incidence of GCs in the outer zone of XpO placentas may be such an adaptive response to placental insufficiency. Studies in mice show that XpO fetuses have a higher risk of being lost during pregnancy, whereas XmO fetuses generally have a better chance of surviving to term [6, 35]. In XX fetuses, the Xp is preferentially inactivated in the TE-derived tissues [48]. Thus, in both females and males, it is the Xm that is active in TE-derived tissues during placental development. Epigenetic differences between Xp and Xm, including genome-wide differences in chromatin condensation or the existence of X-linked paternally imprinted genes in the placenta, could explain why XpO embryos have a higher risk of being lost during pregnancy.

Alternatively, as a smaller trophectoderm ectoplacental cone in XO embryos is often associated with a delay in embryonic development [35, 37, 47], the alteration observed in GCs in outer zone of XpO placentas could reflect a general small delay in development instead of an (active) adaptive response. Interestingly, it has been shown that both the number of GCs and the

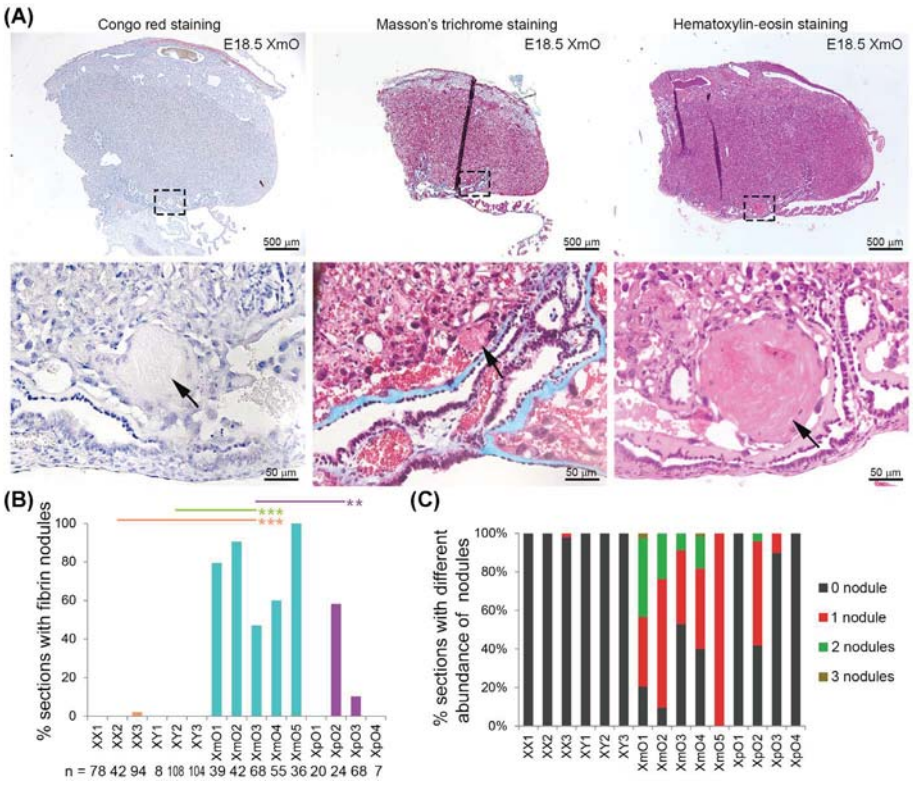

Fig 5. Identifications and quantification of fibrin deposits in term placentas.

(**A**) Representative medial XmO placenta sections with Congo red, Masson's trichrome and Hematoxylin-Eosin staining. The dashed boxes in top panels are shown as magnification in bottom panels. Black arrows point to fibrin deposits. (**B**) Graph depicting the percentage (%) of placental sections with fibrin nodules per histological section (n) in different genotypes. Significant *P* values between XmO placentas and the other genotypes are indicated by ** (*P*<0.01) and *** (*P*<0.001). (**C**) Graph depicting the percentage (%) of placental sections with different abundance of fibrin nodules per histological section (n) in different genotypes.

volume of the junctional zone increases during gestation, peaks at E16.5, followed by reduction until birth [25, 49]. Therefore, if the physiological regression of GCs in XpO placentas was delayed, this would result in relatively more GCs and increased size of the outer zone at E18.5 compared to wild-type placentas.

Abnormal GC numbers, related to impaired glucose transport and glycogen metabolism in placenta [50, 51], have been reported in several mutant mouse placentas, including that of X-linked and imprinted genes, and usually result in runting. Opposite phenotypes regarding GCs numbers can still develop in mouse mutants showing a normal placenta at E10.5. As the XpO phenotype, maternally inherited defects in X-linked *Evx1* also showed higher numbers of GCs, spongiotrophoblasts and secondary TGCs by E14.5 and the mutant pups were smaller at birth [52]. By contrast, *Cited2* KO and the imprinted (paternally-expressed) *Igf2* KO mice show severe reduction of numbers of GCs, spongiotrophoblasts and secondary TGCs at E12.5-13.5 [53, 54], but this also resulted in reduced weight at birth [51]; whereas the imprinted (maternally-expressed) *Cdkn1c* (or *p57Kip2*) KO showed placentomegaly, with larger labyrinth zone and excess of spongiotrophoblasts, but normal number of GCs and TGCs and no difference in the weight of embryos [55].

It is unclear whether Xlr factors are directly involved in glucose metabolism, but they could impact on cell differentiation in the outer zone towards GC cells. We observed similar expression of *Xlr3b* and *Xlr4b/4c* in XpO and XmO outer zones suggesting that these genes are not involved in the production of GCs and are not imprinted in the (TE-derived) outer zone. However, the biological significance of the specific decrease in *Xlr4b/4c* in XpO labyrinth remains to be investigated. If this decrease is not due to imprinting in TE-derived labyrinth cells (mononuclear trophoblast and syncytiotrophoblast cells), then perhaps *Xlr4b/4c* could be imprinted and silenced on the Xp in the EPI-derived endothelial cells of the labyrinth, in line with the reported imprint in the brain (Raefski and O'Neill, 2005). This could explain the 40% reduction in expression observed.

Small fibrin nodules, most probably from maternal blood-clots, were observed in the maternal sinus of all XmO placentas, but not in most of the other placentas. Interestingly, TE-derived cells at the fetal-maternal interface in both mouse and human exhibit endothelial-like properties (endovascular extravillous trophoblast cells and syncytiotrophoblast cells in humans; syncytiotrophoblast cells in mice) and seem to be involved in the regulation of coagulation during pregnancy [56]. Fibrin deposits are occasionally described in the labyrinth and spongiotrophoblast area of mouse placentas [57, 58]; and in the perivillous space, associated with local syncytial denudation, in human placentas [59, 60]. Excessive fibrin deposits at the fetal-maternal interface early during development, such as in *Procr* (or *Epcr*) KO embryos results in severe placental thrombosis and lethality at E10.5 [61]; whereas in *Wnt2* KO embryos showed fibrin deposits between E14-18 with maternal blood accumulation in the labyrinth zone, resulting in 50% viability and smaller pups at birth [62]. The fibrin deposits in XmO placentas indicate excessive activation of the coagulation cascade in the maternal circulation, but this obstruction was not as

severe as in *Wnt2* KO mice and, as such, does not seem to be pathological.

In conclusion, mouse embryos with a single Xp have a lower chance than XmO embryos to survive to term due to placental insufficiency. Here, we show that XmO and XpO term placentas differ significantly in the amount of GCs in the outer zone and that XpO placentas may have shifted towards anaerobic glycolysis. This shift in glucose metabolism does not seem to be a direct consequence of altered expression of X-linked genes involved in this metabolism (although *Pgk1* expression differs between XmO and XpO outer zones), but rather a consequence of an altered cellular composition of the XpO outer zone (large GCs area) due to placental adaptive response earlier during development. Our findings highlight the need to investigate glucose metabolism in the placenta of human Turner patients, which may provide individual potential therapeutic strategies for Turner syndrome.

Acknowledgements

We would like to express our gratitude to A. Ojarikre, and P. Burgoyne, MRC National Institute for Medical Research, the Ridgeway, Mill Hill, London, UK for the work involved in mouse husbandry, the logistics of the crossings and timed mattings and for performing the genotyping/karyotyping of the embryos; L. van Iperen for histology; B. Reinius for isolating RNA; J. Goeman for advise on the statistical test to use and A. Zwijsen and N. Criem for useful discussions.

Funding

NH is funded by the China Scholarship Council (CSC) [NO.201307040026]; JCMdM is funded by Fundação de Amparo à Pesquisa do Estado de São Paulo (FAPESP) [2009/17481-6; 2015/03610-0] and LVP by Fundação de Amparo à Pesquisa do Estado de São Paulo (FAPESP) [CEPID 13/08135-2]; SMCdSL is funded by the Interuniversity Attraction Poles-Phase VII, Belgium [IUAP/PAI P7/14].

References

1. Saenger P: Turner's syndrome. N Engl J Med 1996, 335:1749-1754.
2. Cockwell A, MacKenzie M, Youings S, Jacobs P: A cytogenetic and molecular study of a series of 45,X fetuses and their parents. J Med Genet 1991, 28:151-155.
3. Ranke MB, Saenger P: Turner's syndrome. Lancet 2001, 358:309-314.
4. Burgoyne PS, Evans EP, Holland K: XO monosomy is associated with reduced birthweight and lowered weight gain in the mouse. J Reprod Fertil 1983, 68:381-385.
5. Burgoyne PS, Tam PP, Evans EP: Retarded development of XO conceptuses during early pregnancy in the mouse. J Reprod Fertil 1983, 68:387-393.
6. Hunt PA: Survival of XO mouse fetuses: effect of parental origin of the X chromosome or uterine environment? Development 1991, 111:1137-1141.
7. Payer B, Lee JT: X chromosome dosage compensation: how mammals keep the balance. Annu Rev Genet 2008, 42:733-772.
8. Payer B, Lee JT: Coupling of X-chromosome reactivation with the pluripotent stem cell state. RNA Biol 2014, 11:798-807.
9. Petropoulos S, Panula SP, Schell JP, Lanner F: Single-cell RNA sequencing: revealing human pre-implantation development, pluripotency and germline development. J Intern Med 2016, 280:252-264.
10. Okamoto I, Patrat C, Thepot D, Peynot N, Fauque P, Daniel N, Diabangouaya P, Wolf JP, Renard JP, Duranthon V, Heard E: Eutherian mammals use diverse strategies to initiate X-chromosome inactivation during development. Nature 2011, 472:370-374.
11. Deng X, Berletch JB, Nguyen DK, Disteche CM: X chromosome regulation: diverse patterns in development, tissues and disease. Nat Rev Genet 2014, 15:367-378.
12. Silva J, Nichols J, Theunissen TW, Guo G, van Oosten AL, Barrandon O, Wray J, Yamanaka S, Chambers I, Smith A: Nanog is the gateway to the pluripotent ground state. Cell 2009, 138:722-737.
13. de Mello JCM, de Araujo ESS, Stabellini R, Fraga AM, de Souza JES, Sumita DR, Camargo AA, Pereira LV: Random X inactivation and extensive mosaicism in human placenta revealed by analysis of allele-specific gene expression along the X chromosome. PloS one 2010, 5:e10947.
14. Penaherrera M, Jiang R, Avila L, Yuen R, Brown C, Robinson W: Patterns of placental development evaluated by X chromosome inactivation profiling provide a basis to evaluate the origin of epigenetic variation. Human reproduction 2012, 27:1745-1753.
15. Hamada H, Okae H, Toh H, Chiba H, Hiura H, Shirane K, Sato T, Suyama M, Yaegashi N, Sasaki H: Allele-specific methylome and transcriptome analysis reveals widespread imprinting in the human placenta. The American Journal of Human Genetics 2016, 99:1045-1058.
16. Wegrzyn P, Faro C, Falcon O, Peralta C, Nicolaides K: Placental volume measured by three-dimensional ultrasound at 11 to 13+ 6 weeks of gestation: relation to chromosomal defects. Ultrasound in obstetrics & gynecology 2005, 26:28-32.
17. Mathur A, Stekol L, Schatz D, MacLaren N, Scott M, Lippe B: The parental origin of the single X chromosome in Turner syndrome: lack of correlation with parental age or clinical phenotype. American journal of human genetics 1991, 48:682.
18. Jacobs P, Hassold T, Harvey J, May K: The origin of sex chromosome aneuploidy. Progress in clinical and biological research 1989, 311:135.
19. Álvarez-Nava F, Lanes R, Quintero JM, Miras M, Fideleff H, Mericq V, Marcano H, Zabala W, Soto M, Pardo T: Effect of the parental origin of the X-chromosome on the clinical features, associated complications, the two-year-response to growth hormone (rhGH) and the biochemical profile in patients with turner syndrome. International journal of pediatric endocrinology 2013, 2013:10.
20. Sagi L, Zuckerman-Levin N, Gawlik A, Ghizzoni L, Buyukgebiz A, Rakover Y, Bistritzer T, Admoni O, Vottero A, Baruch O: Clinical significance of the parental origin of the X chromosome in turner syndrome. The Journal of Clinical Endocrinology & Metabolism 2007, 92:846-852.
21. Ko JM, Kim JM, Kim GH, Lee BH, Yoo HW: Influence of parental origin of the X chromosome on physical

phenotypes and GH responsiveness of patients with Turner syndrome. Clinical endocrinology 2010, 73:66-71.

22. Uematsu A, Yorifuji T, Muroi J, Kawai M, Mamada M, Kaji M, Yamanaka C, Momoi T, Nakahata T: Parental origin of normal X chromosomes in Turner syndrome patients with various karyotypes: implications for the mechanism leading to generation of a 45, X karyotype. American journal of medical genetics 2002, 111:134-139.
23. Monroy N, López M, Cervantes A, García-Cruz D, Zafra G, Canún S, Zenteno JC, Kofman-Alfaro S: Microsatellite analysis in Turner syndrome: parental origin of X chromosomes and possible mechanism of formation of abnormal chromosomes. American journal of medical genetics 2002, 107:181-189.
24. Jansson T: Placenta plays a critical role in maternal-fetal resource allocation. Proc Natl Acad Sci U S A 2016, 113:11066-11068.
25. Coan PM, Conroy N, Burton GJ, Ferguson-Smith AC: Origin and characteristics of glycogen cells in the developing murine placenta. Dev Dyn 2006, 235:3280-3294.
26. Adelman DM, Gertsenstein M, Nagy A, Simon MC, Maltepe E: Placental cell fates are regulated in vivo by HIF-mediated hypoxia responses. Genes Dev 2000, 14:3191-3203.
27. Higgins JS, Vaughan OR, Fernandez de Liger E, Fowden AL, Sferruzzi-Perri AN: Placental phenotype and resource allocation to fetal growth are modified by the timing and degree of hypoxia during mouse pregnancy. J Physiol 2016, 594:1341-1356.
28. Ganguly A, Collis L, Devaskar SU: Placental glucose and amino acid transport in calorie-restricted wild-type and Glut3 null heterozygous mice. Endocrinology 2012, 153:3995-4007.
29. Fowden AL, Sferruzzi-Perri AN, Coan PM, Constancia M, Burton GJ: Placental efficiency and adaptation: endocrine regulation. J Physiol 2009, 587:3459-3472.
30. Dimasuay KG, Boeuf P, Powell TL, Jansson T: Placental Responses to Changes in the Maternal Environment Determine Fetal Growth. Front Physiol 2016, 7:12.
31. Hemberger M: The role of the X chromosome in mammalian extra embryonic development. Cytogenet Genome Res 2002, 99:210-217.
32. Himes KP, Koppes E, Chaillet JR: Generalized disruption of inherited genomic imprints leads to wide-ranging placental defects and dysregulated fetal growth. Dev Biol 2013, 373:72-82.
33. Lefebvre L: The placental imprintome and imprinted gene function in the trophoblast glycogen cell lineage. Reprod Biomed Online 2012, 25:44-57.
34. Sandovici I, Hoelle K, Angiolini E, Constancia M: Placental adaptations to the maternal-fetal environment: implications for fetal growth and developmental programming. Reprod Biomed Online 2012, 25:68-89.
35. Jamieson RV, Tan SS, Tam PP: Retarded postimplantation development of X0 mouse embryos: impact of the parental origin of the monosomic X chromosome. Dev Biol 1998, 201:13-25.
36. Zechner U, Reule M, Burgoyne PS, Schubert A, Orth A, Hameister H, Fundele R: Paternal transmission of X-linked placental dysplasia in mouse interspecific hybrids. Genetics 1997, 146:1399-1405.
37. Ishikawa H, Rattigan A, Fundele R, Burgoyne PS: Effects of sex chromosome dosage on placental size in mice. Biol Reprod 2003, 69:483-488.
38. de Melo Bernardo A, Heeren AM, van Iperen L, Fernandes MG, He N, Anjie S, Noce T, Ramos ES, de Sousa Lopes SM: Meiotic wave adds extra asymmetry to the development of female chicken gonads. Mol Reprod Dev 2015.
39. María Emilia Solano KT, Mirka Katharina Kowal, Petra Clara Arck: Identification of suitable reference genes in the mouse placenta. Placenta 2016, 39:7-15.
40. Heeren AM, van Iperen L, Klootwijk DB, de Melo Bernardo A, Roost MS, Gomes Fernandes MM, Louwe LA, Hilders CG, Helmerhorst FM, van der Westerlaken LA, Chuva de Sousa Lopes SM: Development of the follicular basement membrane during human gametogenesis and early folliculogenesis. BMC Dev Biol 2015, 15:4.
41. Romijn HJ, van Uum JF, Emmering J, Goncharuk V, Buijs RM: Colocalization of VIP with AVP in neurons of the human paraventricular, supraoptic and suprachiasmatic nucleus. Brain Res 1999, 832:47-53.
42. Zhao FQ, Keating AF: Functional properties and genomics of glucose transporters. Curr Genomics 2007, 8:113-128.

43. Tuttle S, Stamato T, Perez ML, Biaglow J: Glucose-6-phosphate dehydrogenase and the oxidative pentose phosphate cycle protect cells against apoptosis induced by low doses of ionizing radiation. Radiat Res 2000, 153:781-787.

44. Semenza GL, Roth PH, Fang HM, Wang GL: Transcriptional regulation of genes encoding glycolytic enzymes by hypoxia-inducible factor 1. J Biol Chem 1994, 269:23757-23763.

45. Davies W, Isles A, Smith R, Karunadasa D, Burrmann D, Humby T, Ojarikre O, Biggin C, Skuse D, Burgoyne P: Xlr3b is a new imprinted candidate for X-linked parent-of-origin effects on cognitive function in mice. Nature genetics 2005, 37:625-629.

46. Raefski AS, O'Neill MJ: Identification of a cluster of X-linked imprinted genes in mice. Nature genetics 2005, 37:620-624.

47. Thornhill AR, Burgoyne PS: A paternally imprinted X chromosome retards the development of the early mouse embryo. Development 1993, 118:171-174.

48. Harper MI, Fosten M, Monk M: Preferential paternal X inactivation in extraembryonic tissues of early mouse embryos. J Embryol Exp Morphol 1982, 67:127-135.

49. Coan PM, Ferguson-Smith AC, Burton GJ: Developmental dynamics of the definitive mouse placenta assessed by stereology. Biol Reprod 2004, 70:1806-1813.

50. Redline RW, Chernicky CL, Tan HQ, Ilan J, Ilan J: Differential expression of insulin-like growth factor-II in specific regions of the late (post day 9.5) murine placenta. Molecular reproduction and development 1993, 36:121-129.

51. Sibley C, Coan P, Ferguson-Smith A, Dean W, Hughes J, Smith P, Reik W, Burton G, Fowden A, Constancia M: Placental-specific insulin-like growth factor 2 (Igf2) regulates the diffusional exchange characteristics of the mouse placenta. Proceedings of the National Academy of Sciences of the United States of America 2004, 101:8204-8208.

52. Li Y, Behringer RR: Esx1 is an X-chromosome-imprinted regulator of placental development and fetal growth. Nature genetics 1998, 20:309-311.

53. Withington S, Scott A, Saunders D, Floro KL, Preis J, Michalicek J, Maclean K, Sparrow D, Barbera JM, Dunwoodie S: Loss of Cited2 affects trophoblast formation and vascularization of the mouse placenta. Developmental biology 2006, 294:67-82.

54. Lopez M, Dikkes P, Zurakowski D, Villa-Komaroff L: Insulin-like growth factor II affects the appearance and glycogen content of glycogen cells in the murine placenta. Endocrinology 1996, 137:2100-2108.

55. Takahashi K, Kobayashi T, Kanayama N: p57Kip2 regulates the proper development of labyrinthine and spongiotrophoblasts. Molecular human reproduction 2000, 6:1019-1025.

56. Sood R, Kalloway S, Mast AE, Hillard CJ, Weiler H: Fetomaternal cross talk in the placental vascular bed: control of coagulation by trophoblast cells. Blood 2006, 107:3173-3180.

57. Redecha P, van Rooijen N, Torry D, Girardi G: Pravastatin prevents miscarriages in mice: role of tissue factor in placental and fetal injury. Blood 2009, 113:4101-4109.

58. Vogt E, Ng A-K, Rote NS: A model for the antiphospholipid antibody syndrome: monoclonal antiphosphatidylserine antibody induces intrauterine growth restriction in mice. American journal of obstetrics and gynecology 1996, 174:700-707.

59. Nelson DM, Crouch EC, Curran EM, Farmer DR: Trophoblast interaction with fibrin matrix. Epithelialization of perivillous fibrin deposits as a mechanism for villous repair in the human placenta. Am J Pathol 1990, 136:855-865.

60. Khan HM, Khan MY, Minhas LA: Histological study of the developing mouse placenta. Journal of Rawalpindi Medical College 2011, 15:116-119.

61. Gu J-M, Crawley JT, Ferrell G, Zhang F, Li W, Esmon NL, Esmon CT: Disruption of the endothelial cell protein C receptor gene in mice causes placental thrombosis and early embryonic lethality. Journal of Biological Chemistry 2002, 277:43335-43343.

62. Monkley SJ, Delaney SJ, Pennisi DJ, Christiansen JH, Wainwright BJ: Targeted disruption of the Wnt2 gene results in placentation defects. DEVELOPMENT-CAMBRIDGE- 1996, 122:3343-3353.

6

CHAPTER 7

General discussion and future perspectives

Human (extra)gonadal germ cell development

From the extragonadal location in which they originate, human primordial germ cells (PGCs) migrate and arrive at the developing gonadal primordia at approximately week 7 of gestation (W7, or week 5 post conception) [1-3]. Ectopic PGCs have been described in mouse and bovine adrenals [4-6]. Mostly, these ectopic germ cells are eliminated by apoptosis [7, 8]. However, some of them may escape from entering the normal apoptosis pathway and give rise to extragonadal germ cell tumors [9, 10]. Since the gonads have a common somatic origin as adrenal cortex [11-13], the aim of **Chapter 2** is to investigate whether there are human ectopic germ cells in adrenals and to study the development of human (extra)gonad germ cells in first and second trimesters.

Human germ cells (POU5F1-positive and/or DDX4-positive) are present in all W8.4-W22 adrenal glands, but not in kidney. Between first and second trimesters, germ cells gradually downregulate the pluripotency marker POU5F1 and upregulate late germ cell marker DDX4 in both male and female gonads. Human ovarian germ cells do not enter meiosis synchronously at W22, in agreement with previous reports [3, 14, 15]. Meiotic entry of mouse adrenal and gonadal PGCs has been described to be synchronous [6]. In contrast to mice, human adrenal germ cells show no meiotic entry at least until W21.5, although the possibility that they enter meiosis afterwards cannot be excluded. This work serves as a reference presenting evidence for the existence of human ectopic germ cells in adrenals. Our findings highlight differences in gonadal and extragonadal gametogenesis between humans and mice.

Human PGCs have been suggested to migrate along class III beta-tubulin (TUBB3)-positive neural crest derivations to reach gonadal primordia [2, 10]. Interestingly, early germ cells (POU5F1-positive) in gonads and adrenals are also TUBB3-positive whereas late germ cells (DDX4-positive) are TUBB3-negative. The PGCs that migrate along common routes with neural crest cells to reach the adrenal may thus become ectopic germ cells there. Because the gonads have a common somatic origin as adrenals [11-13], rat PGCs are shown to reach adrenals before gonadal and adrenal primordia are physically separated [16]. This can also explain the colonization of human ectopic germ cells in adrenals. Furthermore, it is important to study the fate of these ectopic germ cells during further development. Whether they will enter meiosis or will lose their germ cell identities?

Ectopic PGCs that escape from entering apoptosis are thought to account for the development of extragonadal germ cell tumors [9, 10, 17, 18]. Interestingly, single-nucleotide polymorphisms (SNPs) located in gene DDX4 have been found to be associated with neuroblastoma tumors [19]. Furthermore, TUBB3-positive neural crest derivatives are thought to be related to the origin of adrenal neuroblastoma tumors [20]. Since there is expression of TUBB3 in ovarian and adrenal POU5F1-positive germ cells, further studies are needed to investigate the potential relationship between ectopic adrenal germ cells and neuroblastoma by studying the expression of additional markers.

Epigenetic regulation in human pre-implantation embryos and first-trimester placental villi

X chromosome inactivation (XCI) and genomic imprinting are two essential specific epigenetic regulation processes established in early development [21], controlling the dosage of X-linked genes and parent-of-origin-specific genes respectively.

Well-studied genetic substrains of mice have revealed two separate XCI waves during mouse female embryo development [22, 23]. However, the XCI dynamics in human female pre-implantation embryos remain unknown, because the parental allelic origin of human embryos is often not available. Recent advances (i.e. single cell RNA-Seq) have enabled the allele-specific expression analysis in human pre-implantation embryos to study XCI status at single-cell resolution [24]. The main aim of **Chapter 3** is to understand the status of XCI in human pre-implantation embryos at single-cell level. Do trophectoderm (TE) cells have different XCI pattern from inner cell mass (ICM) at embryonic day (E)5-E7? If there is X inactivation, whether the XCI pattern is imprinted or random? In this study, X-linked genes are separated into X-sub (X-genes subject to X inactivation) and X-esc (escapees) categories since escapees have biallelic expression, even though some studies do not show significant differences in escapees expression level between sexes [25, 26]. As demonstrated in **Chapter 3**, equal proportion of biallelic expression in X-sub and in autosomal genes suggests that both X chromosomes are active in E3 cells. A smaller proportion of biallelic expression in X-sub than in autosomal genes indicates that one X chromosome is inactive in E4-E6 cells and E7 TE cells, whereas there is reactivation in E7 epiblast (EPI) and primitive endoderm (PE) cells. Additionally, equal DNA methylation of both maternal and paternal alleles in *AR* and *RP2* genes indicates non-imprinted X inactivation in human TE-derived cells, in contrast to the imprinted XCI in mouse TE cells [22]. Results strongly contrast with the previous hypothesis that both X chromosomes are active during human pre-implantation (E3-E7) development [24]. This is because in the allele-specific expression analysis of Petropoulos and colleagues [24], without genome sequencing data, only the SNPs with biallelic expression or random monoallelic expression could be detected as informative SNPs. Therefore, SNPs having imprinted monoallelic expression within an embryo would be missed in the analysis. In addition, those genes with biallelic expression can be X-esc genes at human pre-implantation stage. In another study using RNA FISH for X-linked genes to detect XCI, *ATRX* gene shows biallelic expression in most cells of E5 female blastocysts (without separation of ICM from TE) [27]; however, *ATRX* gene is an X-Y paired gene (thus an escapee) [28] which is supposed to have biallelic expression even on the inactive X chromosome. The first XCI wave in mouse pre-implantation embryos occurs at the two- to four-cell stage [23] while in humans it happens between E3-E4. This difference is probably due to the different timing of zygotic genome activation (ZGA) in mice (at two-cell stage [23]) and in humans (at E4 [24, 29]).

The imprinted *IGF2/H19* cluster domain, controlled by the *IGF2/H19* imprinting control region (ICR1), plays an essential role in placental and embryo growth and development in mammals [30, 31]. According to the parent-offspring conflict theory [32], paternally expressed

IGF2 gene enhances cell proliferation while maternally expressed *H19* gene inhibits embryo growth and somehow negatively affects size of the offspring [33]. Gain or loss of methylation at ICR1 and consequent dysregulation of *IGF2/H19* account for perinatal complications including small for gestational age embryos, intrauterine growth restriction, Beckwith–Wiedemann syndrome (BWS) [34] and Russell–Silver syndrome (RSS) [35]. Chorionic villus sampling (CVS) is a procedure used in prenatal diagnosis of fetal abnormalities. However, it remains unknown whether spatial variation in methylation exists in placental villi and whether the imprinting pattern in placental villi is representative for the fetus. Therefore, the focus of **Chapter 5** is to investigate whether the multiple sites of first-trimester placental villi show the same imprinting pattern of *IGF2/H19* and whether it is the same as in the embryo. In the multiple sites of collection in human first-trimester placental villi (and embryos) analyzed in two pregnancies, demethylated maternal alleles and methylated paternal alleles indicate that multi-site placental villi collections have the same imprinting pattern of the *IGF2/H19* ICR1, also being the same as in embryos. This contrasts with the variability reported between different placental villi at term [36]. The difference may be resulted from the fact that Turan et al analyzed a larger number of placentas, but only one CpG point was analyzed, whereas in our study the methylation status of all CpGs in two placentas are investigated by bisulfite sequencing. In humans, *H19*, but not *IGF2*, has been reported to be biallelically expressed at least in cytotrophoblasts before W10, but to become monoallelically expressed in placentas at term [37-40]. Since there is a mixture of two cell types within placental villi (TE-derived trophoblast cells and ICM-derived mesenchymal cells), it remains to be investigated whether the imprinting patterns of *IGF2/H19* ICR1 in these two cell types are the same as in the embryo.

The epigenome is known to be sensitive to environmental changes [41]. Studies have suggested that treatments and procedures (i.e. ovarian stimulation, intracytoplasmic sperm injection, pre-implantation embryo culture) in assisted reproductive technology (ART) may change epigenetic marks (including *IGF2/H19*) of gametes and embryos [42-46]. Moreover, children conceived by ART are reported to have a higher incidence of imprinted disorders (i.e. Angelman syndrome and BWS) [47-49]. Therefore, the epigenetic dynamics during pre-implantation development is expected to be better understood within the next decades, which shall provide evidence for embryo selection [via pre-implantation genetic diagnosis/screening (PGD/PGS)] and successful pregnancy in assisted reproduction. Although obtaining maternal and/or paternal materials has of course both ethical and practical issues, future work investigating (epi)genetics in human pre-implantation embryos may require embryonic genome sequencing, embryonic RNA-Seq as well as parental genome sequencing data. Furthermore, future investigations could extend to XCI dynamics and imprinting pattern in TE-derived trophoblast cells and ICM-derived mesenchymal cells in placental villi.

Human extravillous trophoblast cells (EVTs) invasion in decidual vasculature during early pregnancy

Fetal EVTs have been described to block the entrance of uterine spiral arteries at W8-W12, thus preventing maternal blood flow into the intervillous space [50-52]. However, exosomes, placental particles [53, 54] and fetal cells [55] have been detected in the maternal blood from W6 onwards, without the presence of robust materno-placental vascular connection. For this reason, the aim of **Chapter 4** is to investigate whether there are alternative routes for EVTs to enter maternal circulation in early pregnancy (W5.5-W12) other than via spiral arteries. As shown in **Chapter 4**, fetal mononuclear EVTs enter veins and lymphatic vessels in decidua basalis directly from W5.5 onwards, much earlier than their remodelling decidual spiral arteries at W8. Same observation in a pregnancy with Klinefelter syndrome in the conceptus (W8.4, mosaic 46,XY and 47,XXY) indicates that efficient entry of maternal (blood and lymph) circulation by interstitial mononuclear EVTs occurs much earlier than previously reported W8 (via entering spiral arteries) [53]. These findings are supported by two very recent studies showing EVTs invasion in decidual veins in the first trimester, based on immunofluorescence for the EVT marker HLA-G [56, 57]. While attention should be paid to the different HLA-G isoforms when using HLA-G to determine EVTs [58], we are the first to combine chrX/chrY fluorescence in situ hybridization (FISH) and immunofluorescence to address the problem for unambiguous (male) EVTs identification. It could be important to investigate the EVTs invasion in decidua in pregnancies with other sex chromosomal disorders (i.e. Turner syndrome).

The entry of maternal circulation by EVTs via decidual veins and lymphatics since W5.5, occurring much earlier than the establishment of maternal-placental vascular connection at W8-W12 [53], enlarges the maternal-fetal interface during early pregnancy. Therefore, while maternal immune response in the uterus include crosstalk between immune cells (natural killer cells, lymphocytes) and EVTs [59, 60], EVTs invading maternal circulation contribute to the response that takes place outside the uterus.

Insufficient invasion of human fetal EVTs into maternal decidua may cause inadequate placental perfusion and consequent pregnancy complications including preeclampsia and intrauterine growth restriction [61-64]. Using the approach provided in **Chapter 4** to identify the (male) EVTs unambiguously in maternal decidua, defective EVTs invasion in pregnancy complications can be further defined and this may lead to identification of underlying mechanism and promising therapy strategies.

Question remaining to be answered is the underlying cellular/molecular mechanism of EVTs invasion in vein and lymphatics in first trimester. Other investigations could focus on the shared invasive characteristics (epithelial–mesenchymal transition) between EVTs and metastasizing malignant cells [65]. This may offer more knowledge on causes of tumor metastasis and provide valuable tumor therapies.

Abnormalities in mouse Turner syndrome placentas

Mice with a genetic form of Turner syndrome (39,XO) harboring either a single paternally inherited (Xp) or maternally inherited (Xm) chromosome show quite different survival rates to term [66-68]. Nevertheless, no detailed comparison of XpO and XmO placentas has been made to explain this difference. The aim of **Chapter 6** is to study whether the transcriptional level of Xp is equal to Xm, by comparing the consequences of Turner syndrome harboring either a single Xp or Xm in mouse E18.5 placenta. The larger area occupied by glycogen cells (GCs) and significantly increased expression level of *Ldha* in the outer zone (junctional zone, trophoblast giant cells and decidua) of XpO placenta indicate that the XpO genotype leads to a more severe placental phenotype than XmO at E18.5, and thus the transcriptional level of Xp is not equal to Xm.

During placental development, TE-derived cells in XX placentas have obligatory active Xm and inactive Xp [69]. The significantly larger amount of GCs in the XpO outer zone might be an adaptive response to defects in the epigenetic regulation of imprinted genes [70-72]. Moreover, abnormal amount of GCs, serving as a potential source of energy in mouse placenta [73], may indicate defects in glycogen metabolism and glucose transport [74, 75]. The higher *Ldha* expression, which encodes the enzyme converting lactate to pyruvate in anaerobic glycolysis, suggests increased anaerobic glycolysis and possible insufficient available oxygen in XpO placentas. This is in accordance with the reported increase in *Ldha* expression in human primary placental trophoblast cells cultured under hypoxic conditions [76].

Although it remains to be clarified how harboring either a single Xp or Xm affects mouse placental development and function, findings in **Chapter 6** contribute to the understanding of different effects of inheriting a single paternal or maternal X chromosome on mouse placental phenotypes and hints to a defect in glucose metabolism. The investigation of glucose metabolism in human Turner syndrome patients and their placentas is needed and may provide new therapeutic strategies for individuals.

Together, the results in this thesis provide new insights into normal development of human (extra)gonadal germ cells, human pre-implantation development as well as placental development in humans and mice. Furthermore, results offer more knowledge on how defects in these processes might cause abnormal pregnancy outcomes and placental functions.

References

1. Byskov AG: Differentiation of mammalian embryonic gonad. Physiol Rev 1986, 66:71-117.
2. Mollgard K, Jespersen A, Lutterodt MC, Yding Andersen C, Hoyer PE, Byskov AG: Human primordial germ cells migrate along nerve fibers and Schwann cells from the dorsal hind gut mesentery to the gonadal ridge. Mol Hum Reprod 2010, 16:621-631.
3. Heeren A, van Iperen L, Klootwijk DB, de Melo Bernardo A, Roost MS, Gomes Fernandes MM, Louwe LA, Hilders CG, Helmerhorst FM, van der Westerlaken LA, Chuva de Sousa Lopes SM: Development of the follicular basement membrane during human gametogenesis and early folliculogenesis. BMC Dev Biol 2015, 15:4.
4. Upadhyay S, Zamboni L: Ectopic germ cells: natural model for the study of germ cell sexual differentiation. Proc Natl Acad Sci U S A 1982, 79:6584-6588.
5. Wrobel KH, Suss F: On the origin and prenatal development of the bovine adrenal gland. Anat Embryol (Berl) 1999, 199:301-318.
6. Zamboni L, Upadhyay S: Germ cell differentiation in mouse adrenal glands. J Exp Zool 1983, 228:173-193.
7. Runyan C, Gu Y, Shoemaker A, Looijenga L, Wylie C: The distribution and behavior of extragonadal primordial germ cells in Bax mutant mice suggest a novel origin for sacrococcygeal germ cell tumors. Int J Dev Biol 2008, 52:333-344.
8. Stallock J, Molyneaux K, Schaible K, Knudson CM, Wylie C: The pro-apoptotic gene Bax is required for the death of ectopic primordial germ cells during their migration in the mouse embryo. Development 2003, 130:6589-6597.
9. Keegan CE, Hammer GD: Recent insights into organogenesis of the adrenal cortex. Trends Endocrinol Metab 2002, 13:200-208.
10. Mamsen LS, Brochner CB, Byskov AG, Mollgard K: The migration and loss of human primordial germ stem cells from the hind gut epithelium towards the gonadal ridge. Int J Dev Biol 2012, 56:771-778.
11. Hanley NA, Ball SG, Clement-Jones M, Hagan DM, Strachan T, Lindsay S, Robson S, Ostrer H, Parker KL, Wilson DI: Expression of steroidogenic factor 1 and Wilms' tumour 1 during early human gonadal development and sex determination. Mech Dev 1999, 87:175-180.
12. Hanley NA, Rainey WE, Wilson DI, Ball SG, Parker KL: Expression profiles of SF-1, DAX1, and CYP17 in the human fetal adrenal gland: potential interactions in gene regulation. Mol Endocrinol 2001, 15:57-68.
13. Morohashi K: The ontogenesis of the steroidogenic tissues. Genes Cells 1997, 2:95-106.
14. Anderson RA, Fulton N, Cowan G, Coutts S, Saunders PT: Conserved and divergent patterns of expression of DAZL, VASA and OCT4 in the germ cells of the human fetal ovary and testis. BMC Dev Biol 2007, 7:136.
15. Kurilo LF: Oogenesis in antenatal development in man. Hum Genet 1981, 57:86-92.
16. Hatano O, Takakusu A, Nomura M, Morohashi K: Identical origin of adrenal cortex and gonad revealed by expression profiles of Ad4BP/SF-1. Genes Cells 1996, 1:663-671.
17. Looijenga LH, Van Agthoven T, Biermann K: Development of malignant germ cells - the genvironmental hypothesis. Int J Dev Biol 2013, 57:241-253.
18. Schneider DT, Schuster AE, Fritsch MK, Hu J, Olson T, Lauer S, Gobel U, Perlman EJ: Multipoint imprinting analysis indicates a common precursor cell for gonadal and nongonadal pediatric germ cell tumors. Cancer Res 2001, 61:7268-7276.
19. Nguyen le B, Diskin SJ, Capasso M, Wang K, Diamond MA, Glessner J, Kim C, Attiyeh EF, Mosse YP, Cole K, et al: Phenotype restricted genome-wide association study using a gene-centric approach identifies three low-risk neuroblastoma susceptibility Loci. PLoS Genet 2011, 7:e1002026.
20. De Preter K, Vandesompele J, Heimann P, Yigit N, Beckman S, Schramm A, Eggert A, Stallings RL, Benoit Y, Renard M, et al: Human fetal neuroblast and neuroblastoma transcriptome analysis confirms neuroblast origin and highlights neuroblastoma candidate genes. Genome Biol 2006, 7:R84.
21. Inbar-Feigenberg M, Choufani S, Butcher DT, Roifman M, Weksberg R: Basic concepts of epigenetics. Fertil Steril 2013, 99:607-615.
22. Okamoto I, Otte AP, Allis CD, Reinberg D, Heard E: Epigenetic dynamics of imprinted X inactivation during

early mouse development. Science 2004, 303:644-649.

23. Deng Q, Ramskold D, Reinius B, Sandberg R: Single-cell RNA-seq reveals dynamic, random monoallelic gene expression in mammalian cells. Science 2014, 343:193-196.

24. Petropoulos S, Edsgard D, Reinius B, Deng Q, Panula SP, Codeluppi S, Plaza Reyes A, Linnarsson S, Sandberg R, Lanner F: Single-Cell RNA-Seq Reveals Lineage and X Chromosome Dynamics in Human Preimplantation Embryos. Cell 2016, 165:1012-1026.

25. Xiong Y, Chen X, Chen Z, Wang X, Shi S, Wang X, Zhang J, He X: RNA sequencing shows no dosage compensation of the active X-chromosome. Nature genetics 2010, 42:1043-1047.

26. Disteche CM: Dosage compensation of the active X chromosome in mammals. Nature genetics 2006, 38:47-53.

27. Okamoto I, Patrat C, Thepot D, Peynot N, Fauque P, Daniel N, Diabangouaya P, Wolf JP, Renard JP, Duranthon V, Heard E: Eutherian mammals use diverse strategies to initiate X-chromosome inactivation during development. Nature 2011, 472:370-374.

28. Bellott DW, Hughes JF, Skaletsky H, Brown LG, Pyntikova T, Cho TJ, Koutseva N, Zaghlul S, Graves T, Rock S, et al: Mammalian Y chromosomes retain widely expressed dosage-sensitive regulators. Nature 2014, 508:494-499.

29. Yan L, Yang M, Guo H, Yang L, Wu J, Li R, Liu P, Lian Y, Zheng X, Yan J, et al: Single-cell RNA-Seq profiling of human preimplantation embryos and embryonic stem cells. Nat Struct Mol Biol 2013, 20:1131-1139.

30. Frost JM, Moore GE: The importance of imprinting in the human placenta. PLoS Genet 2010, 6:e1001015.

31. Demars J, Shmela ME, Rossignol S, Okabe J, Netchine I, Azzi S, Cabrol S, Le Caignec C, David A, Le Bouc Y, et al: Analysis of the IGF2/H19 imprinting control region uncovers new genetic defects, including mutations of OCT-binding sequences, in patients with 11p15 fetal growth disorders. Hum Mol Genet 2010, 19:803-814.

32. Moore T, Haig D: Genomic imprinting in mammalian development: a parental tug-of-war. Trends Genet 1991, 7:45-49.

33. Reik W, Walter J: Genomic imprinting: parental influence on the genome. Nat Rev Genet 2001, 2:21-32.

34. Weksberg R, Shuman C, Beckwith JB: Beckwith-Wiedemann syndrome. Eur J Hum Genet 2010, 18:8-14.

35. Azzi S, Steunou V, Tost J, Rossignol S, Thibaud N, Das Neves C, Le Jule M, Habib WA, Blaise A, Koudou Y, et al: Exhaustive methylation analysis revealed uneven profiles of methylation at IGF2/ICR1/H19 11p15 loci in Russell Silver syndrome. J Med Genet 2015, 52:53-60.

36. Turan N, Katari S, Gerson LF, Chalian R, Foster MW, Gaughan JP, Coutifaris C, Sapienza C: Inter- and intra-individual variation in allele-specific DNA methylation and gene expression in children conceived using assisted reproductive technology. PLoS Genet 2010, 6:e1001033.

37. Adam GI, Cui H, Miller SJ, Flam F, Ohlsson R: Allele-specific in situ hybridization (ASISH) analysis: a novel technique which resolves differential allelic usage of H19 within the same cell lineage during human placental development. Development 1996, 122:839-847.

38. Buckberry S, Bianco-Miotto T, Hiendleder S, Roberts CT: Quantitative allele-specific expression and DNA methylation analysis of H19, IGF2 and IGF2R in the human placenta across gestation reveals H19 imprinting plasticity. PLoS One 2012, 7:e51210.

39. Jinno Y, Ikeda Y, Yun K, Maw M, Masuzaki H, Fukuda H, Inuzuka K, Fujishita A, Ohtani Y, Okimoto T, et al.: Establishment of functional imprinting of the H19 gene in human developing placentae. Nat Genet 1995, 10:318-324.

40. Monk D, Arnaud P, Apostolidou S, Hills FA, Kelsey G, Stanier P, Feil R, Moore GE: Limited evolutionary conservation of imprinting in the human placenta. Proc Natl Acad Sci U S A 2006, 103:6623-6628.

41. el Hajj N, Haaf T: Epigenetic disturbances in in vitro cultured gametes and embryos: implications for human assisted reproduction. Fertility and sterility 2013, 99:632-641.

42. Stouder C, Deutsch S, Paoloni-Giacobino A: Superovulation in mice alters the methylation pattern of imprinted genes in the sperm of the offspring. Reproductive Toxicology 2009, 28:536-541.

43. Sato A, Otsu E, Negishi H, Utsunomiya T, Arima T: Aberrant DNA methylation of imprinted loci in superovulated oocytes. Human reproduction 2007, 22:26-35.

44. Doherty AS, Mann MR, Tremblay KD, Bartolomei MS, Schultz RM: Differential Effects of Culture

on Imprinted H19 Expression in the Preimplantation Mouse Embryo 1. Biology of reproduction 2000, 62:1526-1535.

45. Rivera RM, Stein P, Weaver JR, Mager J, Schultz RM, Bartolomei MS: Manipulations of mouse embryos prior to implantation result in aberrant expression of imprinted genes on day 9.5 of development. Human molecular genetics 2008, 17:1-14.

46. Fernández-Gonzalez R, Moreira P, Bilbao A, Jiménez A, Pérez-Crespo M, Ramírez MA, De Fonseca FR, Pintado B, Gutiérrez-Adán A: Long-term effect of in vitro culture of mouse embryos with serum on mRNA expression of imprinting genes, development, and behavior. Proceedings of the National Academy of Sciences of the United States of America 2004, 101:5880-5885.

47. Pinborg A, Loft A, Romundstad LB, Wennerholm UB, Söderström-Anttila V, Bergh C, Aittomäki K: Epigenetics and assisted reproductive technologies. Acta obstetricia et gynecologica Scandinavica 2016, 95:10-15.

48. DeBaun MR, Niemitz EL, Feinberg AP: Association of in vitro fertilization with Beckwith-Wiedemann syndrome and epigenetic alterations of LIT1 and H19. The American Journal of Human Genetics 2003, 72:156-160.

49. Bowdin S, Allen C, Kirby G, Brueton L, Afnan M, Barratt C, Kirkman-Brown J, Harrison R, Maher ER, Reardon W: A survey of assisted reproductive technology births and imprinting disorders. Human Reproduction 2007, 22:3237-3240.

50. Burton GJ, Jauniaux E, Watson AL: Maternal arterial connections to the placental intervillous space during the first trimester of human pregnancy: the Boyd collection revisited. Am J Obstet Gynecol 1999, 181:718-724.

51. Pijnenborg R, Vercruysse L, Hanssens M: The uterine spiral arteries in human pregnancy: facts and controversies. Placenta 2006, 27:939-958.

52. Jauniaux E, Watson AL, Hempstock J, Bao YP, Skepper JN, Burton GJ: Onset of maternal arterial blood flow and placental oxidative stress. A possible factor in human early pregnancy failure. Am J Pathol 2000, 157:2111-2122.

53. Chamley LW, Holland OJ, Chen Q, Viall CA, Stone PR, Abumaree M: Review: where is the maternofetal interface? Placenta 2014, 35 Suppl:S74-80.

54. Sarker S, Scholz-Romero K, Perez A, Illanes SE, Mitchell MD, Rice GE, Salomon C: Placenta-derived exosomes continuously increase in maternal circulation over the first trimester of pregnancy. J Transl Med 2014, 12:204.

55. Merviel P, Aractingi S, Uzan S: [Detection of fetal cells in maternal blood: myth or reality?]. Gynecol Obstet Fertil 2001, 29:371-376.

56. Moser G, Weiss G, Sundl M, Gauster M, Siwetz M, Lang-Olip I, Huppertz B: Extravillous trophoblasts invade more than uterine arteries: evidence for the invasion of uterine veins. Histochem Cell Biol 2016.

57. Windsperger K, Dekan S, Pils S, Golletz C, Kunihs V, Fiala C, Kristiansen G, Knöfler M, Pollheimer J: Extravillous trophoblast invasion of venous as well as lymphatic vessels is altered in idiopathic, recurrent, spontaneous abortions. Human Reproduction 2017, 32:1208-1217.

58. James JL, Chamley LW: A caution on the use of HLA-G isoforms as markers of extravillous trophoblasts. Placenta 2008, 29:305-306; author reply 307.

59. Gregori S, Amodio G, Quattrone F, Panina-Bordignon P: HLA-G Orchestrates the Early Interaction of Human Trophoblasts with the Maternal Niche. Front Immunol 2015, 6:128.

60. Lash GE: Molecular Cross-Talk at the Feto-Maternal Interface. Cold Spring Harb Perspect Med 2015, 5.

61. Burke SD, Karumanchi SA: Spiral artery remodeling in preeclampsia revisited. Hypertension 2013, 62:1013-1014.

62. Fisher SJ: Why is placentation abnormal in preeclampsia? Am J Obstet Gynecol 2015, 213:S115-122.

63. Plaisier M, Dennert I, Rost E, Koolwijk P, van Hinsbergh VW, Helmerhorst FM: Decidual vascularization and the expression of angiogenic growth factors and proteases in first trimester spontaneous abortions. Hum Reprod 2009, 24:185-197.

64. Plaisier M, Rodrigues S, Willems F, Koolwijk P, van Hinsbergh VW, Helmerhorst FM: Different degrees of vascularization and their relationship to the expression of vascular endothelial growth factor, placental growth factor, angiopoietins, and their receptors in first-trimester decidual tissues. Fertil Steril 2007, 88:176-187.

65. Kokkinos M, Murthi P, Wafai R, Thompson E, Newgreen D: Cadherins in the human placenta–epithelial–mesenchymal transition (EMT) and placental development. Placenta 2010, 31:747-755.

66. Burgoyne PS, Evans EP, Holland K: XO monosomy is associated with reduced birthweight and lowered weight gain in the mouse. J Reprod Fertil 1983, 68:381-385.

67. Burgoyne PS, Tam PP, Evans EP: Retarded development of XO conceptuses during early pregnancy in the mouse. J Reprod Fertil 1983, 68:387-393.

68. Hunt PA: Survival of XO mouse fetuses: effect of parental origin of the X chromosome or uterine environment? Development 1991, 111:1137-1141.

69. Harper MI, Fosten M, Monk M: Preferential paternal X inactivation in extraembryonic tissues of early mouse embryos. J Embryol Exp Morphol 1982, 67:127-135.

70. Hemberger M: The role of the X chromosome in mammalian extra embryonic development. Cytogenet Genome Res 2002, 99:210-217.

71. Lefebvre L: The placental imprintome and imprinted gene function in the trophoblast glycogen cell lineage. Reprod Biomed Online 2012, 25:44-57.

72. Sandovici I, Hoelle K, Angiolini E, Constancia M: Placental adaptations to the maternal-fetal environment: implications for fetal growth and developmental programming. Reprod Biomed Online 2012, 25:68-89.

73. Coan PM, Conroy N, Burton GJ, Ferguson-Smith AC: Origin and characteristics of glycogen cells in the developing murine placenta. Dev Dyn 2006, 235:3280-3294.

74. Redline RW, Chernicky CL, Tan HQ, Ilan J, Ilan J: Differential expression of insulin-like growth factor-II in specific regions of the late (post day 9.5) murine placenta. Molecular reproduction and development 1993, 36:121-129.

75. Sibley C, Coan P, Ferguson-Smith A, Dean W, Hughes J, Smith P, Reik W, Burton G, Fowden A, Constancia M: Placental-specific insulin-like growth factor 2 (IGF2) regulates the diffusional exchange characteristics of the mouse placenta. Proceedings of the National Academy of Sciences of the United States of America 2004, 101:8204-8208.

76. Kay HH, Zhu S, Tsoi S: Hypoxia and lactate production in trophoblast cells. Placenta 2007, 28:854-860.

7

APPENDIX

Summary

Studies aimed at understanding pre-implantation and placental development in humans and mice have provided essential implications for assisted reproductive technology and demonstrated the underlying causes and therapies for infertility, recurrent miscarriage and pregnancy complications. In this thesis, **Chapter 1** presents the state of the literature on early development in both humans and mice, including primordial germ cells (PGCs) development, pre-implantation development, implantation, early placentation and placental development. It also provides a review of two epigenetic regulation processes established in early development: X chromosome inactivation (XCI) and genomic imprinting.

Chapter 2 describes the development of gonadal and extragonadal PGCs in humans, using immunofluorescence for germ cells markers and meiotic markers. Between first and second trimesters, there is a shift towards POU5F1−/DDX4+ germ cells in gonads. Human ectopic germ cells are present in both first- and second-trimester adrenals. Moreover, the asynchronous meiotic entry of human 'adrenal' and 'ovarian' germ cells highlights species-specific differences between human and mouse early gonadal and extragonadal gametogenesis.

Chapter 3 investigates the status of XCI in human pre-implantation embryos at single-cell level, by analyzing online available RNA-seq data of human embryonic day (E)3-E7 embryos. Equal proportion of biallelic expression in "X-sub" (X-genes subject to X inactivation) and in autosomal genes suggests that both X chromosomes are active in E3 cells. Smaller proportion of biallelic expression in "X-sub" than in autosomal genes indicates that one X chromosome is inactive in E4-E6 cells and E7 trophectoderm (TE) cells, whereas it becomes reactivated in E7 epiblast and primitive endoderm cells. In addition, combined human androgen receptor (*AR*)/retinitis pigmentosa 2 (*RP2*) DNA methylation assay shows equal methylation of paternal and maternal alleles in female TE-derived cells, indicating non-imprinted X inactivation in human TE-derived cells, in contrast to the imprinted XCI in mouse TE-derived cells.

Chapter 4 describes in detail the invasion of human fetal extravillous trophoblast cells (EVTs) in maternal decidua and decidual vasculature during early pregnancy (W5.5-W12), using combined immunofluorescence and fluorescence in situ hybridization (FISH) for chrX/chrY to identify (male) EVTs unambiguously. This study serves as a reference for the entering of EVTs in maternal circulation (via decidual veins and lymphatic vessels) since W5.5, much earlier than previously accepted W8 (via decidual spiral arteries). The placental decidua interface of one Klinefelter syndrome embryo (mosaic 47,XXY and 46,XY) is also described.

Chapter 5 studies the spatial imprinting pattern of *IGF2/H19* in multiple-site collection of human first-trimester placental villi, using bisulfite DNA sequencing and allele-specific expression analysis of two informative non-CpG single-nucleotide polymorphism (SNP) sites allowing to discriminate the maternal and paternal alleles. Demethylated maternal alleles and methylated paternal alleles suggest a normal imprinting pattern of *IGF2/H19* in multi-site placental villi collections as in the embryo.

Chapter 6 explores different consequences of Turner syndrome, using a mouse model that harbors either a single maternally inherited (Xm) or paternally inherited (Xp) chromosome, by a detailed analysis of morphology and glucose metabolism in E18.5 XmO and XpO placentas compared to wild type placentas. The significantly larger area occupied by glycogen cells in XpO placental outer zone (junctional zone, trophoblast giant cells and decidua) and the significantly higher expression of *Ldha* in XpO labyrinth zone suggest a more severe placental phenotype in E18.5 XpO placentas than in XmO placentas, with increased anaerobic glycolysis and underlying defects in oxygen availability in XpO placentas.

Finally, **Chapter 7** provides general discussion about the findings described in this thesis. This section also presents and discusses the future perspectives on embryo selection in assisted reproduction and new treatment strategies for infertility, pregnancy complications and sex chromosome related syndromes.

Together, the work in this thesis provides novel insights into gonadal and extragonadal PGCs development in humans and XCI in human pre-implantation embryos. Also we have demonstrated the invasion of decidual vasculature by human extravillous trophoblast cells during early pregnancy, the spatial imprinting pattern of *IGF2/H19* in human first-trimester placental villi and finally the consequences of harboring different combinations of sex chromosomes in the placenta.

Samenvatting

Studies gericht op het begrijpen van preïmplantatie en placentale ontwikkeling bij mensen en muizen zijn belangrijk voor het optimalizeren van voortplantingstechnologien, het vinden van oorzaken en ontwikkelen van therapieën voor onvruchtbaarheid, terugkerende miskraamen en zwangerschapscomplicaties. In dit proefschrift, **hoofdstuk 1** beschrijft de stand van de literatuur over vroege ontwikkeling in zowel mensen als muizen, inclusief de ontwikkeling van kiemcellen (PGC's), pre-implantatie, implantatie, vroege placenta vorming en placenta ontwikkeling. Het geeft ook een overzicht van twee epigenetische regulatieprocessen die zijn vastgesteld in de vroege ontwikkeling: X-chromosoom inactivatie (XCI) en genomische imprinting.

Hoofdstuk 2 beschrijft de ontwikkeling van gonadale en extragonadale PGC's bij mensen, gebruik makend van immunofluorescentie voor kiemcel- en meiotische-markers. Tussen het eerste en tweede trimester is er een verschuiving in de gonaden van POU5F1+/DDX4- kiemcellen naar POU5F1-/DDX4+ kiemcellen. Menselijke ectopische kiemcellen zijn aanwezig in de bijnieren in zowel de eerste als de tweede trimester. De asynchronie in timing van meiosis-entry van menselijk kiemcellen (in the bijnier en ovarium) is een van de aspecten die verschillend is tussen mens en muis gametogenese.

Hoofdstuk 3 onderzoekt de status van XCI in menselijke pre-implantatie embryo's op enkel-cel niveau, door online beschikbare RNA-seq gegevens van embryo's van de menselijke embryonale dag (E)3-E7 te analyseren. Vergelijkend nivos van biallelische expressie in "X-sub" (X genen onderworpen aan X-inactivatie) en in autosomale genen suggereert dat er transcriptie is uit beide X-chromosomen, en dus dat beide actief zijn op E3. Minder biallele expressie in "X-sub" dan in autosomale genen geeft aan dat een van de twee X-chromosomen inactief is in E4-E6-cellen en E7 trophectoderm (TE) cellen, terwijl het wordt geactiveerd in E7 epiblast- en primitieve endodermcellen. Daarnaast blijkt uit een DNA methylatie assay (die de methylatie van humaan androgeen receptor en retinitis pigmentosa genen weergeeft) dat er gelijke methylering van paternale- en maternale-allelen in vrouwelijke TE-afgeleide cellen is. Dit toon aan dat random X-inactivatie in menselijke TE-afgeleide cellen is, in contrast met de imprinted X-inactivatie in muis-TE-afgeleide cellen.

Hoofdstuk 4 beschrijft in detail de invasie van menselijke foetale extravillous trophoblastcellen (EVT's) in de maternale decidua en de deciduale vasculatuur tijdens de vroege zwangerschap (W5.5-W12), met behulp van gecombineerde immunofluorescentie en fluorescente in situ hybridisatie (FISH) voor ChrX en ChrY om (mannelijke). It is noodzakelijk om EVT's met zekerheid te identificeren. Deze studie toont dat er EVT's in de moedercirculatie (via decidale aderen en lymfatische vaten) aanwezig zijn vanaf W5.5, veel eerder dan via de deciduale spiraaladeren op W8. De placenta-decidua interface van een human embryo met Klinefelter syndroom (mozaïek 47, XXY en 46, XY) wordt in deze hoofdstuk ook beschreven.

Hoofdstuk 5 onderzoekt het imprinting status van het *IGF2/H19* gebied op meerdere plaatsen van menselijke placenta villi tijdens de eerste trimester. Dit is gedaan met behulp van

bisulfiet DNA sequencing en allel-specifieke expressie analyse van twee informatieve non-CpG SNPs die de paternale- en maternale-allelen kunnen onderscheiden. Gedemetyleerde maternale allelen en gemethyleerde paternale allelen suggereren een normaal imprintings status in het *IGF2/H19* gebied in de verschillende placenta villi, zoals gevonden in het embryo.

Hoofdstuk 6 onderzoekt verschillende gevolgen van het Turner syndroom, met behulp van een muismodel dat zowel een enkel X chromosoom van maternaal (Xm) of paternaal (Xp) origine. Dit wordt bestudeerd door een gedetailleerde analyse van de morfologie, maar ook het glucose metabolisme, in zowel XmO en XpO E18.5 muizen placenta's. Er is een aanzienlijk grotere gebied met glycogeencellen in de buitenste zone (junctionale zone, reuze trophoblast cellen en decidua) van XpO placenta's en deen significant hogere expressie van *Ldha* in de XpO labyrintzone. Dit wijst op ernstiger afwijkingen in E18.5 XpO placenta's dan in XmO placenta's. Er is een verder een verhoogde anaërobe glycolyse en onderliggende defecten in zuurstof beschikbaarheid in XpO placenta's.

Ten slotte is **hoofdstuk 7** een algemene discussie over de bevindingen die in dit proefschrift zijn beschreven. Toekomstperspectieven op embryo selectie bij geassisteerde voortplanting en nieuwe behandelingsstrategieën voor onvruchtbaarheid, zwangerschapscomplicaties en sekschromosoom gerelateerde syndromen worden behandeld.

Het werk in dit proefschrift geeft nieuwe inzichten in gonadale en extragonadale ontwikkeling van PGC's bij mensen en XCI in menselijke pre-implantatie embryo's weer. Ook presenteren we onze bevindingen over de invasie van deciduele vasculatuur door fetal EVT's tijdens de vroege zwangerschap, het imprinting status van *IGF2/H19* in menselijke eerste trimester placenta villi en tenslotte de gevolgen van het verschaffen van verschillende combinaties van sekschromosomen in de placenta.

论文概述

关于人和鼠植入前胚胎发育和胎盘发育的研究为辅助生殖技术提供了重要的应用价值，并且为不孕症、习惯性流产和妊娠并发症等找到潜在的病因和治疗方法。本论文第一章综述了人和鼠的早期发育过程，包括原始生殖细胞发育、植入前胚胎发育、植入和早期胎盘发育，也阐述了在早期发育阶段就建立的两个表观遗传调控过程：X染色体失活和基因印记。

第二章通过免疫荧光染色方法测定生殖细胞标志物和减数分裂标记物的表达，研究了人性腺内和性腺外原始生殖细胞的发育过程。从第一至第二孕期，性腺原始生殖细胞中POU5F1（早期生殖细胞标记物）的表达逐渐下降，而DDX4（晚期生殖细胞标记物）的表达渐增。此外，在第一和第二孕期的肾上腺中都存在异位的原始生殖细胞。但与鼠不同的是，人性腺和肾上腺中的原始生殖细胞非同步进入减数分裂，这突出了人与鼠早期性腺内外配子发生过程的物种特异性。

第三章通过分析RNA测序数据来研究单细胞水平上人植入前胚胎(E3-E7)的X染色体失活状态。在E3胚胎中，两个等位基因都表达的比例在X染色体基因和常染色体基因中无差异，表明E3胚胎细胞中两条染色体都是有活性的。在E4-E6胚胎和E7滋养外胚层细胞中，X染色体基因中两个等位基因都表达的比例显著低于常染色体基因，表明一条X染色体在E4-E6细胞和E7滋养层细胞中是失活的，而在E7上胚层细胞和下胚层细胞中它又恢复活性。此外，人雄激素受体基因(*AR*)/色素性视网膜炎2基因(*RP2*)的DNA甲基化联合试验显示，在人滋养层衍生细胞中父源基因和母源基因的甲基化比例相当，表明人滋养层细胞中的X染色体失活是随机的，这与鼠滋养层细胞中总是父源X染色体失活不同。

第四章联合使用免疫荧光和荧光原位杂交（X和Y染色体）技术来精确标记蜕膜组织中男性胎儿绒毛外滋养层细胞，从而研究第一孕期（孕5.5-12周）胎儿绒毛外滋养层细胞对子宫蜕膜和蜕膜血管的侵入。这项研究为胎儿绒毛外滋养层细胞自孕5.5周经蜕膜静脉和淋巴管侵入母体血液循环提供依据，远早于之前普遍认为的自孕8周绒毛外滋养层细胞经子宫螺旋动脉进入母体血液循环。此外，本研究对一例性染色体异常胎儿（克莱恩费尔特氏综合征，47,XXY/46,XY嵌合体）的胎盘-蜕膜交接部位进行了描述。

第五章通过亚硫酸氢盐DNA测序法和对两个单核苷酸多态性位点的等位基因特异性表达分析研究了人第一孕期胎盘绒毛多点采集样本中的*IGF2/H19*基因印记类型。两个单核苷酸多态性位点用来区分母源性和父源性等位基因。结果显示，在多点绒毛样本中，当母源性等位基因表达时，*IGF2/H19*印记控制区呈去甲基化状态；当父源性等位基因表达时，*IGF2/H19*印记控制区呈甲基化状态。这表明绒毛不同位置样本的*IGF2/H19*印记类型正常，也与胚胎中的印记类型相同。

第六章使用鼠特纳综合征(39,XO)模型探讨了携带单一母源性X染色体(Xm)或父源性X染色体(Xp)对胎盘的不同影响。对 E18.5 XmO,XpO和野生型胎盘的形态和葡萄糖代谢的详细比较结果显示，XpO胎盘外区（包括海绵带，滋养层巨细胞和蜕膜）中糖原细胞所占的面积明显增加，而且XpO胎盘迷路区*Ldha*（乳酸脱氢酶）基因表达

明显升高，表明胎盘厌氧糖酵解的增加和潜在的胎盘供氧缺陷。研究提示，相比于XmO, E18.5 XpO能导致更异常的胎盘表型。

最后，第七章是对本论文研究结果的综合讨论，也为辅助生殖中胚胎选择以及不育症、妊娠并发症和性染色体异常的治疗策略提出了新的展望。

综上，本论文为人性腺内外原始生殖细胞的发育和人植入前胚胎的发育中X染色体失活提供了新见解，并对孕早期人绒毛外滋养层细胞对蜕膜血管的侵入、*IGF2/H19*在第一孕期胎盘绒毛中的印记表达和性染色体异常在胚胎发育中的影响进行了研究。

List of Publications

Roost MS, Slieker RC, Bialecka M, van Iperen L, Fernandes MMG, **He N**, Suchiman HE, Carlotti F, Szuhai K, de Koning E, Mummery C, Heijmans B, Chuva de Sousa Lopes SM. DNA methylation and transcriptional trajectories during human development and reprogramming of isogenic pluripotent stem cells.
Nature Communications 2017, in press.

He N, Lim SJ, Moreira de Mello JC, Navarro I, Bialecka M, Salvatori DCF, van der Westerlaken LAJ, Pereira LV, Chuva de Sousa Lopes SM. At term, XmO and XpO mouse placentas show differences in glucose metabolism in the trophectoderm-derived outer zone.
Frontiers in Cell and Developmental Biology 2017, 5(63).

He N, van Iperen L, de Jong D, Szuhai K, Helmerhorst FM, van der Westerlaken LAJ, Chuva de Sousa Lopes SM. Human extravillous trophoblasts penetrate decidual veins and lymphatics before remodeling spiral arteries during early pregnancy.
PLOS ONE 2017, 12:e0169849.

Heeren AM*, **He N***, de Souza AF, Goercharn-Ramlal A, van Iperen L, Roost MS, Fernandes MMG, van der Westerlaken LAJ, Chuva de Sousa Lopes SM. On the development of extragonadal and gonadal human germ cells.
Biology Open 2016, 5:185-194.
*Equal first authorship contribution

de Melo Bernardo A, Heeren AM, van Iperen L, Fernandes MMG, **He N**, Anjie S, Noce T, Ramos ES, Chuva de Sousa Lopes SM. Meiotic wave adds extra asymmetry to the development of female chicken gonads.
Molecular Reproduction and Development 2015, 82:774-786.

Roovers EF, Rosenkranz D, Mahdipour M, Han CT, **He N**, Chuva de Sousa Lopes SM, van der Westerlaken LAJ, Zischler H, Butter F, Roelen BA, Ketting RF. Piwi proteins and piRNAs in mammalian oocytes and early embryos.
Cell Reports 2015, 10:2069-2082.

Curriculum Vitae

Nannan He was born on June 15th, 1989 in Jiaozuo, Henan, China. After obtaining her Bachelor's degree in Clinical Medicine in 2011 at Zhengzhou University (Zhengzhou, China), Nannan continued with her Master studies in Reproductive Medical Centre of the First Affiliated Hospital of Zhengzhou University, under the supervision of Prof. Dr. Yingpu Sun. During her two-year master program, Nannan carried out her research project "Prevalence of Y chromosome microdeletion in blood and sperms of males with idiopathic severe oligozoospermia". She received her Master's diploma in June 2013. In October of the same year, supported by China Scholarship Council (NO.201307040026), Nannan started her PhD training in the group of Dr. Susana M. Chuva de Sousa Lopes at the Department of Anatomy and Embryology at Leiden University Medical Center (Leiden, the Netherlands), with Prof. Dr. Christine L. Mummery and Prof. Dr. Frans M. Helmerhorst as her promotors and Dr. Susana M. Chuva de Sousa Lopes as co-promotor. Her research focused on pre-implantation and placental development in humans and mice. The results of her research are presented in this thesis.

Acknowledgements

I would like to convey my sincere appreciation to everyone who has helped and encouraged me during my PhD studies. Your support and contribution made this thesis possible.

First of all, I would like to express my sincere thanks to my two promotors Professor Christine L. Mummery and Professor Frans M. Helmerhorst for providing me this opportunity to conduct my PhD studies in LUMC. All your input, help, encouragement and advice was essential for my PhD and the thesis.

My deep gratitude also goes to my daily supervisor Dr. Susana M. Chuva de Sousa Lopes, in whose group I received high-quality research training in the last four years. Dear Susana, your guidance, inspiration, critical thinking, scientific understanding, friendship, input in various aspects, were crucial for me to carry out all the doctoral work and o vercome the challenges along the path. May the force be with you! I am also extremely grateful to all (former and current) members of the group, particularly Liesbeth, Maria, Matthias, Monika, Aline, Fang, Marijne, Julia, Carmen, Maaike, Sara and Michael. Your help, kindness, advice, fruitful discussions and suggestions supported me through all the adventures. We had a wonderful time together and I will not forget! Additional thanks to Maaike for translating my summary to Dutch.

My sincere thanks also go to my fellow PhD students Verena, Oleh, Xu, Lettine, Yang, Joshua, Viola, Karina, Elisa and Beerend for the kind support and talks not only about science but also about life. Thank you every current and previous fellow labmate from the department, particularly Saskia, Lisa, Mervyn, Daniela, Dorien, Conny, Bert, Margot and Jantine for lab techniques, software and hardware support; Atie for all administrative issues; and Daniel for the IT support.

I would like to thank all the input and support beyond the Department of Anatomy and Embryology: Lucette and Gonneke from Department of Gynaecology; Karoly, Danielle, Joop, Annelies, Hans and Willem from Department of Molecular Cell Biology; Leon and Ioannis from the Sequencing Analysis Support Core; Jelle and Szymon from the Department of Medical Statistics; Brendy from Department of Pathology, Mihaela from Graduate School and Haoyu from Department of Human Genetics. Additional special thanks to Sailaja for the artwork in my thesis.

My heartfelt gratitude goes to my dear friends and their unconditional support. Man, Yatwai, Susanna, Chinjung, Hui, Cui, Speeder, Kiki, Alan, Xinxin, Zhenyu, Min, Chunli, Gelilla, Piet, Leo, Piet, Els, Andy, Helen, Yage and Na, many thanks for sharing joys, gratefulness, trials and healing in life. We are witnesses to many miracles! I express profound thanks to Xiaoyu, for accompanying this four-year journey with me from the very beginning. We share so many unforgotten memories of the Europe. Many thanks to Fang for the cooking for over a year. Additional honest thanks to Mei and Zhao, for keeping me connected to Zhengzhou, China.

I greatly appreciate the financial support from the China Scholarship Council (CSC) during my PhD training at LUMC.

At the end, I owe my sincerest gratitude towards my family. My dear parents, sister and brother-in-law, thank you for unflagging love and support throughout my life. My deepest love and immense appreciation also go to my boyfriend Fei.